

Phase transitions between dilute and dense axion stars

Pierre-Henri Chavanis

Laboratoire de Physique Théorique, Université Paul Sabatier, 118 route de Narbonne 31062 Toulouse, France

We study the nature of phase transitions between dilute and dense axion stars interpreted as self-gravitating Bose-Einstein condensates. We develop a Newtonian model based on the Gross-Pitaevskii-Poisson equations for a complex scalar field with a self-interaction potential $V(|\psi|^2)$ involving an attractive $|\psi|^4$ term and a repulsive $|\psi|^6$ term. Using a Gaussian ansatz for the wave function, we analytically obtain the mass-radius relation of dilute and dense axion stars for arbitrary values of the self-interaction parameter $\lambda \leq 0$. We show the existence of a critical point $|\lambda|_c \sim (m/M_P)^2$, where m is the axion mass and M_P the Planck mass, above which a first order phase transition takes place. We qualitatively estimate general relativistic corrections on the mass-radius relation of axion stars. For weak self-interactions $|\lambda| < |\lambda|_c$, a system of self-gravitating axions forms a stable dilute axion star below a general relativistic maximum mass $M_{\text{max,GR}}^{\text{dilute}} \sim M_P^2/m$ and collapses into a black hole above that mass. For strong self-interactions $|\lambda| > |\lambda|_c$, a system of self-gravitating axions forms a stable dilute axion star below a Newtonian maximum mass $M_{\text{max,N}}^{\text{dilute}} = 5.073M_P/\sqrt{|\lambda|}$ [P.H. Chavanis, Phys. Rev. D **84**, 043531 (2011)], collapses into a dense axion star above that mass, and collapses into a black hole above a general relativistic maximum mass $M_{\text{max,GR}}^{\text{dense}} \sim \sqrt{|\lambda|}M_P^3/m^2$. Dense axion stars explode below a Newtonian minimum mass $M_{\text{min,N}}^{\text{dense}} \sim m/\sqrt{|\lambda|}$ and form dilute axion stars of large size or disperse away. We determine the phase diagram of self-gravitating axions and show the existence of a triple point ($|\lambda|_*$, $M_*/(M_P^2/m)$) separating dilute axion stars, dense axion stars, and black holes. We make numerical applications for QCD axions and ultralight axions. Our approximate analytical results are in good agreement with the exact numerical results of Braaten *et al.* [Phys. Rev. Lett. **117**, 121801 (2016)] for Newtonian dense axion stars. They are also qualitatively similar to those obtained by Helfer *et al.* [JCAP **03**, 055 (2017)] for general relativistic axion stars but they differ quantitatively for weak self-interactions due presumably to the use of a different self-interaction potential $V(|\psi|^2)$. We point out analogies between the evolution of self-gravitating axions (bosons) at zero temperature evolving from dilute axion stars to dense axion stars and black holes, and the evolution of compact degenerate (fermion) stars at zero temperature evolving from white dwarfs to neutron stars and black holes. We also discuss some analogies between the phase transitions of axion stars at zero temperature and the phase transitions of self-gravitating fermions at finite temperature. Finally, we suggest that a dense axionic nucleus may form at the center of dark matter halos through the collapse of a dilute axionic core (soliton) passing above the maximum mass $M_{\text{max,N}}^{\text{dilute}}$. It would have a mass $1.11 \times 10^9 (f/m) M_\odot$, a radius $0.949/(mf^{1/3})$ pc, a density $2.10 \times 10^{-8} (m^2 f^2) \text{ g/m}^3$, a pulsation period $8.24/(mf^{1/3})$ yrs and an energy $-5.59 \times 10^{62} (f/m)$ ergs, where the axion mass m is measured in units of $10^{-22} \text{ eV}/c^2$ and the axion decay constant f is measured in units of 10^{15} GeV . This dense axionic nucleus could be the remnant of a bosonova associated with the emission of a characteristic radiation [Levkov *et al.*, Phys. Rev. Lett. **118**, 011301 (2017)].

PACS numbers: 95.30.Sf, 95.35.+d, 98.80.-k

I. INTRODUCTION

The nature of dark matter (DM) is still unknown and constitutes one of the greatest mysteries of modern cosmology. The cold dark matter (CDM) model in which DM is assumed to be made of weakly interacting massive particles (WIMPs) works remarkably well at large (cosmological) scales but encounters some problems at small (galactic) scales. These problems are known as the cusp problem [1], the missing satellite problem [2], and the too big to fail problem [3]. In order to solve this “CDM crisis”, it has been proposed to take the quantum nature of the particles into account. For example, it has been suggested that DM may be made of bosons in the form of Bose-Einstein condensates (BECs) at absolute zero temperature [4–80] (see the Introduction of [34] for a short historic of this model). In this model, DM halos are in-

terpreted as gigantic boson stars described by a scalar field (SF) that may represent the wavefunction ψ of the BEC. The mass of the DM boson has to be very small (see below) for quantum mechanics to manifest itself at galactic scales. The bosons may be noninteracting or have a repulsive or attractive self-interaction. Different names have been given to this model such as SFDM, fuzzy dark matter (FDM), BECDM, and ψ DM. In the fully general relativistic context, the evolution of the SF is described by the Klein-Gordon-Einstein (KGE) equations. At the scale of DM halos, Newtonian gravity can be used so the evolution of the wave function of the self-gravitating BEC is governed by the Gross-Pitaevskii-Poisson (GPP) equations.

Using the transformations introduced by Madelung [81] and de Broglie [82–84], hydrodynamic representations of the GPP and KGE equations have been intro-

duced in [25, 29, 34–36, 40, 41, 46, 59, 60, 74] (see the Introduction of [74] for a short historic of the hydrodynamic interpretation of [74] for a short historic of the hydrodynamic interpretation of quantum mechanics). The quantum Euler equations are similar to the hydrodynamic equations of CDM except that they include a quantum force arising from the Heisenberg uncertainty principle and a pressure force due to the self-interaction of the bosons measured by their scattering length a_s . In the BEC model, DM halos are stable stationary solutions of the KGE, GPP, or quantum Euler equations. They satisfy a condition of hydrostatic equilibrium corresponding to the balance between the gravitational attraction, the repulsive quantum force (Heisenberg’s uncertainty principle), and the pressure force due to the self-interaction (scattering) that can be repulsive ($a_s > 0$) or attractive ($a_s < 0$). The mass-radius relation of self-gravitating BECs at $T = 0$ has been obtained numerically (exactly) and analytically (approximately) in [34, 35] for any value (positive or negative) of the scattering length a_s of the bosons.¹ For bosons with a positive scattering length ($a_s > 0$), corresponding to a repulsive self-interaction, this study makes the link between the noninteracting limit $GM^2ma_s/\hbar^2 \ll 1$ in which the pressure due to the scattering can be neglected and the Thomas-Fermi (TF) limit $GM^2ma_s/\hbar^2 \gg 1$ in which the quantum potential can be neglected. In that case, an equilibrium state exists for any mass. For bosons with a negative scattering length ($a_s < 0$), corresponding to an attractive self-interaction, this study shows that stable halos can exist only below a maximum mass. The cosmological evolution of a relativistic self-interacting complex SF described by the KGE equations has been studied in [54, 77]. The gravitational instability of an infinite homogeneous complex SF described by the KGE and GPP equations (quantum Jeans problem) has been treated through the hydrodynamical picture in [5, 29, 34, 40, 41, 59, 80].

One possible DM candidate is the axion [85]. Axions are hypothetical pseudo-Nambu-Goldstone bosons of the Peccei-Quinn [86] phase transition associated with a $U(1)$ symmetry that solves the strong charge parity (CP) problem of quantum chromodynamics (QCD). The axion is a spin-0 particle with a very small mass $m = 10^{-4} \text{ eV}/c^2$ and an extremely weak self-interaction $a_s = -5.8 \times 10^{-53} \text{ m}$ arising from nonperturbative effects in QCD. Their role in cosmology has been first investigated in [87–90]. They are produced in the early universe by non-thermal mechanisms, either by vacuum misalignment [87–89] or cosmic string decay [90]. Axions are extremely nonrelativistic and have huge occupation numbers, so they can be described by a classical field. Recently, it has been proposed that gravitational inter-

actions can thermalize the axions, so axionic DM can form a BEC during the radiation-dominated era [91, 92]. Axions can thus be described by a relativistic quantum field theory with a real scalar field φ whose evolution is governed by the KGE equations. In the nonrelativistic limit, they can be described by an effective field theory with a complex scalar field ψ whose evolution is governed by the GPP equations. Therefore, axions are good candidates for the BECDM scenario. One particularity of the QCD axion is to have a negative scattering length ($a_s < 0$) corresponding to an attractive self-interaction.

The formation of structures in an axion-dominated Universe was investigated by Hogan and Rees [93] and Kolb and Tkachev [94]. In the very early Universe, the axions are relativistic but self-gravity can be neglected with respect to their attractive self-interaction. These authors found that the attractive self-interaction of the axions generates very dense structures corresponding to pseudo-soliton configurations that they called “axion miniclusters” [93] or “axitons” [94]. These axitons have a mass $M_{\text{axiton}} \sim 10^{-12} M_\odot$ and a radius $R_{\text{axiton}} \sim 10^9 \text{ m}$. At later times, self-gravity must be taken into account. Kolb and Tkachev [94] mentioned the possibility to form boson stars² by Jeans instability through Bose-Einstein relaxation in the gravitationally bound clumps of axions. In other words, axitons are expected to collapse into boson stars due to Jeans instability when self-gravity becomes important. This possibility was originally proposed by Tkachev [98, 100] who introduced the names “gravitationally bound axion condensates” [98] and “axionic Bose stars” [100], becoming later “axion stars”. It is important to stress, however, that Tkachev [98, 100] and Kolb and Tkachev [94] considered boson stars with a repulsive self-interaction ($a_s > 0$). Since axions have an attractive self-interaction ($a_s < 0$), one cannot directly apply the standard results of boson stars [95–99] to axion stars.

The case of self-interacting boson stars with an attractive self-interaction ($a_s < 0$), possibly representing axion stars, has been considered only recently [34, 35, 73, 101–114]. The analytical expression of the maximum mass of Newtonian self-gravitating BECs with an attractive self-interaction was first obtained in [34, 35]. For QCD axions, this leads to a maximum mass $M_{\text{max}}^{\text{exact}} = 6.46 \times 10^{-14} M_\odot = 1.29 \times 10^{17} \text{ kg} = 2.16 \times 10^{-8} M_\oplus$ and a minimum radius $(R_{99}^*)^{\text{exact}} = 3.26 \times 10^{-4} R_\odot = 227 \text{ km} = 3.56 \times 10^{-2} R_\oplus$. This is the maximum mass of dilute QCD axion stars. These values correspond to the typical

¹ This mass-radius relation describes ultracompact dwarf DM halos like Fornax that are completely condensed (ground state), and the solitonic core of large BECDM halos. It does not describe the virialized envelope of large DM halos that has a Navarro-Frenk-White (NFW) profile (see, e.g., [52, 78] for more details).

² Boson stars, that are the solutions of the KGE equations, were introduced by Kaup [95] and Ruffini and Bonazzola [96] in the case where the bosons have no self-interaction. Boson stars in which the bosons have a repulsive self-interaction were considered later by Colpi *et al.* [97], Tkachev [98] and Chavanis and Harko [99]. These authors showed that boson stars can exist only below a maximum mass (see Appendixes A 5 and A 6) due to general relativistic effects.

size of asteroids. Obviously, QCD axions cannot form giant BECs with the dimension of DM halos. By contrast, they may form mini axion stars that could be the constituents of DM halos under the form of mini massive compact halo objects (mini MACHOs) [73].³ These mini axion stars are Newtonian self-gravitating BECs of QCD axions with an attractive self-interaction stabilized by the quantum pressure (Heisenberg uncertainty principle). They may cluster into structures similar to standard CDM halos but made of scalar field MACHOs instead of WIMPs. However, mini axion stars (MACHOs) behave essentially as CDM and do not solve the small-scale crisis of CDM.

Other types of axions with a very small mass may exist and are called ultralight axions (ULA) [72]. Such axions appear in string theory [117] leading to the notion of string axiverse [118]. ULAs can form very big objects of the size of DM halos. For an ULA with a mass $m = 2.19 \times 10^{-22} \text{ eV}/c^2$ and a very small attractive self-interaction $a_s = -1.11 \times 10^{-62} \text{ fm}$, one finds [73] that the maximum mass and the minimum radius of an axionic DM halo are $M_{\text{max}}^{\text{exact}} = 10^8 M_{\odot}$ and $R = 1 \text{ kpc}$, comparable to the dimensions of dwarf spheroidal galaxies (dSphs) like Fornax.⁴ Therefore, ULAs can form giant BECs with the dimensions of DM halos.

The previous discussion shows that QCD axions and ULAs behave very differently. QCD axions form mini axion stars of the asteroid size which behave like CDM. On the other hand, ULAs form DM halos which can solve the small-scale problems of CDM. In the following, to simplify the discussion, we shall always speak of “axion stars” but we stress that this term can refer either to “mini axion stars” (QCD axions) or “axionic DM halos” (ULAs). Our formalism is general and can handle these two situations.

One may wonder what happens when the mass of an axion star is larger than the maximum mass M_{max} [34, 35]. In that case, there is no equilibrium state and the star undergoes gravitational collapse. Similarly, white dwarf stars [119], neutron stars [120] and boson stars [95–99] exist only below a maximum mass and collapse when they are too massive. The collapse of massive stars leads to black holes. We note, however, that the

maximum mass of the axion stars is a Newtonian non-relativistic result (essentially due to the attractive self-interaction of the axions) while the maximum mass of white dwarf stars, neutron stars and boson stars arises from special and/or general relativity. As a result, the collapse of axion stars is expected to be very different from the collapse of white dwarfs, neutron stars and boson stars.

The collapse of dilute axion stars above M_{max} was first discussed in [73]. In this paper, we determined the general expression of the collapse time $t_{\text{coll}}(M, R_0)$ as a function of the mass $M \geq M_{\text{max}}$ of the axion star and its initial radius R_0 .⁵ We used an approximation based on a Gaussian ansatz which is expected to be very good close to the critical point M_{max} . However, in order to determine the final fate of an axion star experiencing gravitational collapse, a more precise study is necessary.

Let us first consider, as in [73], axion stars with a purely attractive $|\psi|^4$ self-interaction potential in the framework of Newtonian gravity. The dynamical evolution above M_{max} of a nonrelativistic self-gravitating BEC with a purely attractive $|\psi|^4$ interaction described by the GPP equations is interesting in its own right even if this model may not be realistic on a physical point of view (see below). In that case, we expect that the collapse will ultimately lead to a Dirac peak $\rho(\vec{x}) = M\delta(\vec{x})$ because the effective potential is not bounded from below (see Appendix C). However, the evolution of the system is not trivial. In the early stage of the collapse, self-gravity must be taken into account. By contrast, in the late stages of the collapse, the attractive self-interaction of the bosons dominates, and self-gravity can be neglected. The collapse of a nongravitational BEC with an attractive self-interaction ($a_s < 0$) has been studied extensively and is well-known [121, 122]. After an initial smooth evolution where the BEC density profile is close to a Gaussian (if it is Gaussian initially), the system undergoes a self-similar collapse (called “wave collapse”) leading to a finite time singularity: at $t = t_{\text{coll}}(M, R_0)$,⁶ the central density $\rho_0(t)$ becomes infinite and the core radius $r_0(t)$ tends to zero leading to a singular den-

³ The mass M of the mini MACHOs must be less than $2 \times 10^{-9} M_{\odot}$ to be consistent with the observational constraints imposed by gravitational microlensing [115, 116]. The maximum mass $M_{\text{max}}^{\text{exact}} = 6.46 \times 10^{-14} M_{\odot}$ of QCD axion stars satisfies this constraint. Coincidentally, these mini axion stars have a mass comparable to the mass of the axitons [94] but their mechanism of formation is completely different. In particular, the maximum mass of a mini axion star is obtained by balancing the quantum pressure against the gravitational and self-interaction forces whereas the mass of a minicluster is determined by the volume of the horizon when the axion starts to oscillate.

⁴ See Appendix D of [77] for a more detailed discussion about the mass of ULAs, including noninteracting bosons and bosons with a repulsive or an attractive self-interaction.

⁵ The main purpose of our paper was to obtain the expression of the collapse time $t_{\text{coll}}(M, R_0)$, not to study accurately the collapse dynamics of the axion star or determine what is the final outcome of the collapse. We mentioned the possibility to form black holes, but we also stressed the limitation of our approach and mentioned other scenarios when a more realistic self-interaction potential is considered. We note that the order of magnitude of the collapse time $t_{\text{coll}}(M, R_0)$ obtained in [73] is totally insensitive to the precise nature of the final object that is formed as a result of the collapse as long as it is sufficiently small (see Appendix B).

⁶ This collapse time corresponds precisely to the function $t_{\text{coll}}(M, R_0)$ studied in [73]. It cannot be obtained from the self-similar solution of the GP equations because it appears as an undetermined constant of integration [121, 122]. Therefore, a complementary study, such as the one performed in [73], is necessary to obtain $t_{\text{coll}}(M, R_0)$.

sity profile $\rho(r, t = t_{\text{coll}}) \propto r^{-2}$ diverging at the origin. During the self-similar evolution, the central density increases as $\rho_0(t) = \rho(0, t) \sim (t_{\text{coll}} - t)^{-1}$ and the core radius decreases as $r_0(t) \sim (t_{\text{coll}} - t)^{1/2}$. Note that the singularity at $t = t_{\text{coll}}$ contains no central mass: $M(r) = 4\pi \int_0^r \rho(r') r'^2 dr' \rightarrow 0$ as $r \rightarrow 0$. However, the evolution continues in the post collapse regime $t > t_{\text{coll}}$, where a Dirac peak $\rho(\vec{x}, t) = M_D(t) \delta(\vec{x})$ with an increasing mass $M_D(t)$ forms at $r = 0$ by accreting particles around it.⁷ If we take general relativity into account, using the KGE equations with a purely attractive ϕ^4 interaction, we expect that the Dirac peak will be replaced by a black hole. Of course, the postcollapse dynamics of the GPP and KGE equations is difficult to study mathematically and numerically because one needs to cross the r^{-2} singularity at $t = t_{\text{coll}}$. It would be interesting to study this model in detail at a mathematical level even if it is purely academic on a physical point of view for the reasons explained below.

First, the previous scenario assumes that the system remains spherically symmetric and compact during the collapse. Recently, Cotner [105] has numerically solved the GPP equations with a purely attractive self-interaction. When $M > M_{\text{max}}$, he found that the system collapses and first forms an extremely dense core surrounded by a fluctuating halo of scalar waves (suggesting a large amount of interference). Then, he observed that the core fragments into several stable pieces (axion “drops”) of mass $M' < M_{\text{max}}$, thereby avoiding its catastrophic collapse into a singularity. This fragmentation process was previously suggested in [104].

On the other hand, even in the case of a spherical collapse, new physical processes can come into play when the system becomes dense enough and can prevent the formation of a finite time singularity at $t = t_{\text{coll}}$. In particular, when the system becomes dense, the $|\psi|^4$ approximation is not valid anymore and we have to take into account higher order terms in the expansion of the SF potential (or, better, consider the exact axionic self-interaction potential). These higher order terms, which can be repulsive (unlike the ϕ^4 term), can account for strong collisions between axions. These collisions may have important consequences on the collapse dynamics. Three possibilities have been considered in the recent literature:

(i) The first possibility is to form *dense axion stars*. Indeed, when repulsive terms are taken into account, the SF potential becomes bounded from below. In that case, the

collapse is halted by the repulsion of the bosons that becomes dominant at high densities. An equilibrium state exists in which the self-gravity is balanced by the repulsive self-interaction. This possibility was first proposed by Braaten *et al.* [103] who calculated numerically the equilibrium configurations of dense axion stars.

(ii) The second possibility is a *bosenova* phenomenon. The collapse of the axion star may be accompanied by a burst of relativistic axions (radiation) produced by inelastic reactions when the density reaches high values. Relativistic collisions between axions can stop the collapse and even drive a re-expansion of the system. In that case, the collapse (implosion) is followed by an explosion. This phenomenon was shown experimentally by Donley *et al.* [129] for nongravitational relativistic BECs with an attractive self-interaction. Braaten *et al.* [103] and Eby *et al.* [108] argued that axion stars, as they collapse, emit many highly energetic free axions. This could cause the partial, or even complete, disappearance of the axion star. Recently, the validity of this scenario (bosenova) for relativistic axion stars was demonstrated by Levkov *et al.* [110] from direct numerical simulations of the KGE equations with the exact axionic potential taking collisions into account. In these simulations, the system does not reach an equilibrium state (i.e. it does not form a dense axion star) but undergoes a series of collapses and explosions. Multiparticle relativistic interactions in the dense center create an outgoing stream of mildly relativistic particles which carries away an essential part of the star mass (about 30%). The explosion is a period of violent oscillations accompanied by strong emission of outgoing high-frequency waves with a characteristic spectrum (see Fig. 3 in [110]).

(iii) The third possibility, in the case where general relativity is taken into account, is the formation of a black hole if the mass of the axion star is sufficiently large or if the self-interaction is sufficiently weak. This possibility has been demonstrated numerically by Helfer *et al.* [112]. For small masses or strong self-interactions, they obtained either a stable axion star or a dispersion phenomenon similar to that reported by Levkov *et al.* [110]. For large masses or weak self-interactions, a black hole was formed.

Other works have been considered in relation to axion stars. In particular, it has been proposed that Fast radio bursts (FRBs), whose origin is one of the major mysteries of high energy astrophysics, could be caused by axion stars that can engender bursts when undergoing conversion into photons during their collision with the magnetosphere of neutron stars (magnetars), during their collision with the magnetized accretion disk of a black hole, or during their collapse above the maximum mass. We refer to [130–134] for the suggestion of this scenario and to [135] for an interesting critical discussion.

For all these reasons, it is important to study the phase transitions between dilute and dense axion stars in detail. The aim of this paper is to perform an exhaustive analytical study of this problem and to isolate charac-

⁷ As far as we know, this postcollapse regime has not been studied in detail for the GP equation with an attractive self-interaction. Therefore, our discussion should be confirmed, or infirmed, by numerical simulations. Our claim that a Dirac peak is formed in the postcollapse regime comes from the analogy between the GP equation with an attractive self-interaction and the Smoluchowski-Poisson equations describing self-gravitating Brownian particles [123–128].

teristic mass, length, density and energy scales that play an important role. Even if our analytical approach is approximate, these typical scales are fully relevant and determine the gross characteristic features of the system. In general, in astrophysics, we are more interested by orders of magnitude than by exact values. Our study provides the correct orders of magnitude. Furthermore, when it was possible to compare our approximate analytical results with exact numerical results [35, 103], we found that our study proves to be relatively accurate.

The paper is organized as follows. In Sec. II, starting from the KGE equations for a real SF, and considering the nonrelativistic limit, we derive the hydrodynamic equations describing axionic dark matter in an expanding universe taking into account the self-interaction of the axions. In Sec. III, we determine the general equation of state of axionic dark matter and introduce the simplified equation of state studied in this paper. In Sec. IV, we recall important results concerning the maximum mass of dilute axion stars and express it with different parameters that are relevant to our problem. In Sec. V, we derive the analytical mass-radius relation of dilute and dense axion stars within the Gaussian ansatz. In Sec. VI, we consider the TF approximation which is particularly well-suited to describe dense axion stars. In Sec. VII, we derive the energy and pulsation of dilute and dense axion stars and derive a simplified version of Poincaré's turning point argument based on the Gaussian ansatz. In Sec. VIII, we derive the radius of the axion star resulting from a collapse or an explosion at a critical point. In Sec. IX, we study the stability of axion stars and the nature of phase transitions between dilute and dense configurations. In Sec. X, we take into account general relativistic effects in a qualitative manner and obtain an estimate of the maximum mass of axion stars above which they collapse into a black hole. This allows us to obtain a phase diagram exhibiting a triple point separating dilute axion stars, dense axion stars, and black holes. In Sec. XI, we summarize our main results and discuss analogies and differences between axion stars and fermion stars. The Appendixes present important complementary results giving, for example, the fundamental scalings of mass, radius, density, energy... or providing exact results (going beyond the Gaussian ansatz) in particular limits of the problem.

II. HYDRODYNAMIC EQUATIONS OF AXIONIC DARK MATTER IN AN EXPANDING UNIVERSE

In this section, we derive the hydrodynamic equations describing axionic DM in an expanding universe in the nonrelativistic limit $c \rightarrow +\infty$, starting from the KGE equations for a real SF. The nonrelativistic approximation is extremely well justified for axions. We compare the resulting equations with those obtained in our previous papers [59, 60] for a complex SF.

A. The KGE equations

We consider the weak field gravity limit and work with the Newtonian gauge which is a perturbed form of the Friedmann-Lemaître-Robertson-Walker (FLRW) line element [136]. We use the simplest form of Newtonian gauge, only taking into account scalar perturbations which are the ones that contribute to the formation of structures in cosmology. Vector perturbations (which are supposed to be always small) vanish during cosmic inflation and tensor perturbations (which account for gravitational waves) are neglected [137]. We also neglect anisotropic stresses. We finally assume that the Universe is flat in agreement with the observations of the cosmic microwave background (CMB). Under these conditions, the line element is given by

$$ds^2 = c^2 \left(1 + 2\frac{\Phi}{c^2}\right) dt^2 - a(t)^2 \left(1 - 2\frac{\Phi}{c^2}\right) \delta_{ij} dx^i dx^j, \quad (1)$$

where $\Phi/c^2 \ll 1$. In this metric, $\Phi(\vec{x}, t)$ represents the gravitational potential of classical Newtonian gravity and $a(t)$ is the scale factor. Working with this metric enables us to obtain exact equations at the order $O(\Phi/c^2)$ taking into account both relativistic and gravitational contributions inside an expanding Universe.

We consider a real SF φ with a potential $V(\varphi^2)$ whose evolution is governed by the KGE equations. In the weak field approximation $\Phi/c^2 \ll 1$, using the Newtonian gauge, the KGE equations write

$$\frac{1}{c^2} \frac{\partial^2 \varphi}{\partial t^2} + \frac{3H}{c^2} \frac{\partial \varphi}{\partial t} - \frac{1}{a^2} \left(1 + \frac{4\Phi}{c^2}\right) \Delta \varphi - \frac{4}{c^4} \frac{\partial \Phi}{\partial t} \frac{\partial \varphi}{\partial t} + \left(1 + \frac{2\Phi}{c^2}\right) \frac{m^2 c^2}{\hbar^2} \varphi + 2 \left(1 + \frac{2\Phi}{c^2}\right) \frac{dV}{d\varphi^2} \varphi = 0, \quad (2)$$

$$\begin{aligned} \frac{\Delta \Phi}{4\pi G a^2} &= \frac{1}{2c^4} \left(1 - \frac{2\Phi}{c^2}\right) \left(\frac{\partial \varphi}{\partial t}\right)^2 \\ &+ \frac{1}{2a^2 c^2} \left(1 + \frac{2\Phi}{c^2}\right) (\vec{\nabla} \varphi)^2 + \frac{m^2}{2\hbar^2} \varphi^2 \\ &+ \frac{1}{c^2} V(\varphi^2) - \frac{3H^2}{8\pi G} + \frac{3H}{4\pi G c^2} \left(\frac{\partial \Phi}{\partial t} + H\Phi\right), \end{aligned} \quad (3)$$

where $H = \dot{a}/a$ is the Hubble parameter. They can be compared to the KGE equations (12) and (18) of [60] for a complex SF.

B. The GPE equations

To ultimately obtain the nonrelativistic limit $c \rightarrow +\infty$, we make the transformation

$$\varphi = \frac{1}{\sqrt{2}} \frac{\hbar}{m} \left[\psi(\vec{x}, t) e^{-imc^2 t/\hbar} + \psi^*(\vec{x}, t) e^{imc^2 t/\hbar} \right]. \quad (4)$$

This is the counterpart of the Klein transformation for a complex SF φ (see Eq. (24) of [60]). Equation (4) introduces a complex function $\psi(\vec{x}, t)$ that we shall call the pseudo wave function. This transformation allows us to separate the fast oscillations of the SF with pulsation $\omega = mc^2/\hbar$ caused by its rest mass from the slow evolution of $\psi(\vec{x}, t)$. Neglecting the oscillatory terms that average out to zero in the fast oscillation regime $\omega \gg H$, we find that⁸

$$\varphi^2 \simeq \frac{\hbar^2}{m^2} |\psi|^2. \quad (5)$$

We define the pseudo rest-mass density by

$$\rho = |\psi|^2. \quad (6)$$

We stress that it is only in the nonrelativistic limit $c \rightarrow +\infty$ that ψ has the interpretation of a wave function and that ρ has the interpretation of a rest-mass density (see below). In the relativistic regime, ψ and ρ do not have a clear physical interpretation but they can always be defined as convenient notations [59, 60].

Substituting Eq. (4) into Eqs. (2) and (3), and neglecting the oscillatory terms again (see footnote 8), we obtain the GPE equations

$$\begin{aligned} i\hbar \frac{\partial \psi}{\partial t} - \frac{\hbar^2}{2mc^2} \frac{\partial^2 \psi}{\partial t^2} - \frac{3}{2} H \frac{\hbar^2}{mc^2} \frac{\partial \psi}{\partial t} \\ + \frac{\hbar^2}{2ma^2} \left(1 + \frac{4\Phi}{c^2}\right) \Delta \psi \\ - m\Phi \psi - \left(1 + \frac{2\Phi}{c^2}\right) m \frac{dV}{d|\psi|^2} \psi + \frac{3}{2} i\hbar H \psi \\ + \frac{2\hbar^2}{mc^4} \frac{\partial \Phi}{\partial t} \left(\frac{\partial \psi}{\partial t} - \frac{imc^2}{\hbar} \psi\right) = 0, \end{aligned} \quad (7)$$

$$\begin{aligned} \frac{\Delta \Phi}{4\pi G a^2} = & \left(1 - \frac{\Phi}{c^2}\right) |\psi|^2 + \frac{\hbar^2}{2m^2 c^4} \left(1 - \frac{2\Phi}{c^2}\right) \left|\frac{\partial \psi}{\partial t}\right|^2 \\ & + \frac{\hbar^2}{2a^2 m^2 c^2} \left(1 + \frac{2\Phi}{c^2}\right) |\vec{\nabla} \psi|^2 + \frac{1}{c^2} V(|\psi|^2) \\ & - \frac{\hbar}{mc^2} \left(1 - \frac{2\Phi}{c^2}\right) \text{Im} \left(\frac{\partial \psi}{\partial t} \psi^*\right) - \frac{3H^2}{8\pi G} \\ & + \frac{3H}{4\pi G c^2} \left(\frac{\partial \Phi}{\partial t} + H\Phi\right). \end{aligned} \quad (8)$$

These equations look similar to those obtained for a complex SF without making any approximation (see Eqs. (25) and (26) of [60]). However, there is a crucial difference. In the present case, $V(|\psi|^2)$ is an effective potential

deduced from $V(\varphi^2)$ by substituting φ from Eq. (4) and neglecting the oscillatory terms. Therefore, it is different from the potential that one would get by directly substituting φ (already averaged) from Eq. (5) into $V(\varphi^2)$, as we can do when φ is complex [60]. The instantonic potential of axions is worked out explicitly in Sec. III A following [108].

In the nonrelativistic limit $c \rightarrow +\infty$,⁹ the GPE equations (7) and (8) reduce to the GPP equations

$$i\hbar \frac{\partial \psi}{\partial t} + \frac{3}{2} i\hbar H \psi = -\frac{\hbar^2}{2ma^2} \Delta \psi + m\Phi \psi + m \frac{dV}{d|\psi|^2} \psi, \quad (9)$$

$$\frac{\Delta \Phi}{4\pi G a^2} = |\psi|^2 - \frac{3H^2}{8\pi G}, \quad (10)$$

similar to Eqs. (29) and (30) of [60] (with the same warning as before concerning the effective potential). When $V = 0$, they reduce to the Schrödinger-Poisson equations in an expanding Universe. The GP equation (9) can be rewritten as

$$i\hbar \frac{\partial \psi}{\partial t} + \frac{3}{2} i\hbar H \psi = -\frac{\hbar^2}{2ma^2} \Delta \psi + m[\Phi + h(|\psi|^2)] \psi \quad (11)$$

where

$$h(|\psi|^2) = \frac{dV}{d|\psi|^2}, \quad \text{i.e.} \quad h(\rho) = V'(\rho). \quad (12)$$

Remark: In the full relativistic theory, the axions are represented by a real SF φ and the particle number is not conserved. However, in the nonrelativistic limit, they are just spinless particles described by a complex wavefunction ψ and their number $N = \frac{1}{m} \int |\psi|^2 d\mathbf{r}$ is conserved. Physically, the particle number is conserved because, by removing the fast oscillating terms, we have eliminated the particle number violating processes that are energetically forbidden for nonrelativistic particles.

C. The hydrodynamic representation

Using the Madelung [81] transformation, we can write the GPP equations under the form of hydrodynamic equations. To that purpose, we write the wave function ψ as

$$\psi(\vec{x}, t) = \sqrt{\rho(\vec{x}, t)} e^{iS(\vec{x}, t)/\hbar}, \quad (13)$$

where $\rho = |\psi|^2$ is the density and $S = (1/2)i\hbar \ln(\psi^*/\psi)$ is the real action. Following Madelung, we also define a velocity field and an energy field by

$$\vec{v}(\vec{x}, t) = \frac{\vec{\nabla} S}{ma}, \quad E(\vec{x}, t) = -\frac{\partial S}{\partial t}, \quad (14)$$

⁸ This approximation may lead to incorrect results in the relativistic regime but it becomes exact in the nonrelativistic limit $c \rightarrow +\infty$ considered after Eq. (8). Note that there is no such approximation for a complex SF since the relation $|\varphi|^2 = (\hbar^2/m^2)|\psi|^2$ is always valid in that case (see Eq. (24) of [60]).

⁹ Although we take the $c \rightarrow +\infty$ limit in the field equations, we keep relativistic contributions in the SF potential (see Sec. III A).

where the scale factor a has been introduced in the velocity field in order to take into account the expansion of the Universe. Since the velocity is potential, the flow is irrotational: $\nabla \times \mathbf{u} = \mathbf{0}$. Substituting Eq. (13) into Eq. (11) and separating real and imaginary parts, we obtain the quantum Euler-Poisson (EP) equations in an expanding background [41, 60, 74]:

$$\frac{\partial \rho}{\partial t} + 3H\rho + \frac{1}{a} \vec{\nabla} \cdot (\rho \vec{v}) = 0, \quad (15)$$

$$\frac{\partial S}{\partial t} + \frac{(\vec{\nabla} S)^2}{2ma^2} = \frac{\hbar^2}{2ma^2} \frac{\Delta \sqrt{\rho}}{\sqrt{\rho}} - m\Phi - mh(\rho), \quad (16)$$

$$\begin{aligned} \frac{\partial \vec{v}}{\partial t} + H\vec{v} + \frac{1}{a} (\vec{v} \cdot \vec{\nabla}) \vec{v} &= \frac{\hbar^2}{2m^2 a^3} \vec{\nabla} \left(\frac{\Delta \sqrt{\rho}}{\sqrt{\rho}} \right) \\ &- \frac{1}{a} \vec{\nabla} \Phi - \frac{1}{\rho a} \vec{\nabla} P, \end{aligned} \quad (17)$$

$$\frac{\Delta \Phi}{4\pi G a^2} = \rho - \frac{3H^2}{8\pi G}. \quad (18)$$

The hydrodynamic equations (15)-(18) have a clear physical interpretation. Equation (15), corresponding to the imaginary part of the GP equation, is the continuity equation. It accounts for the local conservation of mass $M = \int \rho \, d\mathbf{r}$. Equation (16), corresponding to the real part of the GP equation, is the quantum Hamilton-Jacobi equation. It can also be interpreted as a generalized Bernoulli equation for a potential flow. It involves a quantum potential

$$Q = -\frac{\hbar^2}{2ma^2} \frac{\Delta \sqrt{\rho}}{\sqrt{\rho}} = -\frac{\hbar^2}{4ma^2} \left[\frac{\Delta \rho}{\rho} - \frac{1}{2} \frac{(\nabla \rho)^2}{\rho^2} \right] \quad (19)$$

which takes into account the Heisenberg uncertainty principle. Equation (17), obtained by taking the gradient of Eq. (16), is the quantum Euler equation. It involves a quantum force (per unit of mass) $\mathbf{F}_Q = -(1/ma)\nabla Q$. It also involves a pressure force $-(1/\rho a)\nabla P$ where the pressure is given by a barotropic equation of state $P(\rho)$ determined by the nonlinearity $h(\rho)$ in the GP equation (11) through the relation

$$h'(\rho) = \frac{P'(\rho)}{\rho}. \quad (20)$$

This equation shows that h can be interpreted as an enthalpy in the hydrodynamic representation [34]. Equation (20) can be integrated into [60, 74]:

$$P(\rho) = \rho h(\rho) - V(\rho) = \rho V'(\rho) - V(\rho). \quad (21)$$

The speed of sound is

$$c_s^2 = P'(\rho) = \rho V''(\rho). \quad (22)$$

Finally, Eq. (17) involves the gravitational force $-\nabla\Phi$, where Φ is determined by the Poisson equation (18).

Remarks: We stress that the hydrodynamic equations (15)-(18) do not involve viscous terms because they are equivalent to the GPP equations (9) and (10). As a result, they describe a superfluid. We also note that the hydrodynamic equations (15)-(18) with the quantum potential (proportional to \hbar^2) neglected provide a TF, or semiclassical, description of nonrelativistic SFs. When $\hbar = P = 0$, one recovers the classical equations of CDM.

D. The spatially homogeneous SF

For a spatially homogeneous SF ($\rho(\vec{x}, t) = \rho_b(t)$, $\vec{v}_b(\vec{x}, t) = \vec{0}$, $\Phi_b(\vec{x}, t) = 0$, $S_b(\vec{x}, t) = S_b(t)$), the fluid equations (15)-(18) reduce to [41, 60, 74]:

$$\frac{d\rho_b}{dt} + 3H\rho_b = 0, \quad E = mV'(\rho_b), \quad H^2 = \frac{8\pi G}{3}\rho_b, \quad (23)$$

where $E(t) = -dS_b/dt$ is the time-dependent energy of the spatially homogeneous SF in the comoving frame. The wave function of the SF is $\psi_b(\vec{x}, t) = \psi_b(t) = \sqrt{\rho_b(t)} e^{-i(\hbar)^{-1} \int E(t) dt}$. These equations govern the evolution of the cosmological background. We find that $\rho_b \propto a^{-3}$, $a \propto t^{2/3}$, $H = 2/3t$ and $\rho_b = 1/6\pi G t^2$, corresponding to the Einstein-de Sitter (EdS) solution. Therefore, in the nonrelativistic era, and for the homogeneous background, BECDM behaves as CDM. Using Eq. (23), the Poisson equation (18) can be rewritten as

$$\Delta \Phi = 4\pi G a^2 (\rho - \rho_b), \quad (24)$$

where $\rho_b(t)$ is the background density.

E. The equations for the density contrast

Let us write the density in the form $\rho(\vec{x}, t) = \rho_b(t)[1 + \delta(\vec{x}, t)]$, where $\rho_b \propto 1/a^3$ and $\delta(\vec{x}, t)$ is the density contrast. Substituting this expression into Eqs. (15)-(18), we obtain the following equations for the density contrast [41]:

$$\frac{\partial \delta}{\partial t} + \frac{1}{a} \vec{\nabla} \cdot [(1 + \delta)\vec{v}] = 0, \quad (25)$$

$$\begin{aligned} \frac{\partial \vec{v}}{\partial t} + H\vec{v} + \frac{1}{a} (\vec{v} \cdot \vec{\nabla}) \vec{v} &= \frac{\hbar^2}{2m^2 a^3} \vec{\nabla} \left(\frac{\Delta \sqrt{1 + \delta}}{\sqrt{1 + \delta}} \right) \\ &- \frac{1}{a} \vec{\nabla} \Phi - \frac{c_s^2}{(1 + \delta)a} \vec{\nabla} \delta, \end{aligned} \quad (26)$$

$$\Delta \Phi = 4\pi G \rho_b a^2 \delta, \quad (27)$$

where $c_s^2 = P'(\rho) = P'[\rho_b(1 + \delta)]$ is the square of the speed of sound in the inhomogeneous Universe. We stress that

these equations are exact in the nonrelativistic limit, i.e. they do not rely on the assumption $\delta \ll 1$. The linearized quantum EP equations have been studied in [41, 59] in the context of structure formation for BECDM.

III. THE EQUATION OF STATE OF AXIONS

A. The instantonic potential of axions

The instantonic potential of the axions is [86, 138, 139]:

$$V(\varphi) = \frac{m^2 c f^2}{\hbar^3} \left[1 - \cos \left(\frac{\hbar^{1/2} c^{1/2} \varphi}{f} \right) \right] - \frac{m^2 c^2}{2\hbar^2} \varphi^2, \quad (28)$$

where m is the mass of the axion and f is the axion decay constant.¹⁰ Expanding the cosine term in Taylor series, we get

$$V(\varphi) = -\frac{m^2 c f^2}{\hbar^3} \sum_{n=2}^{+\infty} \frac{(-1)^n}{(2n)!} \left(\frac{\hbar^{1/2} c^{1/2} \varphi}{f} \right)^{2n}. \quad (29)$$

If we keep only the first two terms of this expansion, we obtain the φ^6 potential

$$V(\varphi) = -\frac{m^2 c^3}{24 f^2 \hbar} \varphi^4 + \frac{m^2 c^4}{720 f^4} \varphi^6. \quad (30)$$

The effective potential $V(|\psi|^2)$ appearing in the GP equation (9) can be obtained from the following heuristic procedure introduced by Eby *et al.* [108]. Raising φ in Eq. (4) to the power $2n$ thanks to the binomial formula and keeping only terms that do not oscillate, we obtain

$$\varphi^{2n} = \frac{1}{2^n} \left(\frac{\hbar}{m} \right)^{2n} C_{2n}^n |\psi|^{2n}, \quad (31)$$

where $C_{2n}^n = (2n)!/(n!)^2$. Substituting this expression into Eq. (29), we get

$$V(|\psi|^2) = -\frac{m^2 c f^2}{\hbar^3} \sum_{n=2}^{+\infty} \frac{(-1)^n}{(n!)^2} \left(\frac{\hbar^3 c |\psi|^2}{2 f^2 m^2} \right)^n. \quad (32)$$

The series can be performed analytically leading to an effective potential of the form

$$V(|\psi|^2) = \frac{m^2 c f^2}{\hbar^3} \left[1 - \frac{\hbar^3 c}{2 f^2 m^2} |\psi|^2 - J_0 \left(\sqrt{\frac{2 \hbar^3 c |\psi|^2}{f^2 m^2}} \right) \right], \quad (33)$$

where J_0 is the Bessel function of zeroth order. If we keep only the first two terms in the expansion of Eq. (32), we obtain the $|\psi|^6$ potential

$$V(|\psi|^2) = -\frac{\hbar^3 c^3}{16 f^2 m^2} |\psi|^4 + \frac{\hbar^6 c^4}{288 f^4 m^4} |\psi|^6. \quad (34)$$

We note that $V(|\psi|^2)$ is different from the expression obtained by substituting Eq. (5) into $V(\varphi)$. The difference is apparent already in the first term of the expansion of the potential which involves a coefficient $-1/16$ [see Eq. (34)] instead of $-1/24$ [see Eq. (30)].

In the nonrelativistic limit $c \rightarrow +\infty$, or for dilute systems satisfying $|\psi|^2 \ll f^2 m^2 / \hbar^3 c$, the potential $V(|\psi|^2)$ is dominated by the $|\psi|^4$ term. A $|\psi|^4$ potential is usually written as

$$V(|\psi|^2) = \frac{2\pi a_s \hbar^2}{m^3} |\psi|^4, \quad (35)$$

where a_s is the s-scattering length of the bosons [141]. Comparing this expression with the first term of Eq. (34), we obtain

$$a_s = -\frac{\hbar c^3 m}{32\pi f^2}. \quad (36)$$

Using this relationship, the potential of Eq. (34) can be rewritten as

$$V(|\psi|^2) = \frac{2\pi a_s \hbar^2}{m^3} |\psi|^4 + \frac{32\pi^2 \hbar^4 a_s^2}{9m^6 c^2} |\psi|^6. \quad (37)$$

We note that the first term is nonrelativistic while the second term is relativistic in nature since it involves the speed of light c . It provides a relativistic correction of order $1/c^2$ to the $|\psi|^4$ potential.

For dilute configurations satisfying $|\psi|^2 \ll m^3 c^2 / |a_s| \hbar^2$, it is sufficient to keep only the first term in the expansion of the potential $V(|\psi|^2)$ given by Eq. (32). Since the axions have a negative scattering length ($a_s < 0$), we see from Eq. (37) that the $|\psi|^4$ term corresponds to an attraction between axions. This term is sufficient to describe dilute axion stars below the maximum mass M_{\max} [34, 35]. However, for $M > M_{\max}$, dilute axion stars undergo gravitational collapse and their density increases. When the star becomes dense enough, we need to take into account higher order terms in the expansion of the potential. We see that the $|\psi|^6$ term from Eq. (37) corresponds to a repulsion between axions. Therefore, this term can stop the collapse and lead to equilibrium states corresponding to dense axion stars [103]. This repulsion has a relativistic origin. In this paper, we will consider a simplified model where we only retain the first two terms in the expansion of the potential, i.e., we will use Eq. (37) as an approximation of the potential $V(|\psi|^2)$ given by Eq. (33). Because of this approximation, our study may present differences with respect to the studies of [103, 108] based on the potential (33). However, we will see that these differences are small.

Remark: the expression of the effective potential $V(|\psi|^2)$ given by Eq. (33), obtained from the heuristic procedure of Eby *et al.* [108], is not exact. Braaten *et al.* [107] have shown that the first two terms in the expansion of the exact potential are given by

$$V_{\text{exact}}(|\psi|^2) \simeq -\frac{\hbar^3 c^3}{16 f^2 m^2} |\psi|^4 - \frac{\hbar^6 c^4}{256 f^4 m^4} |\psi|^6 + \dots \quad (38)$$

¹⁰ Another, more relevant, axionic potential is the chiral potential [139, 140].

The exact potential (38) differs from Eq. (34) at the level of the $|\psi|^6$ term. Not only the value of the prefactor is different but its sign also is different. For the potential of Eq. (34), the $|\psi|^6$ term corresponds to a repulsion while for the exact potential of Eq. (38) it corresponds to an attraction. Therefore, our study based on the potential (37), and the studies of [103, 108] based on the potential (33), may present quantitative differences with respect to the studies of [110, 112] based on the exact axionic potential (28).

B. The general equation of state

The general equation of state of an axion star is given by Eq. (21) with the potential

$$V(\rho) = \frac{m^2 c f^2}{\hbar^3} \left[1 - \frac{\hbar^3 c}{2 f^2 m^2} \rho - J_0 \left(\sqrt{\frac{2 \hbar^3 c \rho}{f^2 m^2}} \right) \right]. \quad (39)$$

Using $J'_0(x) = -J_1(x)$, we obtain

$$P(\rho) = \frac{m^2 c f^2}{\hbar^3} \left[\frac{1}{2} \sqrt{\frac{2 \hbar^3 c \rho}{f^2 m^2}} J_1 \left(\sqrt{\frac{2 \hbar^3 c \rho}{f^2 m^2}} \right) + J_0 \left(\sqrt{\frac{2 \hbar^3 c \rho}{f^2 m^2}} \right) - 1 \right]. \quad (40)$$

This equation of state involves the function

$$f(x) = \frac{x}{2} J_1(x) + J_0(x) - 1 \quad (41)$$

that is plotted in Fig. 1. For $x \rightarrow 0$,

$$f(x) \simeq -\frac{x^4}{64} + \frac{x^6}{1152}. \quad (42)$$

For $x \rightarrow +\infty$,

$$f(x) \sim \sqrt{\frac{x}{2\pi}} \cos \left(x - \frac{\pi}{2} - \frac{\pi}{4} \right). \quad (43)$$

The equation of state (40) has a complicated oscillatory behavior for $\rho \rightarrow +\infty$. To understand the meaning of these oscillations, let us progressively increase the density of axion stars, from dilute axion stars to dense axion stars. At low densities, the pressure force is attractive (because $a_s < 0$) and adds to the gravitational attraction. A dilute axion star can resist this attraction thanks to the repulsive quantum force arising from Heisenberg's uncertainty principle. However, above a critical density, corresponding to the maximum mass M_{\max} [34, 35], the axion star becomes unstable and collapses. During the collapse, its density increases. At sufficiently high densities the pressure force becomes repulsive and counteracts the gravitational attraction. An equilibrium state is reached, corresponding to a dense axion star [103]. If we keep increasing the density, the pressure force becomes

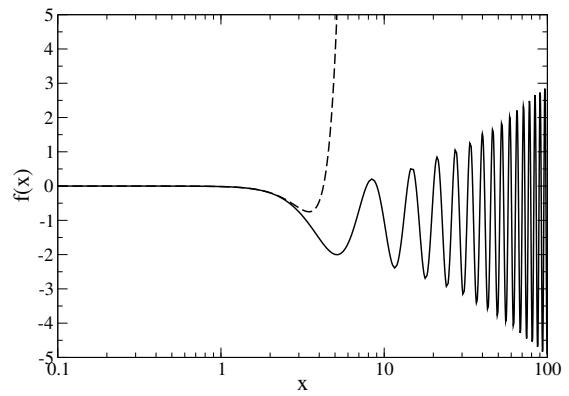


FIG. 1: The function $f(x)$ characterizing the equation of state of axions. For comparison, we have plotted in dashed line the function obtained by keeping only the two first terms in the expansion of $f(x)$ for $x \rightarrow 0$ [see Eq. (42)]. It corresponds to the simplified equation of state of Sec. III C studied in this paper.

attractive again. The dense axion star becomes unstable and collapses until, at even higher densities, the pressure force becomes repulsive and stops the collapse. This process of stabilization/destabilization occurs periodically at higher and higher densities. As a result, the mass-radius relation of axion stars should exhibit a branch of dilute axion stars and several branches of dense axion stars. In this paper, we shall only consider the first branch of dense axion stars. Therefore, it is sufficient to consider the approximation of the equation of state for sufficiently low densities until the first stabilization takes place. This is discussed in the following section.

C. The simplified equation of state

In our simplified model, the equation of state of an axion star is given by Eq. (21) with the potential

$$V(\rho) = \frac{2\pi a_s \hbar^2}{m^3} \rho^2 + \frac{32\pi^2 \hbar^4 a_s^2}{9m^6 c^2} \rho^3. \quad (44)$$

This yields

$$P(\rho) = \frac{2\pi a_s \hbar^2}{m^3} \rho^2 + \frac{64\pi^2 \hbar^4 a_s^2}{9m^6 c^2} \rho^3. \quad (45)$$

The equation of state can be written as

$$P(\rho) = K_2 \rho^2 + K_3 \rho^3, \quad (46)$$

where $K_2 = 2\pi a_s \hbar^2 / m^3$ and $K_3 = 64\pi^2 \hbar^4 a_s^2 / 9m^6 c^2$. This is the sum of two polytropic equations of state of index $\gamma = 2$ ($n = 1$) and $\gamma = 3$ ($n = 1/2$). The first equation of state has an attractive effect ($K_2 < 0$) and the second equation of state has a repulsive effect ($K_3 > 0$).

The equation of state (45) can also be obtained from the exact equation of state (40) by keeping only the first

two terms in its expansion for $\rho \rightarrow 0$. The approximate equation of state (45) is plotted in dashed line in Fig. 1 and compared with the exact equation of state (40). We see that the approximate equation of state has a behavior similar to the exact equation of state at low densities. Starting from $P = 0$, the pressure first decreases (being therefore negative), reaches a minimum and finally increases up to infinity. At low densities, corresponding to dilute axion stars, the two equations of state coincide. At higher densities, when the repulsive self-interaction comes into play, they differ quantitatively but present nevertheless the same qualitative behaviour, both reaching a minimum before increasing. This is the minimum requirement for the validity of our study.

In this paper, we will study in detail the simplified equation of state (45), corresponding to the complex SF potential (37) involving an attractive $|\psi|^4$ term and a repulsive $|\psi|^6$ term. This polynomial potential is interesting in its own right even if it does not exactly correspond to the potential of axions. A more precise treatment of axion stars should consider the general equation of state (40), associated with the effective potential (33), as in Braaten *et al.* [103] and Eby *et al.* [108]. An even more precise treatment should be based on the instantonic potential [86, 117, 139] [see Eq. (28)], or on the chiral potential [139, 140], as in Levkov *et al.* [110] and Helfer *et al.* [112]. An interest of our model is that it leads to a fully analytical study that allows us to identify characteristic mass, length and density scales of fundamental importance. Furthermore, as we shall see, it gives results that are in good agreement with the exact numerical results of Braaten *et al.* [103] based on the potential (33).

IV. THE MAXIMUM MASS OF DILUTE AXION STARS

The mass-radius relation of a nonrelativistic self-gravitating BEC/SF at $T = 0$ described by a purely $|\psi|^4$ potential [see Eq. (35)] has been obtained analytically (approximately) and numerically (exactly) in [34, 35]. When $a_s > 0$, the short-range interaction between the bosons is repulsive. When $a_s < 0$, it is attractive. In this paper, we restrict ourselves to attractive self-interactions.

A. Maximum mass, minimum radius, and maximum average density

When the self-interaction between the bosons is attractive ($a_s < 0$), like in the case of axions, an equilibrium state exists only below a maximum mass [34, 35]:

$$M_{\max}^{\text{exact}} = 1.012 \frac{\hbar}{\sqrt{Gm|a_s|}}. \quad (47)$$

This is the maximum mass of stable dilute Newtonian axion stars. The radii of the stable configurations satisfy

$R_{99} \geq (R_{99}^*)^{\text{exact}}$ where [34, 35]:

$$(R_{99}^*)^{\text{exact}} = 5.5 \left(\frac{|a_s| \hbar^2}{Gm^3} \right)^{1/2} \quad (48)$$

is the radius corresponding to the maximum mass. This is the minimum radius of stable dilute Newtonian axion stars. The subscript 99 means that R_{99} is the radius containing 99% of the mass (the density profile has not a compact support but extends to infinity so the radius of the axion star is formally infinite). The minimum radius is related to the maximum mass by the relation

$$R_{99}^* = 5.57 \frac{\hbar^2}{GM_{\max} m^2}. \quad (49)$$

The maximum average density of stable dilute Newtonian axion stars, defined by $\bar{\rho}_{\max} = 3M_{\max}/4\pi(R_{99}^*)^3$, is

$$\bar{\rho}_{\max}^{\text{exact}} = 1.45 \times 10^{-3} \frac{Gm^4}{a_s^2 \hbar^2}. \quad (50)$$

For $M \ll M_{\max}$ and $R_{99} \gg R_{99}^*$, the mass-radius relation is given by [6, 34, 35]:

$$R_{99}^{\text{exact}} = 9.946 \frac{\hbar^2}{GMm^2}, \quad (51)$$

corresponding to the noninteracting limit. This branch is stable.

For $M \ll M_{\max}$ and $R_{99} \ll R_{99}^*$, the mass-radius relation is given by [34, 35]:

$$R_{99}^{\text{exact}} = 3.64 \frac{|a_s|}{m} M, \quad (52)$$

corresponding to the nongravitational limit. This branch is unstable.

Remark: For future reference, we recall that when the self-interaction between the bosons is repulsive ($a_s > 0$), an equilibrium state exists, in the TF approximation, at a unique radius [9, 16, 23, 25, 34]:

$$R^{\text{exact}} = \pi \left(\frac{a_s \hbar^2}{Gm^3} \right)^{1/2}, \quad (53)$$

independent of the mass. We note that its scaling coincides with that of $(R_{99}^*)^{\text{exact}}$ in Eq. (48).

B. Alternative expressions

Alternative expressions of the maximum mass of axion stars can be given. Introducing the dimensionless self-interaction constant (see, e.g., Appendix A of [73]):

$$\lambda = \frac{8\pi a_s m c}{\hbar}, \quad (54)$$

we get [34, 35]:

$$M_{\max}^{\text{exact}} = 5.073 \frac{M_P}{\sqrt{|\lambda|}}, \quad (55)$$

where $M_P = (\hbar c/G)^{1/2} = 2.18 \times 10^{-5} \text{ g}$ is the Planck mass.¹¹ Similarly, the minimum radius can be written as [34, 35]:

$$(R_{99}^*)^{\text{exact}} = 1.1 \sqrt{|\lambda|} \frac{M_P}{m} \lambda_C, \quad (56)$$

where $\lambda_C = \hbar/mc$ is the Compton wavelength of the bosons. The maximum average density is

$$\bar{\rho}_{\text{max}}^{\text{exact}} = 0.917 \frac{1}{\lambda^2} \left(\frac{m}{M_P} \right)^4 \frac{M_P^2}{m \lambda_C^3}. \quad (57)$$

We can also express the maximum mass, minimum radius, and maximum average density of axion stars in terms of the axion decay constant [see Eq. (36)]:

$$f = \left(\frac{\hbar c^3 m}{32\pi |a_s|} \right)^{1/2}. \quad (58)$$

We obtain

$$M_{\text{max}}^{\text{exact}} = 10.15 \frac{f}{M_P c^2} \frac{M_P^2}{m}, \quad (59)$$

$$(R_{99}^*)^{\text{exact}} = 0.55 \frac{M_P c^2}{f} \lambda_C, \quad (60)$$

$$\bar{\rho}_{\text{max}}^{\text{exact}} = 14.7 \left(\frac{f}{M_P c^2} \right)^4 \frac{M_P^2}{m \lambda_C^3}. \quad (61)$$

Remark: We note the relation $f = mc^2/2|\lambda|^{1/2}$. We also note that the scalings from Eqs. (55)-(61) artificially involve the speed of light c because of the definition of λ and f . Actually, c should not appear in the equations since the maximum mass, minimum radius, and maximum average density of dilute axion stars are nonrelativistic results, as shown in the scalings of Eqs. (47)-(50).

C. Maximum scattering length

Instead of expressing the maximum mass as a function of the scattering length, we can express the maximum scattering length of the bosons (in absolute value) as a

function of the mass of the star. Self-gravitating BECs with an attractive self-interaction can be at equilibrium only if the scattering length of the bosons is less than a maximum value [34, 35]:

$$|a_s|_{\text{max}}^{\text{exact}} = 1.024 \frac{\hbar^2}{GmM^2}. \quad (62)$$

This corresponds to

$$|\lambda|_{\text{max}}^{\text{exact}} = 25.74 \left(\frac{M_P}{M} \right)^2, \quad (63)$$

$$\frac{f_{\text{min}}^{\text{exact}}}{M_P c^2} = 9.855 \times 10^{-2} \frac{mM}{M_P^2}. \quad (64)$$

D. Numerical applications

Let us make numerical applications for different types of axions.

1. QCD axions

Considering QCD axions with $m = 10^{-4} \text{ eV}/c^2$ and $a_s = -5.8 \times 10^{-53} \text{ m}$ [85], corresponding to $\lambda = -7.39 \times 10^{-49}$ and $f = 5.82 \times 10^{19} \text{ eV} = 4.77 \times 10^{-9} M_P c^2$, we obtain $M_{\text{max}}^{\text{exact}} = 6.46 \times 10^{-14} M_\odot = 1.29 \times 10^{17} \text{ kg} = 2.16 \times 10^{-8} M_\oplus$, $(R_{99}^*)^{\text{exact}} = 3.26 \times 10^{-4} R_\odot = 227 \text{ km} = 3.56 \times 10^{-2} R_\oplus$, and $\bar{\rho}_{\text{max}} = 2.62 \times 10^3 \text{ g/m}^3$ (the maximum number of bosons is $N_{\text{max}} = M_{\text{max}}/m = 7.21 \times 10^{56}$). These values correspond to the typical size of asteroids. QCD axions cannot form DM halos of relevant mass and size. However, they can form mini boson stars (mini axion stars or dark matter stars) of very low mass which are stable gravitationally bound BECs. They might play a role as DM components (i.e. DM halos could be made of mini axion stars interpreted as MACHOs) if they exist in the universe in abundance.

Remark: For QCD axions, the product $mf \equiv (\Lambda_{\text{QCD}}/c)^2$ of the mass and decay constant is fixed to the value $\Lambda_{\text{QCD}} = 7.6 \times 10^7 \text{ eV}$ [85]. Astrophysical and cosmological constraints restrict f to the interval $0.5 \times 10^{18} \text{ eV} < f < 7.6 \times 10^{21} \text{ eV}$. The axion mass lies therefore in the interval $7.7 \times 10^{-7} \text{ eV}/c^2 < m < 1.2 \times 10^{-2} \text{ eV}/c^2$. According to Eq. (36), we have

$$\frac{|a_s|}{m^3} = \frac{\hbar c^3}{32\pi f^2 m^2} = \frac{\hbar c^7}{32\pi \Lambda_{\text{QCD}}^4}. \quad (65)$$

Since mf is fixed for QCD axions, then $|a_s|/m^3$ is fixed. From Eq. (48), this implies that the minimum radius R_{99}^* is fixed to the value $(R_{99}^*)^{\text{exact}} = 0.55(M_P c^2/\Lambda_{\text{QCD}})^2 l_P = 227 \text{ km}$, independently of the axion mass m (here $l_P = (\hbar G/c^3)^{1/2} = 1.62 \times 10^{-35} \text{ m}$ is the Planck length). By contrast, the maximum mass $M_{\text{max}} = 10.15(\Lambda_{\text{QCD}}/M_P c^2)^2 M_P^3/m^2$ from Eq. (47) scales with the mass of the axion as m^{-2} .

¹¹ This scaling can be compared to the scaling $M_{\text{max}} = 0.384 M_P^3/m^2$ of the maximum mass of fermion stars [120], to the scaling $M_{\text{max}} = 0.633 M_P^2/m$ of the maximum mass of non-interacting boson stars [95, 96], and to the scaling $M_{\text{max}} = 0.0612 \sqrt{\lambda} M_P^3/m^2$ of the maximum mass of self-interacting boson stars [97–99]. We emphasize, however, that the maximum mass of dilute axion stars given by Eq. (55) is a Newtonian result contrary to the other limits that come from general relativity. The usually very small mass-radius ratio of dilute axion stars (see below) justifies *a posteriori* why a Newtonian treatment is sufficient to describe them.

2. Ultralight axions

Considering ULAs with $m = 2.19 \times 10^{-22} \text{ eV}/c^2$ and $a_s = -1.11 \times 10^{-62} \text{ fm}$ corresponding to $\lambda = -3.10 \times 10^{-91}$ and $f = 1.97 \times 10^{23} \text{ eV} = 1.61 \times 10^{-5} M_P c^2$ (see Appendix D of [77]), we obtain $M_{\text{max}}^{\text{exact}} = 10^8 M_\odot$, $(R_{99}^*)^{\text{exact}} = 1 \text{ kpc}$, and $\bar{\rho}_{\text{max}} = 1.62 \times 10^{-18} \text{ g/m}^3$ (the maximum number of bosons is $N_{\text{max}} = 5.09 \times 10^{95}$). These values are typical of dwarf DM halos like Fornax, or typical of the solitonic core of large DM halos (see footnote 1).

Remark: We note that a halo of mass $M = 10^8 M_\odot$ made of ULAs with mass $m = 2.19 \times 10^{-22} \text{ eV}/c^2$ is stable if $a_s = 0$ but becomes unstable, and collapses, if the scattering length of the axions is larger (in absolute value) than $|a_s|_{\text{max}} = 1.11 \times 10^{-62} \text{ fm}$ [73]. This corresponds to $|\lambda|_{\text{max}} = 3.10 \times 10^{-91}$ and $f_{\text{min}} = 1.97 \times 10^{23} \text{ eV} = 1.61 \times 10^{-5} M_P c^2$. Therefore $\lambda = 0$ is very different from $\lambda = -3.10 \times 10^{-91}$ (!) The extraordinarily small value of $|\lambda|_{\text{max}} = 3.10 \times 10^{-91}$ was stressed in our previous papers [35, 73, 77].

3. White dwarfs and neutron stars

It is interesting to compare these results with other systems exhibiting a maximum mass like white dwarfs [119] and neutron stars [120]. For ideal ${}^4_2\text{He}$ white dwarfs treated within the framework of general relativity [142], we have $M_{\text{max}} = 1.39 M_\odot$, $R_{\text{min}} = 1.02 \times 10^3 \text{ km}$ and $(\rho_0)_{\text{max}} = 2.35 \times 10^{16} \text{ g/m}^3$. For ideal neutron stars [120], we have $M_{\text{max}} = 0.710 M_\odot$, $R_{\text{min}} = 9.16 \text{ km}$ and $(\rho_0)_{\text{max}} = 3.54 \times 10^{21} \text{ g/m}^3$.

E. Validity of the Newtonian treatment for dilute axion stars

The previous results are valid for Newtonian dilute axion stars. We note that the maximum mass given by Eq. (47) increases as the self-interaction decreases. This result is expected to be valid for sufficiently small masses, i.e., for sufficiently strong self-interactions (in a sense made precise below). When the mass becomes large, i.e., for weak self-interactions, general relativity must be taken into account. Helfer *et al.* [112] numerically solved the general relativistic KGE equations with the instantonic potential (28) and studied the formation of black holes from axion stars. They obtained the phase diagram sketched in Fig. 2. For a sufficiently strong self-interactions (small f), the maximum mass of dilute axion stars is given by Eq. (47). It can be rewritten as

$$\frac{M_{\text{max}}^{\text{exact}}}{M_P^2/m} = 10.15 \frac{f}{M_P c^2}. \quad (66)$$

This formula gives a relatively good agreement with the numerical results of Helfer *et al.* [112] up to about

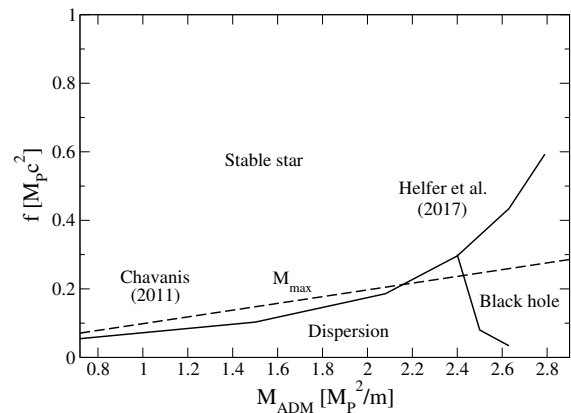


FIG. 2: Sketch of the phase diagram obtained by Helfer *et al.* [112] by numerically solving the KGE equations with the instantonic potential (28). The dashed line corresponds to the Newtonian maximum mass of dilute axion stars given by Eq. (66) obtained in [34]. It is valid for $f \ll M_P c^2$ (strong self-interactions). We see that it gives a fair agreement with the numerical results of [112] up to the triple point at $(f, M) \sim (0.3 M_P c^2, 2.4 M_P^2/m)$.

$f \sim 0.25 M_P c^2$ and $M \sim 2.54 M_P^2/m$ (corresponding approximately to the position of the triple point in their phase diagram). For weaker self-interactions (larger f), the general relativistic results of Helfer *et al.* [112] start to substantially deviate from the expression of the Newtonian maximum mass given by Eq. (66).

We can estimate the validity of our Newtonian description of dilute axion stars as follows. The Newtonian theory of gravitation is valid if the radius R of a star of mass M is much larger than its Schwarzschild radius

$$R_S = \frac{2GM}{c^2}. \quad (67)$$

Using Eq. (47), the Schwarzschild radius of a dilute axion star with the maximum mass can be written as

$$R_S^{\text{exact}} = 2.024 \left(\frac{G\hbar^2}{|a_s|mc^4} \right)^{1/2}. \quad (68)$$

We note the alternative expressions

$$R_S^{\text{exact}} = 10.146 \frac{l_P}{\sqrt{|\lambda|}} = 20.30 \frac{f}{M_P c^2} \frac{M_P}{m} l_P. \quad (69)$$

If axion stars with the maximum mass can be treated with Newtonian gravity, then all the branch of dilute axion stars can be treated with Newtonian gravity (see Appendix E of [73]). Therefore, the condition of validity of the Newtonian treatment for dilute axion stars is

$$\frac{R_{99}^*}{R_S} = \frac{R_{99}^* c^2}{2GM_{\text{max}}} \gg 1. \quad (70)$$

Using Eqs. (47) and (48), we get

$$\frac{R_{99}^* c^2}{2GM_{\text{max}}} \sim \frac{|a_s|c^2}{2Gm}, \quad (71)$$

where we have not written the prefactors since Eq. (70) just gives an estimate of the validity of the Newtonian approximation. We note the exact relations

$$\frac{|a_s|c^2}{Gm} = \frac{2|a_s|}{r_S} = \frac{1}{32\pi} \left(\frac{M_P c^2}{f} \right)^2 = \frac{|\lambda|}{8\pi} \left(\frac{M_P}{m} \right)^2, \quad (72)$$

where

$$r_S = \frac{2Gm}{c^2} \quad (73)$$

is the effective Schwarzschild radius of a particle of mass m (we have introduced this quantity in [77]). As a result, the criterion (70) expressing the validity of the Newtonian approach at the critical point can be written in the equivalent forms

$$|a_s| \gg r_S, \quad f \ll M_P c^2, \quad |\lambda| \gg \left(\frac{m}{M_P} \right)^2. \quad (74)$$

The Newtonian approach is therefore valid for sufficiently strong self-interactions. By contrast, when $|a_s| \sim r_S$, $f \sim M_P c^2$ and $|\lambda| \sim (m/M_P)^2$, general relativity must be taken into account. In that case, the maximum mass and minimum radius of axion stars, obtained by substituting these equivalents into Eqs. (47)-(61), become of the order of

$$M_{\max} \sim \frac{M_P^2}{m}, \quad R_* \sim \lambda_C, \quad (75)$$

corresponding to the Kaup scales (see Appendix A 5). A more detailed general relativistic treatment is performed in Sec. X.

Let us make some numerical applications to complete those reported in Sec. IV D.

For QCD axions with $m = 10^{-4} \text{ eV}/c^2$ and $a_s = -5.8 \times 10^{-53} \text{ m}$, we find $R_S^{\text{exact}} = 1.91 \times 10^{-10} \text{ m}$, $r_S = 2.65 \times 10^{-67} \text{ m}$, $M_P c^2 = 1.22 \times 10^{28} \text{ eV}$ and $(m/M_P)^2 = 6.71 \times 10^{-65}$, implying $(R_{99}^*/R_S)_{\text{exact}} = 1.19 \times 10^{15}$.

For ULAs with $m = 2.19 \times 10^{-22} \text{ eV}/c^2$ and $a_s = -1.11 \times 10^{-62} \text{ fm}$, we find $R_S^{\text{exact}} = 9.57 \times 10^{-6} \text{ pc}$, $r_S = 1.88 \times 10^{-101} \text{ pc}$, $M_P c^2 = 1.22 \times 10^{28} \text{ eV}$ and $(m/M_P)^2 = 3.22 \times 10^{-100}$, implying $(R_{99}^*/R_S)_{\text{exact}} = 1.04 \times 10^8$.

In the following sections, we shall assume that the condition $f \ll M_P c^2$ (strong self-interaction) is fulfilled so that the Newtonian treatment is valid for dilute axion stars and for dense axion stars whose masses are not too large. General relativistic corrections for large values of f (weak self-interaction), or for large masses, will be obtained qualitatively in Sec. X. We see from the previous numerical applications that QCD axions and ULAs are in the strongly self-interacting regime. Therefore, the Newtonian approximation generally provides an excellent description of axion stars made of QCD axions and ULAs, except if they have very large masses.

V. MASS-RADIUS RELATION OF DILUTE AND DENSE AXION STARS WITHIN THE GAUSSIAN ANSATZ

When $M > M_{\max}$, dilute axion stars undergo gravitational collapse [34, 35]. As discussed in the Introduction, one possibility is that the collapse ends with the formation of dense axion stars [103]. In this section, we study phase transitions between dilute and dense axion stars and establish their mass-radius relation. We consider a simplified model corresponding to the polynomial SF potential (37) leading to the equation of state (45). We develop an analytical approach based on a Gaussian ansatz. This is a generalization of our previous work [34] for dilute axion stars. This ansatz usually proves to be accurate to study the equilibrium configurations of self-gravitating BECs [34, 35]. We shall compare our analytical results with the exact numerical results obtained by Braaten *et al.* [103] and find good agreement.

A. The effective potential

Using a Gaussian ansatz for the wave function [34, 73, 78], one can show that the total energy of an axion star of mass M and radius R described by the equation of state (45) is given by

$$E_{\text{tot}} = \frac{1}{2} \alpha M \left(\frac{dR}{dt} \right)^2 + V(R) \quad (76)$$

with the effective potential

$$V(R) = \sigma \frac{\hbar^2 M}{m^2 R^2} - \nu \frac{GM^2}{R} + \zeta \frac{2\pi a_s \hbar^2 M^2}{m^3 R^3} + \zeta \frac{32\pi^2 \hbar^4 a_s^2 M^3}{9m^6 c^2 R^6}. \quad (77)$$

The coefficients are $\alpha = 3/2$, $\sigma = 3/4$, $\zeta = 1/(2\pi)^{3/2}$ and $\nu = 1/\sqrt{2\pi}$.¹² The first term in Eq. (76) is the classical kinetic energy Θ_c and the second term is the potential energy V . The potential energy includes the contribution of the quantum kinetic energy Θ_Q (or quantum potential), the gravitational energy W , the internal energy U_2 due to the repulsive self-interaction (corresponding to a polytropic equation of state of index $\gamma = 2$ and polytropic constant $K_2 < 0$), and the internal energy U_3 due to the attractive self-interaction (corresponding to a polytropic equation of state of index $\gamma = 3$ and polytropic constant $K_3 > 0$). The general formalism needed to obtain the expression (77) of the effective potential can be found in [78]. Writing $\dot{E}_{\text{tot}} = 0$ expressing the conservation of

¹² Other types of ansatz give the same results with slightly different values of the coefficients. For the sake of generality, we will express our results in terms of α , σ , ζ and ν so they can be applied to more general situations if necessary.

energy, we find that the dynamical equation satisfied by the radius of the BEC is

$$\alpha M \frac{d^2 R}{dt^2} = -V'(R). \quad (78)$$

This equation is similar to the equation of motion of a fictive particle of mass αM moving in an effective potential $V(R)$.

B. Maximum mass of dilute axion stars

Within the Gaussian ansatz, the maximum mass and the minimum radius of dilute axion stars are [34]:

$$M_{\max} = \left(\frac{\sigma^2}{6\pi\zeta\nu} \right)^{1/2} \frac{\hbar}{\sqrt{Gm|a_s|}} = 1.085 M_a, \quad (79)$$

$$R_* = \left(\frac{6\pi\zeta}{\nu} \right)^{1/2} \left(\frac{|a_s|\hbar^2}{Gm^3} \right)^{1/2} = 1.732 R_a, \quad (80)$$

where the scales M_a and R_a are defined in Appendix A 1. For a Gaussian density profile, the relation between the radius R and the radius R_{99} containing 99% of the mass is $R_{99} = 2.38167R$ [34]. The expressions (79) and (80) can be compared with the exact results (47) and (48).

We define a density scale, a pressure scale, an energy scale and a dynamical time scale by

$$\rho_0 = \frac{\sigma\nu}{(6\pi\zeta)^2} \frac{Gm^4}{a_s^2\hbar^2} = 0.209 \rho_a, \quad (81)$$

$$P_0 = \frac{2\pi\sigma^2\nu^2}{(6\pi\zeta)^4} \frac{G^2m^5}{|a_s|^3\hbar^2} = 0.274 P_a, \quad (82)$$

$$V_0 = \frac{\sigma^2\nu^{1/2}}{(6\pi\zeta)^{3/2}} \frac{\hbar m^{1/2}G^{1/2}}{|a_s|^{3/2}} = 0.271 E_a, \quad (83)$$

$$t_D = \frac{6\pi\zeta}{\nu} \left(\frac{\alpha}{\sigma} \right)^{1/2} \frac{|a_s|\hbar}{Gm^2} = 4.24 t_a, \quad (84)$$

where the scales ρ_a , P_a , E_a and t_a are defined in Appendix A 1. We note the identities

$$M_{\max} = \frac{\sigma}{\nu} \frac{\hbar^2}{Gm^2 R_*}, \quad \rho_0 = \frac{M_{\max}}{R_*^3}, \quad (85)$$

$$V_0 = \nu \frac{GM_{\max}^2}{R_*}, \quad t_D = \left(\frac{\alpha}{\nu} \right)^{1/2} \frac{1}{\sqrt{G\rho_0}} \quad (86)$$

Considering QCD axions with $m = 10^{-4} \text{ eV}/c^2$ and $a_s = -5.8 \times 10^{-53} \text{ m}$, we obtain $M_{\max} = 6.92 \times 10^{-14} M_\odot = 1.37 \times 10^{17} \text{ kg} = 2.31 \times 10^{-8} M_\oplus$, $N_{\max} = 7.72 \times 10^{56}$, $R_* = 1.03 \times 10^{-4} R_\odot = 71.5 \text{ km} = 1.12 \times 10^{-2} R_\oplus$, $\rho_0 = 3.76 \times 10^5 \text{ g/m}^3$, $V_0 = 7.06 \times 10^{25} \text{ ergs}$, and $t_D = 1.22 \times 10^4 \text{ s} = 3.40 \text{ hrs}$.

Considering ultralight axions (ULAs) with $m = 2.19 \times 10^{-22} \text{ eV}/c^2$ and $a_s = -1.11 \times 10^{-62} \text{ fm}$, we obtain $M_{\max} = 1.07 \times 10^8 M_\odot$, $N_{\max} = 5.45 \times 10^{95}$, $R_* = 0.313 \text{ kpc}$, $\rho_0 = 2.36 \times 10^{-16} \text{ g/m}^3$, $V_0 = 1.25 \times 10^{54} \text{ ergs}$, and $t_D = 4.88 \times 10^{14} \text{ s} = 15.5 \text{ Myrs}$.

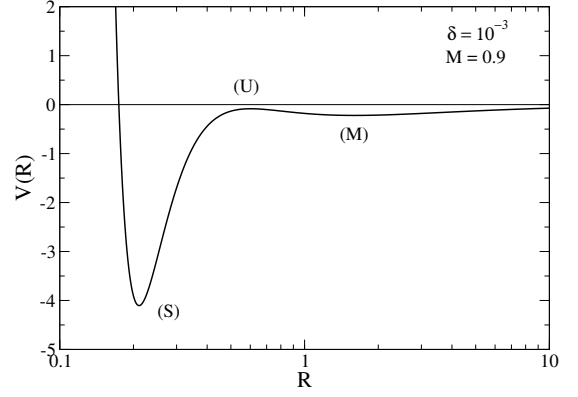


FIG. 3: Effective potential $V(R)$ as a function of the radius R for $\delta = 10^{-3}$ and $M = 0.9 < M_{\max} = 1$. It presents a local minimum (M) corresponding to a metastable dilute axion star, a global minimum (S) corresponding to a fully stable dense axion star, and a local maximum (U) corresponding to an unstable axion star.

C. Dimensionless variables

We introduce the dimensionless variables

$$\hat{M} = \frac{M}{M_{\max}}, \quad \hat{R} = \frac{R}{R_*}, \quad \hat{\rho} = \frac{\rho}{\rho_0}, \quad (87)$$

$$\hat{P} = \frac{P}{P_0}, \quad \hat{V} = \frac{V}{V_0}, \quad \hat{t} = \frac{t}{t_D}, \quad \hat{\omega} = \omega t_D. \quad (88)$$

We shall work with these dimensionless variables but, from now on, we forget the “hats” in order to simplify the notations.

With these dimensionless variables, the average density and the total energy write

$$\rho = \frac{3M}{4\pi R^3} \quad (89)$$

and

$$E_{\text{tot}} = \frac{1}{2} M \left(\frac{dR}{dt} \right)^2 + V(R). \quad (90)$$

The effective potential is given by

$$V(R) = \frac{M}{R^2} - \frac{M^2}{R} - \frac{M^2}{3R^3} + \delta \frac{M^3}{R^6}, \quad (91)$$

where

$$\delta = \frac{16\pi\nu\sigma}{27(6\pi\zeta)^2} \frac{Gm}{|a_s|c^2} = 0.389 \frac{Gm}{|a_s|c^2} \quad (92)$$

is a dimensionless interaction parameter. For illustration, the effective potential $V(R)$ is plotted in Fig. 3 for $\delta = 10^{-3}$ and $M = 0.9$. The dynamical equation satisfied by the radius of the BEC is

$$M \frac{d^2 R}{dt^2} = -V'(R). \quad (93)$$

Remark: In terms of the dimensionless variables, the general equation of state (40) writes

$$P = \frac{4}{729\delta^2} f(\sqrt{108\delta\rho}) \quad (94)$$

and the simplified equation of state (45) writes

$$P = -\rho^2 + 6\delta\rho^3. \quad (95)$$

D. The interaction parameter δ

Using Eq. (72), we can write the interaction parameter δ as

$$\delta = \frac{16\pi\nu\sigma}{27(6\pi\zeta)^2} \frac{r_S}{2|a_s|} = 0.194 \frac{r_S}{|a_s|}, \quad (96)$$

$$\delta = \frac{16\pi\nu\sigma}{27(6\pi\zeta)^2} 32\pi \left(\frac{f}{M_P c^2} \right)^2 = 39.1 \left(\frac{f}{M_P c^2} \right)^2, \quad (97)$$

$$\delta = \frac{16\pi\nu\sigma}{27(6\pi\zeta)^2} \frac{8\pi}{|\lambda|} \left(\frac{m}{M_P} \right)^2 = 9.77 \frac{1}{|\lambda|} \left(\frac{m}{M_P} \right)^2. \quad (98)$$

From the discussion of Sec. IV E, we note that the validity of the Newtonian treatment at the critical point expressed by the condition (70) can be written as

$$\delta \ll 1. \quad (99)$$

Considering QCD axions with $m = 10^{-4} \text{ eV}/c^2$ and $a_s = -5.8 \times 10^{-53} \text{ m}$, we obtain $\delta = 8.88 \times 10^{-16}$.

Considering ultralight axions (ULAs) with $m = 2.19 \times 10^{-22} \text{ eV}/c^2$ and $a_s = -1.11 \times 10^{-62} \text{ fm}$, we obtain $\delta = 1.02 \times 10^{-8}$.

These numerical applications confirm that the Newtonian approach is valid for axion stars made of QCD axions and ULAs, except if the mass M is large.

E. The mass-radius relation

A stable equilibrium state corresponds to a minimum of the effective potential $V(R)$. Its first derivative is

$$V'(R) = -\frac{2M}{R^3} + \frac{M^2}{R^2} + \frac{M^2}{R^4} - 6\delta \frac{M^3}{R^7}. \quad (100)$$

The condition $V'(R) = 0$ leads to the mass-radius relation

$$-\frac{2M}{R^3} + \frac{M^2}{R^2} + \frac{M^2}{R^4} - 6\delta \frac{M^3}{R^7} = 0, \quad (101)$$

which can be rewritten as

$$6\delta M^2 - R^3(1 + R^2)M + 2R^4 = 0. \quad (102)$$

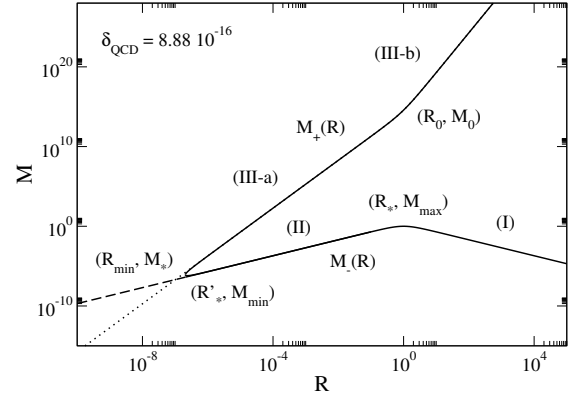


FIG. 4: Mass-radius relationship of QCD axion stars ($\delta = 8.88 \times 10^{-16}$). The dashed line corresponds to the mass-radius relation of dilute axion stars with $\delta = 0$ [34]. The dotted line corresponds to the TF approximation of dense axion stars (see Sec. VI).

This is a second degree equation whose solutions are

$$M = \frac{R^3(1 + R^2) \pm \sqrt{R^6(1 + R^2)^2 - 48\delta R^4}}{12\delta}. \quad (103)$$

The mass-radius relation $M(R)$ has two branches (+) and (-) determined by the sign in front of the square root.

In the general case, the equilibrium state results from the balance between the gravitational attraction, the repulsion due to the quantum potential arising from the Heisenberg uncertainty principle, the attractive self-interaction and the repulsive self-interaction. All these contributions are present in the mass-radius relation (103).

The mass-radius relation (103) is plotted in Fig. 4 for $\delta = 8.88 \times 10^{-16}$ corresponding to QCD axions. We have also plotted the mass-density relation in Fig. 5, where ρ represents the average density defined by Eq. (89). These curves present different critical points that will be studied specifically in the following sections. There is a local maximum mass $M_{\max}(\delta)$ at a radius $R_*(\delta)$ and a local minimum mass $M_{\min}(\delta)$ at a radius $R'_*(\delta)$. There is also a minimum radius $R_{\min}(\delta)$ corresponding to a mass $M_*(\delta)$.

The mass-radius relation $M(R)$ defines a series of equilibria (see Appendix D). There can be several solutions with the same mass M . A stable equilibrium state must be a minimum of $V(R)$ so it must satisfy $V''(R) > 0$. Computing the second derivative of $V(R)$ from Eq. (91), we get

$$V''(R) = \frac{6M}{R^4} - \frac{2M^2}{R^3} - \frac{4M^2}{R^5} + 42\delta \frac{M^3}{R^8}. \quad (104)$$

We can distinguish three branches in the curve $R(M)$ delimited by the maximum mass $M_{\max}(\delta)$ and the minimum mass $M_{\min}(\delta)$. As will be shown below (see Secs. VII D and IX), the branch (I) corresponds to stable dilute axion stars, the branch (III) corresponds to stable

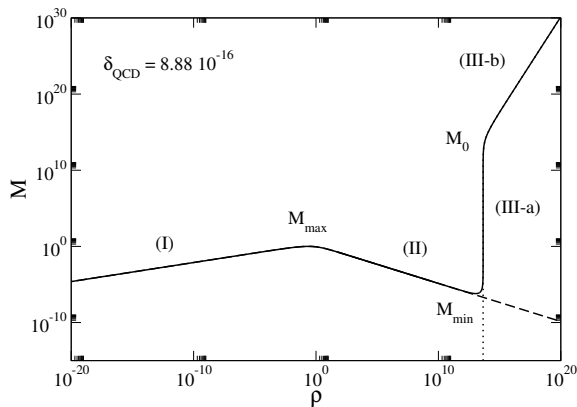


FIG. 5: Mass-density relationship of QCD axion stars ($\delta = 8.88 \times 10^{-16}$).

dense axion stars, and the intermediate branch (II) corresponds to unstable axion stars. The change of stability in the series of equilibria takes place at the maximum and minimum masses $M_{\max}(\delta)$ and $M_{\min}(\delta)$ in agreement with the Poincaré theory of linear series of equilibria [143], the $M(R)$ theorem of Wheeler introduced in the physics of compact objects (white dwarfs and neutron stars) [144], and the catastrophe (or bifurcation) theory [145] (see Appendix D).¹³

Remark: In the nongravitational limit, corresponding to $R \ll 1$, the mass-radius relation (103) can be simplified by neglecting R^2 in front of 1. This approximation describes the branches (II) and (III-a) for $\delta \ll 1$. However, since this approximation does not significantly simplify the equations, we shall not consider this limit specifically.

F. The mass-radius relation of dilute axion stars

When $\delta = 0$, we recover the mass-radius relation of dilute axion stars [34]:

$$M = \frac{2R}{1+R^2} \quad \text{or} \quad R = \frac{1 \pm \sqrt{1-M^2}}{M}. \quad (105)$$

This relation also provides a good approximation of the branches (I) and (II) of the general mass-radius relation (103) for $\delta \ll 1$ (the approximation being better and better as $\delta \rightarrow 0$).¹⁴ This amounts to neglecting the self-repulsion (nonrepulsive limit). The relation (105)

describes the equilibrium between the self-gravity, the quantum potential, and the attractive self-interaction. This curve exhibits a maximum mass $M_{\max} = 1$ at $R_* = 1$ with a maximum average density $\rho_{\max} = 3/4\pi$.

For $R \gg 1$, we obtain

$$M \sim \frac{2}{R}. \quad (106)$$

This is also the asymptotic behavior of the general mass-radius relation (103) for $R \rightarrow +\infty$ and $M \rightarrow 0$. In that limit, the self-interaction is negligible and Eq. (106) describes a stable equilibrium between the self-gravity and the quantum potential. This corresponds to the noninteracting limit. The density is given by $\rho \sim 3/2\pi R^4$ so the mass-density relation is $M \sim 2(2\pi/3)^{1/4} \rho^{1/4}$. Since $\rho \rightarrow 0$ for $R \rightarrow +\infty$, this branch corresponds to dilute axion stars. Coming back to dimensional variables, we get

$$M = \frac{2\sigma}{\nu} \frac{\hbar^2}{GRm^2} = 3.76 \frac{\hbar^2}{GRm^2}. \quad (107)$$

This relation can be compared with the exact result (51).

For $R \ll 1$, we obtain

$$M \sim 2R. \quad (108)$$

In that limit, the self-gravity is negligible and Eq. (108) describes an unstable equilibrium between the quantum potential and the attractive self-interaction. This corresponds to the nongravitational limit. The density is given by $\rho \sim 3/(2\pi R^2)$ so the mass-density relation is $M \sim 2(3/2\pi\rho)^{1/2}$. Since $\rho \rightarrow +\infty$ for $R \rightarrow 0$, this branch corresponds to unstable dense axion stars. Coming back to dimensional variables, we get

$$M = \frac{2\sigma}{6\pi\zeta} \frac{mR}{|a_s|} = 1.25 \frac{mR}{|a_s|}. \quad (109)$$

This relation can be compared with the exact result (52).

G. The minimum radius

Equilibrium states only exist above a minimum radius $R_{\min}(\delta)$ where the branches (+) and (-) merge. The minimum radius $R_{\min}(\delta)$, corresponding to the vanishing of the discriminant of Eq. (102), is determined by the equation

$$\delta = \frac{R_{\min}^2}{48} (1 + R_{\min}^2)^2. \quad (110)$$

¹³ To be complete, we also quote the necessary Vakhitov-Kolokolov condition of stability $dM/d\rho > 0$ [122, 146] mentioned in [110]. Applied to the mass-density relationship of Fig. 5 this criterion indicates that the branch (II) is unstable.

¹⁴ More precisely, when $\delta \rightarrow 0$, the branches (I) and (II) tend towards the mass-radius relation of dilute axion stars ($\delta = 0$) while the branch (III-a) is pushed towards the vertical axis $R = 0$ and

the branch (III-b) is rejected at infinity. Therefore, the general mass-radius relation (103) tends towards the mass-radius relation of dilute axion stars (105) except for small radii (see Appendix C for a more detailed description of the differences between the limit $\delta \rightarrow 0$ and the nonrepulsive case $\delta = 0$).

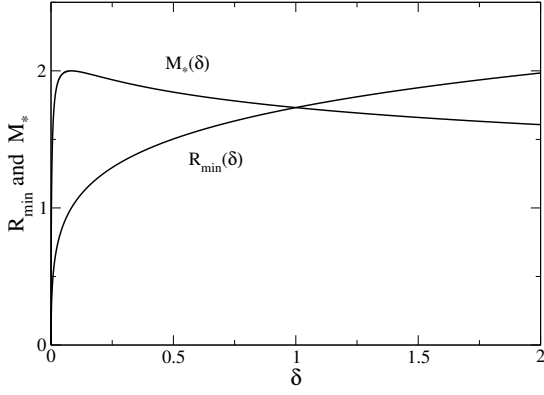


FIG. 6: The minimum radius $R_{\min}(\delta)$ and the corresponding mass $M_*(\delta)$ as a function of δ . We note, parenthetically, that these curves cross each other at $\delta = 1$ (at that point $R_{\min} = M_* = \sqrt{3}$).

This is a third degree equation whose physical solution is

$$R_{\min} = \frac{1}{18^{1/3}} \left(9\sqrt{48\delta} + \sqrt{12 + 3888\delta} \right)^{1/3} - \left(\frac{2}{3} \right)^{1/3} \left(9\sqrt{48\delta} + \sqrt{12 + 3888\delta} \right)^{-1/3}. \quad (111)$$

The mass $M_*(\delta)$ at the minimum radius is determined by the equation

$$M_* = \frac{4R_{\min}}{1 + R_{\min}^2}, \quad (112)$$

obtained by substituting for δ from Eq. (110) into Eq. (103). For $\delta \rightarrow 0$:

$$R_{\min} \sim 4\sqrt{3\delta}, \quad M_* \sim 16\sqrt{3\delta}, \quad M_* \sim 4R_{\min}. \quad (113)$$

For $\delta \rightarrow +\infty$:

$$R_{\min} \sim 2^{2/3}(3\delta)^{1/6}, \quad M_* \sim \frac{2^{4/3}}{(3\delta)^{1/6}}, \quad M_* \sim \frac{4}{R_{\min}}. \quad (114)$$

The functions $R_{\min}(\delta)$ and $M_*(\delta)$ are plotted in Fig. 6. The mass $M_*(\delta)$ reaches a maximum $M_* = 2$ at $\delta = \delta_0 = 1/12 = 0.083333\dots$. At that point, $R_{\min} = 1$. The function $M_*(R_{\min})$ given by Eq. (112) is plotted in Fig. 7.

Coming back to dimensional variables, we get for $|a_s| \gg r_S$:

$$R_{\min} \sim 16\sqrt{3} \left(\frac{\pi}{27} \right)^{1/2} \left(\frac{\sigma}{6\pi\zeta} \right)^{1/2} \frac{\hbar}{mc} \sim 7.48 R_i, \quad (115)$$

$$M_* \sim 64\sqrt{3} \left(\frac{\pi}{27} \right)^{1/2} \left(\frac{\sigma}{6\pi\zeta} \right)^{3/2} \frac{\hbar}{|a_s|c} \sim 18.7 M_i, \quad (116)$$

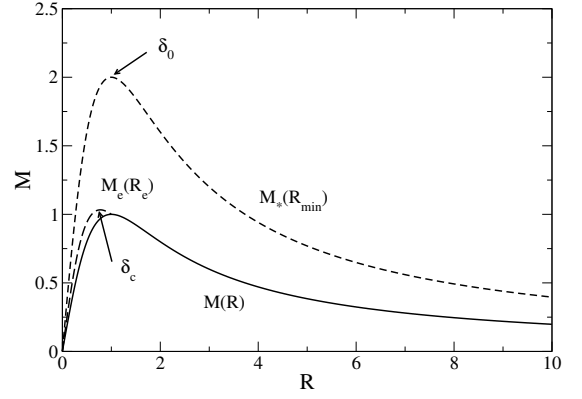


FIG. 7: The curve $M_*(R_{\min})$ (short-dashed) and the curve $M_e(R_e)$ (long-dashed). For comparison, we have also plotted the mass-radius relation (105) of dilute axion stars with $\delta = 0$ in full lines.

$$\rho \sim \frac{27}{256\pi^2} \frac{m^3 c^2}{|a_s| \hbar^2} \sim 1.07 \times 10^{-2} \rho_i, \quad (117)$$

where the scales M_i , R_i and ρ_i are defined in Appendix A 2. We note that the gravitational constant G does not appear in these scales since they are obtained in the nongravitational limit $R \ll 1$ (see the Remark at the end of Sec. V E).

For QCD axions with $\delta = 8.88 \times 10^{-16}$, we obtain $R_{\min} = 2.06 \times 10^{-7}$, $M_* = 8.26 \times 10^{-7}$, and $\rho \sim 1/(16\pi\delta) = 2.26 \times 10^{13}$ (in terms of dimensional variables, this corresponds to $R_{\min} = 1.47$ cm, $M_* = 5.72 \times 10^{-20} M_\odot$, and $\rho = 8.48 \times 10^{18}$ g/m³).

For ULAs with $\delta = 1.02 \times 10^{-8}$, we obtain $R_{\min} = 7.00 \times 10^{-4}$, $M_* = 2.80 \times 10^{-3}$, and $\rho \sim 1/(16\pi\delta) = 1.95 \times 10^6$ (in terms of dimensional variables, this corresponds to $R_{\min} = 0.219$ pc, $M_* = 3.00 \times 10^5 M_\odot$, and $\rho = 4.60 \times 10^{-10}$ g/m³).

H. The maximum and minimum masses

The maximum mass $M_{\max}(\delta)$ corresponding to the radius $R_*(\delta)$ and the minimum mass $M_{\min}(\delta)$ corresponding to the radius $R'_*(\delta)$ are located on the branch $(-)$. They are determined by the condition $M'(R_e) = 0$. Taking the derivative of Eq. (103) with respect to R , and setting it equal to zero, we obtain after simplification the equation

$$\delta = \frac{R_e^2}{192} (3 + 2R_e^2 - 5R_e^4). \quad (118)$$

This equation determines $R_*(\delta)$ and $R'_*(\delta)$. Substituting for δ from Eq. (118) into Eq. (103) we obtain after some algebra

$$M_e = \frac{8R_e}{3 + 5R_e^2}. \quad (119)$$

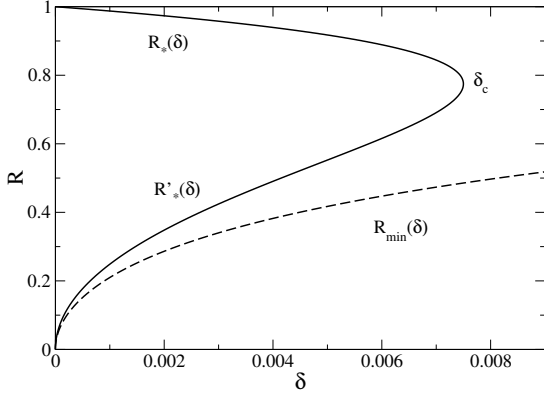


FIG. 8: The radius $R_*(\delta)$ corresponding to the maximum mass $M_{\max}(\delta)$ and the radius $R'_*(\delta)$ corresponding to the minimum mass $M_{\min}(\delta)$ as a function of δ . They coincide at the critical point δ_c (see Sec. VI). We have also plotted the minimum radius $R_{\min}(\delta)$ for comparison.

This equation can be obtained more rapidly by differentiating Eq. (102) and setting $dM = 0$. Equation (119) determines $M_{\max}(R_*)$ and $M_{\min}(R'_*)$. Equations (118) and (119) determine $M_{\max}(\delta)$ and $M_{\min}(\delta)$ in parametric form with parameter R_e .

For $\delta \rightarrow 0$:

$$R'_* \sim 8\sqrt{\delta}, \quad M_{\min} \sim \frac{64}{3}\sqrt{\delta}, \quad M_{\min} \sim \frac{8}{3}R'_*, \quad (120)$$

$$R_* \simeq 1 - 12\delta, \quad M_{\max} \simeq 1 + 3\delta. \quad (121)$$

The functions $R_*(\delta)$ and $R'_*(\delta)$ are plotted in Fig. 8. The functions $M_{\max}(\delta)$ and $M_{\min}(\delta)$ are plotted in Fig. 9. The functions $M_{\max}(R_*)$ and $M_{\min}(R'_*)$, corresponding to the right and left branches of the curve $M_e(R_e)$ defined by Eq. (119), are plotted in Fig. 7.

Coming back to dimensional variables, we get for $|a_s| \gg r_S$:

$$M_{\min} \sim \frac{256}{3} \left(\frac{\pi}{27}\right)^{1/2} \left(\frac{\sigma}{6\pi\zeta}\right)^{3/2} \frac{\hbar}{|a_s|c} \sim 14.4M_i, \quad (122)$$

$$R'_* \sim 32 \left(\frac{\pi}{27}\right)^{1/2} \left(\frac{\sigma}{6\pi\zeta}\right)^{1/2} \frac{\hbar}{mc} \sim 8.64 R_i, \quad (123)$$

$$\rho \sim \frac{27}{512\pi^2} \frac{m^3 c^2}{|a_s| \hbar^2} \sim 5.34 \times 10^{-3} \rho_i. \quad (124)$$

For QCD axions with $\delta = 8.88 \times 10^{-16}$, we obtain $R_* = 1$, $M_{\max} = 1$, $\rho = 3/(4\pi) = 0.239$, $R'_* = 2.38 \times 10^{-7}$, $M_{\min} = 6.36 \times 10^{-7}$ and $\rho \sim 1/(32\pi\delta) = 1.12 \times 10^{13}$ (in terms of dimensional variables, this corresponds to $R_* = 71.5$ km, $M_{\max} = 6.92 \times 10^{-14} M_\odot$, $\rho = 8.98 \times 10^4$ g/m³, $R'_* = 1.70$ cm, $M_{\min} = 4.40 \times 10^{-20} M_\odot$ and $\rho = 4.21 \times 10^{18}$ g/m³).

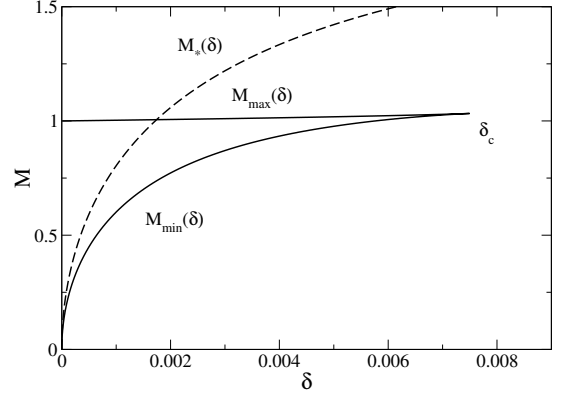


FIG. 9: The maximum mass $M_{\max}(\delta)$ and the minimum mass $M_{\min}(\delta)$ as a function of δ . They coincide at the critical point δ_c (see Sec. VI). We have also plotted the mass $M_*(\delta)$ corresponding to the minimum radius for comparison (we note, parenthetically, that $M_* = M_{\max}$ for $\delta = 1.74 \times 10^{-3}$ and $M = 1.005$). Since the functions $\delta(R_e)$ and $M(R_e)$ are maximum at the critical point (see Sec. VI) the curve $M_e(\delta)$ presents a spike at $\delta = \delta_c$.

For ULAs with $\delta = 1.02 \times 10^{-8}$, we obtain $R_* = 1$, $M_{\max} = 1$, $\rho = 3/(4\pi) = 0.239$, $R'_* = 8.08 \times 10^{-4}$, $M_{\min} = 2.15 \times 10^{-3}$ and $\rho \sim 1/(32\pi\delta) = 9.75 \times 10^5$ (in terms of dimensional variables, this corresponds to $R_* = 0.313$ kpc, $M_{\max} = 1.07 \times 10^8 M_\odot$, $\rho = 5.63 \times 10^{-17}$ g/m³, $R'_* = 0.253$ pc, $M_{\min} = 2.30 \times 10^5 M_\odot$ and $\rho = 2.30 \times 10^{-10}$ g/m³).

Remark: The exact result of Braaten *et al.* [103] for the radius of the dense axion star with the minimum mass is $R'_* = 9.2(\hbar/mc)$, which is very close to our estimate $R'_* = 8.64(\hbar/mc)$ from Eq. (123). Other comparisons between our approximate results and the exact results of Braaten *et al.* [103] are made in the caption of Fig. 34.

I. The critical point

There is a critical point when the maximum mass and the minimum mass coincide. This corresponds to the maximum of the function $M_e(R_e)$ or, equivalently, to the maximum of the function $\delta(R_e)$. We find

$$\delta_c = \frac{3}{400} = 0.0075. \quad (125)$$

For this critical value of δ , the mass-radius relation $M(R)$ presents an inflexion point at

$$R_c = \sqrt{\frac{3}{5}} = 0.774597\dots \quad M_c = \frac{4}{\sqrt{15}} = 1.0327955\dots \quad (126)$$

We also have

$$(R_{\min})_c = 0.485537\dots, \quad (M_*)_c = 1.57164\dots \quad (127)$$

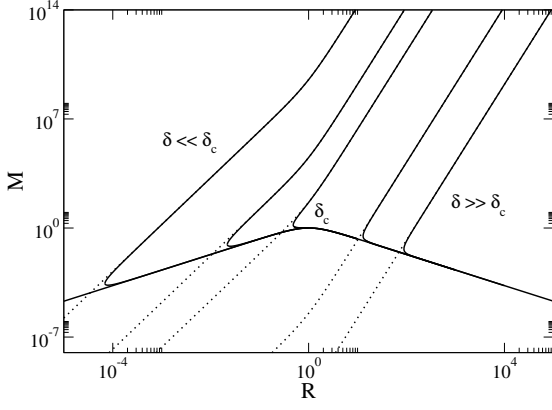


FIG. 10: Mass-radius relationship for different values of the interaction parameter ($\delta = 10^{-10}, 10^{-5}, \delta_c, 10^5, 10^{10}$).

The mass-radius relation is plotted in Fig. 10 for different values of δ including the critical value δ_c . The curve $R(M)$ is multivalued for $\delta < \delta_c$ and univalued for $\delta > \delta_c$.

Using Eqs. (96)-(98), this critical point corresponds to

$$|a_s|_c = \frac{3200\pi\nu\sigma}{81(6\pi\zeta)^2} r_S = 25.9 r_S, \quad (128)$$

$$f_c = \frac{9(6\pi\zeta)}{320\pi\sqrt{2\nu\sigma}} M_P c^2 = 1.38 \times 10^{-2} M_P c^2, \quad (129)$$

$$|\lambda|_c = \frac{51200\pi^2\nu\sigma}{81(6\pi\zeta)^2} \left(\frac{m}{M_P}\right)^2 = 1.30 \times 10^3 \left(\frac{m}{M_P}\right)^2. \quad (130)$$

We will see that a first order phase transition between dilute axion stars and dense axion stars occurs for $\delta < \delta_c$. This condition can be written as $|a_s| > |a_s|_c$, $f < f_c$, or $|\lambda| > |\lambda|_c$. We will comment on the typical values of $|a_s|_c$, f_c and $|\lambda|_c$ in Sec. X where we take general relativity into account and introduce similar quantities $|a_s|_*$, f_* and $|\lambda|_*$ separating the strongly self-interacting regime from the weakly self-interacting regime.

VI. THE TF APPROXIMATION FOR DENSE AXION STARS

In the TF approximation where the quantum potential energy (first term in Eq. (91)) can be neglected, the mass-radius relation reduces to

$$M = \frac{R^3(1 + R^2)}{6\delta}. \quad (131)$$

The curve $M(R)$ is monotonically increasing. It is plotted in dotted line in Figs. 4 and 10. This curve almost coincides with the branch (III) of stable dense axion stars. Therefore, dense axion stars are very well-described by the TF approximation. It is only close to the minimum mass M_{\min} that the effect of the quantum potential is important. Two regimes can be evidenced.

A. Nongravitational limit

For $R \ll 1$, we obtain

$$M \sim \frac{R^3}{6\delta}. \quad (132)$$

In that limit, self-gravity is negligible and Eq. (132) describes the equilibrium between the attractive self-interaction and the repulsive self-interaction (see Appendix E). This corresponds to the nongravitational limit defining the branch (III-a) in Fig. 4. In that limit, the axion stars all have the same density (independent of M or R) given by

$$\rho_{\text{dense}} = \frac{1}{8\pi\delta}. \quad (133)$$

The constancy of the density is clearly visible in Fig. 5. Since $\rho \gg 1$ for $\delta \ll 1$, the axion stars on the branch (III-a) are dense. Coming back to dimensional variables, we get

$$M \sim \frac{9}{32\pi} \frac{m^3 c^2}{|a_s| \hbar^2} R^3 = 8.95 \times 10^{-2} \frac{m^3 c^2}{|a_s| \hbar^2} R^3 \quad (134)$$

and

$$\rho_{\text{dense}} = \frac{27}{128\pi^2} \frac{m^3 c^2}{|a_s| \hbar^2} = 2.14 \times 10^{-2} \rho_i. \quad (135)$$

These relations can be compared with the exact results from Eqs. (E4) and (E5).

For QCD axions with $\delta = 8.88 \times 10^{-16}$, we obtain $\rho_{\text{dense}} = 4.48 \times 10^{13}$ (in terms of dimensional variables, this corresponds to $\rho_{\text{dense}} = 1.68 \times 10^{19} \text{ g/m}^3$).

For ULAs with $\delta = 1.02 \times 10^{-8}$, we obtain $\rho_{\text{dense}} = 3.90 \times 10^6$ (in terms of dimensional variables, this corresponds to $\rho_{\text{dense}} = 9.21 \times 10^{-10} \text{ g/m}^3$).

Remark: If we consider the intersection between the nongravitational limit of dilute axion stars ($M \sim 2R$ for $R \ll 1$) and the nongravitational limit of dense axion stars ($M \sim R^3/6\delta$ for $R \ll 1$), we obtain a point with radius $R \sim (12\delta)^{1/2}$ and mass $M \sim 2(12\delta)^{1/2}$ whose scaling with δ agrees with (R_{\min}, M_*) and (R'_*, M_{\min}) for $\delta \rightarrow 0$.

B. Nonattractive limit

For $R \gg 1$, we obtain

$$M \sim \frac{R^5}{6\delta}. \quad (136)$$

This is also the asymptotic behavior of the general mass-radius relation (103) for $R \rightarrow +\infty$ and $M \rightarrow +\infty$. In that limit, the attractive self-interaction is negligible and Eq. (136) describes the equilibrium between the self-gravity and the repulsive self-interaction. This corresponds to the nonattractive limit defining the branch

(III-b) in Fig. 4. In that limit, the axion stars are equivalent to polytropes of index $n = 1/2$ (see Appendix F). The density is given by $\rho \sim R^2/8\pi\delta$ so the mass-density relation is $M \sim (1/6\delta)(8\pi\delta\rho)^{5/2}$. Since $\rho \gg 1$ for $\delta \ll 1$ and/or $R \gg 1$, the axion stars on the branch (III-b) are dense. Coming back to dimensional variables, we get

$$M \sim \frac{9}{32\pi} \frac{\nu}{6\pi\zeta} \frac{Gm^6c^2}{a_s^2\hbar^4} R^5 = 2.98 \times 10^{-2} \frac{Gm^6c^2}{a_s^2\hbar^4} R^5. \quad (137)$$

This relation can be compared with the exact result (F3) for a polytrope $n = 1/2$.

Remark: If we consider the intersection between the noninteracting limit of dilute axion stars ($M \sim 2/R$ for $R \gg 1$) and the nonattractive limit of dense axion stars ($M \sim R^5/6\delta$ for $R \gg 1$), we obtain a point with radius $R \sim (12\delta)^{1/6}$ and mass $M \sim 2/(12\delta)^{1/6}$ whose scaling with δ agrees with (R_{\min}, M_*) for $\delta \rightarrow +\infty$.

C. Transition between the nongravitational and nonattractive TF regimes

Dense axion stars are well-described by the mass-radius relation of Eq. (131) obtained in the TF approximation. We have evidenced two regimes: a regime (III-a), corresponding to $R \ll 1$, where self-gravity is negligible [see Eq. (132)] and a regime (III-b), corresponding to $R \gg 1$, where the attractive self-interaction is negligible [see Eq. (136)]. Qualitatively, the transition between these two regimes occurs at

$$R_0 = 1, \quad M_0 = \frac{1}{6\delta}. \quad (138)$$

Coming back to dimensional variables, we get

$$R_0 = \left(\frac{6\pi\zeta}{\nu} \right)^{1/2} \left(\frac{|a_s|\hbar^2}{Gm^3} \right)^{1/2} = 1.73R_r = R_*, \quad (139)$$

$$M_0 = \frac{9}{32\pi} \left(\frac{6\pi\zeta}{\nu} \right)^{3/2} \left(\frac{|a_s|\hbar^2c^4}{G^3m^3} \right)^{1/2} = 0.465M_r, \quad (140)$$

where the scales R_r and M_r are defined in Appendix A 6. These relations can be compared with the exact results from Eqs. (G1) and (G2).

The regime (III-a) exists provided that $R_0 > R_{\min}$, implying $\delta < \delta_0$ with

$$\delta_0 = \frac{1}{12}. \quad (141)$$

At that point, $M_0 = M_* = 2$ (see Sec. V G). When $\delta < \delta_0$ and $M < M_0$, dense axion stars are in the regime (III-a) where self-gravity is negligible. In that case, a dense axion star of mass M has a radius

$$R \sim (6M\delta)^{1/3}. \quad (142)$$

When $\delta < \delta_0$ and $M > M_0$, or when $\delta > \delta_0$, dense axion stars are in the regime (III-b) where the attractive self-interaction is negligible. In that case, a dense axion star of mass M has a radius

$$R \sim (6M\delta)^{1/5}. \quad (143)$$

We will see in Sec. X B that the solutions (III-b) are unphysical, or at most only marginally physical, because general relativistic effects become important precisely when $M \sim M_0$. However, for mathematical completeness, we will continue to discuss these solutions in the Newtonian framework, but keep this limitation in mind.

For QCD axions with $\delta = 8.88 \times 10^{-16}$, we obtain $R_0 = 1$, $M_0 = 1.88 \times 10^{14}$ and $\rho_{\text{dense}} = 1/(8\pi\delta) = 4.48 \times 10^{13}$ (in terms of dimensional variables, this corresponds to $R_0 = 71.5$ km, $M_0 = 13.0M_\odot$, and $\rho_{\text{dense}} = 1.68 \times 10^{19}$ g/m³).

For ULAs with $\delta = 1.02 \times 10^{-8}$, we obtain $R_0 = 1$, $M_0 = 1.63 \times 10^7$ and $\rho_{\text{dense}} = 1/(8\pi\delta) = 3.90 \times 10^6$ (in terms of dimensional variables, this corresponds to $R_0 = 0.313$ kpc, $M_0 = 1.75 \times 10^{15}M_\odot$, and $\rho_{\text{dense}} = 9.21 \times 10^{-10}$ g/m³).

VII. ENERGY AND PULSATION

A. The total energy

At equilibrium ($\dot{R} = 0$), the total energy of an axion star is given by $E_{\text{tot}} = V(R)$. Therefore

$$E_{\text{tot}} = \frac{M}{R^2} - \frac{M^2}{R} - \frac{M^2}{3R^3} + \delta \frac{M^3}{R^6}. \quad (144)$$

We can obtain the functions $E_{\text{tot}}(R)$ and $E_{\text{tot}}(M)$ by combining Eqs. (103) and (144). These functions are plotted in Figs. 11 and 12.

The functions $M(R)$ and $E_{\text{tot}}(R)$ achieve their extrema at the same points.¹⁵ The local minimum energy $E_{\text{tot}}^{\min}(\delta)$ is reached at the local maximum mass point $(M_{\text{max}}(\delta), R_*(\delta))$ and the local maximum energy $E_{\text{tot}}^{\max}(\delta)$ is reached at the local minimum mass point $(M_{\text{min}}(\delta), R'_*(\delta))$. As a consequence, the function $E_{\text{tot}}(M)$ presents a spike at the local maximum and minimum masses (see Fig. 12).

For dilute axion stars with $\delta = 0$ at the critical point ($M = R = 1$), we get

$$E_{\text{tot}} = -\frac{1}{3}. \quad (145)$$

Coming back to dimensional variables, we obtain

$$E_{\text{tot}} = -\frac{1}{3} \frac{\sigma^2\nu^{1/2}}{(6\pi\zeta)^{3/2}} \frac{\hbar m^{1/2}G^{1/2}}{|a_s|^{3/2}} = -9.03 \times 10^{-2} E_a, \quad (146)$$

¹⁵ The intrinsic reason is explained in Appendix D. See also the Remark at the end of this section.

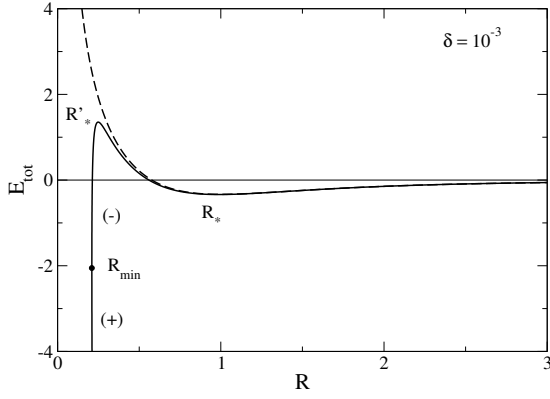


FIG. 11: Total energy E_{tot} as a function of the radius R for axion stars with $\delta = 10^{-3}$ (for illustration, we have taken a relatively large value of δ to facilitate the reading of the figure). The dashed line corresponds to dilute axion stars with $\delta = 0$.

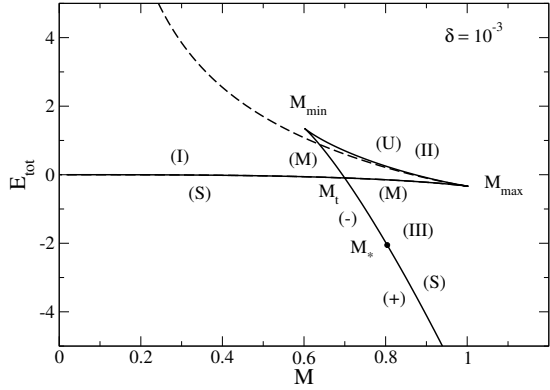


FIG. 12: Total energy E_{tot} as a function of the mass M for axion stars with $\delta = 10^{-3}$. The dashed line corresponds to dilute axion stars with $\delta = 0$.

where the scale E_a is defined in Appendix A 1. For QCD axions with $m = 10^{-4} \text{ eV}/c^2$ and $a_s = -5.8 \times 10^{-53} \text{ m}$, we get $E_{\text{tot}} = -2.35 \times 10^{25} \text{ ergs}$. For ULAs with $m = 2.19 \times 10^{-22} \text{ eV}/c^2$ and $a_s = -1.11 \times 10^{-62} \text{ fm}$, we get $E_{\text{tot}} = -4.17 \times 10^{53}$.

In the TF approximation, the first term in Eq. (144) can be neglected. Using Eq. (131), the total energy can be written as

$$E_{\text{tot}} = -\frac{R^3(1+R^2)^2}{216\delta^2}(5R^2+1). \quad (147)$$

For $R \ll 1$ (nongravitational limit):

$$E_{\text{tot}} \sim -\frac{R^3}{216\delta^2}, \quad E_{\text{tot}} \sim -\frac{M}{36\delta}. \quad (148)$$

Coming back to dimensional variables, we obtain

$$E_{\text{tot}} \sim -\frac{81\zeta}{1024\pi} \frac{m^3 c^4}{|a_s| \hbar^2} R^3 = -1.60 \times 10^{-3} \frac{m^3 c^4}{|a_s| \hbar^2} R^3, \quad (149)$$

$$E_{\text{tot}} \sim -\frac{3(6\pi\zeta)}{64\pi} M c^2 = -1.79 \times 10^{-2} M c^2. \quad (150)$$

These relations can be compared with the exact results from Eq. (E14).

For $R \gg 1$ (nonattractive limit):

$$E_{\text{tot}} \sim -\frac{5R^9}{216\delta^2}, \quad E_{\text{tot}} \sim -\frac{5M^{9/5}}{6^{6/5}\delta^{1/5}}. \quad (151)$$

This is also the asymptotic behavior of the general relations (103) and (144) for $R \rightarrow +\infty$ and $M \rightarrow +\infty$. We note that $E_{\text{tot}} \sim -(5/6)M^2/R$. Coming back to dimensional variables, we obtain

$$E_{\text{tot}} \sim -\frac{5\nu}{6} \frac{GM^2}{R} \sim -0.332 \frac{GM^2}{R}. \quad (152)$$

This relation can be compared with the exact result (F16) valid for a polytrope $n = 1/2$.

Remark: Let us recover from our approach based on the Gaussian ansatz the fact that the energy and the mass achieve their extrema at the same points. The total energy can be written as $E_{\text{tot}} = V(M(R), R)$, where $M(R)$ corresponds to the mass-radius relation (103). Therefore

$$\frac{dE_{\text{tot}}}{dR} = \frac{\partial V}{\partial M} \frac{dM}{dR} + \frac{\partial V}{\partial R}. \quad (153)$$

Since $V'(R) = 0$ for every state on the series of equilibria, there remains

$$\frac{dE_{\text{tot}}}{dR} = \frac{\partial V}{\partial M} \frac{dM}{dR}. \quad (154)$$

In general $\partial V/\partial M \neq 0$ at an equilibrium state. Therefore, $E'_{\text{tot}}(R) = 0$ if, and only if, $M'(R) = 0$.

B. The eigenenergy

For a self-gravitating BEC described by a polytropic equation of state, the quantity NE (representing N times the eigenenergy E) can be deduced from the total energy E_{tot} by multiplying the gravitational term by 2 and the internal energy by γ (see Sec. 5.2.1 of [78]). Therefore, according to Eq. (144), the eigenenergy of an axion star with the equation of state (45) which is the sum of two polytropic equations of state of index $\gamma = 2$ and $\gamma = 3$ is given by

$$NE = \frac{M}{R^2} - \frac{2M^2}{R} - \frac{2M^2}{3R^3} + 3\delta \frac{M^3}{R^6}. \quad (155)$$

We can obtain the functions $NE(R)$ and $NE(M)$ by combining Eqs. (103) and (155). These functions are plotted in Figs. 13 and 14.

For dilute axion stars with $\delta = 0$ at the critical point ($M = R = 1$), we get

$$NE = -\frac{5}{3}. \quad (156)$$

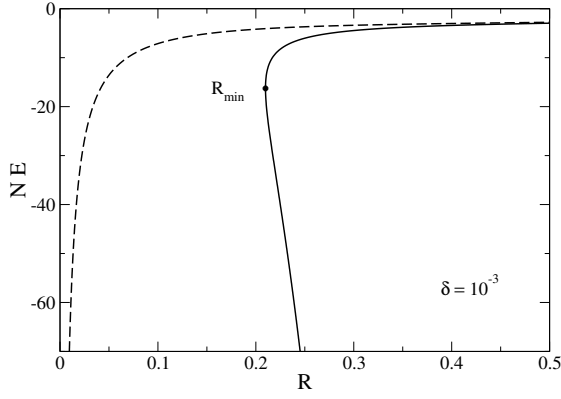


FIG. 13: Eigenenergy NE as a function of the radius R for axion stars with $\delta = 10^{-3}$. The dashed line corresponds to dilute axion stars with $\delta = 0$.

Coming back to dimensional variables, we obtain

$$NE = -\frac{5}{3} \frac{\sigma^2 \nu^{1/2}}{(6\pi\zeta)^{3/2}} \frac{\hbar m^{1/2} G^{1/2}}{|a_s|^{3/2}} = -0.452 E_a \quad (157)$$

or

$$E = -\frac{5}{3} \frac{\sigma \nu}{6\pi\zeta} \frac{Gm^2}{|a_s|} = -0.417 \frac{E_a}{N_a}. \quad (158)$$

These relations can be compared with the exact results given in [35]. We note that $|E| \ll mc^2$ for $|a_s| \gg 2Gm/c^2$ (i.e. $\delta \ll 1$) which justifies our nonrelativistic treatment. For QCD axions with $m = 10^{-4} \text{ eV}/c^2$ and $a_s = -5.8 \times 10^{-53} \text{ m}$, we get $NE = -1.175 \times 10^{26} \text{ ergs}$ and $E = -1.52 \times 10^{-31} \text{ ergs}$. For ULAs with $m = 2.19 \times 10^{-22} \text{ eV}/c^2$ and $a_s = -1.11 \times 10^{-62} \text{ fm}$, we get $NE = -2.085 \times 10^{54} \text{ ergs}$ and $E = -3.83 \times 10^{-42} \text{ ergs}$.

In the TF approximation, the first term in Eq. (155) can be neglected. Using Eq. (131), the eigenenergy can be written as

$$NE = -\frac{R^3(1+R^2)^2}{216\delta^2}(9R^2+1). \quad (159)$$

For $R \ll 1$ (nongravitational limit):

$$NE = E_{\text{tot}}. \quad (160)$$

This is an exact result independent of the Gaussian ansatz (see Appendix E).

For $R \gg 1$ (nonattractive limit):

$$NE = \frac{9}{5} E_{\text{tot}}. \quad (161)$$

This is an exact result for a polytrope $n = 1/2$ independent of the Gaussian ansatz (see Appendix F). This is also the asymptotic behavior of the general relations (103) and (155) for $R \rightarrow +\infty$ and $M \rightarrow +\infty$.

Remark: According to Eqs. (D4) and (D8), one has $E/m = dE_{\text{tot}}/dM$ or, equivalently,

$$NE = M \frac{dE_{\text{tot}}}{dM}. \quad (162)$$

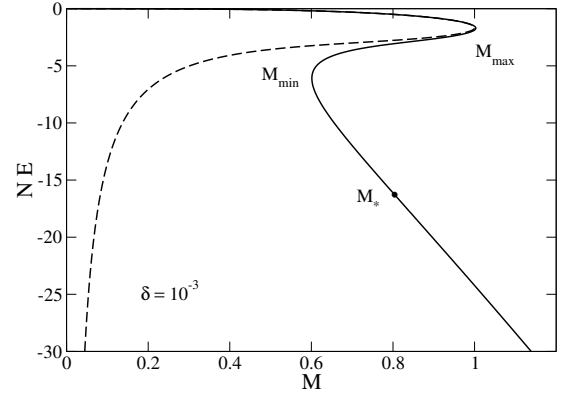


FIG. 14: Eigenenergy NE as a function of the mass M for axion stars with $\delta = 10^{-3}$. The dashed line corresponds to dilute axion stars with $\delta = 0$.

Let us check that this exact relation is satisfied by our approximate approach based on the Gaussian ansatz. The total energy can be written as $E_{\text{tot}} = V(M, R(M))$, where $R(M)$ corresponds to the mass-radius relation (103). Therefore

$$\frac{dE_{\text{tot}}}{dM} = \frac{\partial V}{\partial M} + \frac{\partial V}{\partial R} \frac{dR}{dM}. \quad (163)$$

Since $V'(R) = 0$ for every state on the series of equilibria, there remains

$$\frac{dE_{\text{tot}}}{dM} = \frac{\partial V}{\partial M}. \quad (164)$$

This relation is equivalent to Eq. (154). Therefore, we have to show that $E/m = \partial V/\partial M$ or, equivalently,

$$NE = M \frac{\partial V}{\partial M}. \quad (165)$$

Taking the partial derivative of $V(R, M)$ given by Eq. (91) with respect to M , and comparing the result with Eq. (155), we find that this relation is indeed satisfied.

C. The pulsation

The complex pulsation of an axion star slightly displaced from equilibrium is given by [34, 78]:

$$\omega^2 = \frac{V''(R)}{M}. \quad (166)$$

Using Eq. (104), we get

$$\omega^2 = \frac{6}{R^4} - \frac{2M}{R^3} - \frac{4M}{R^5} + 42\delta \frac{M^2}{R^8}. \quad (167)$$

We can obtain the functions $\omega^2(R)$ and $\omega^2(M)$ by combining Eqs. (103) and (167). These functions are plotted in Figs. 15-18. The pulsation vanishes at the critical

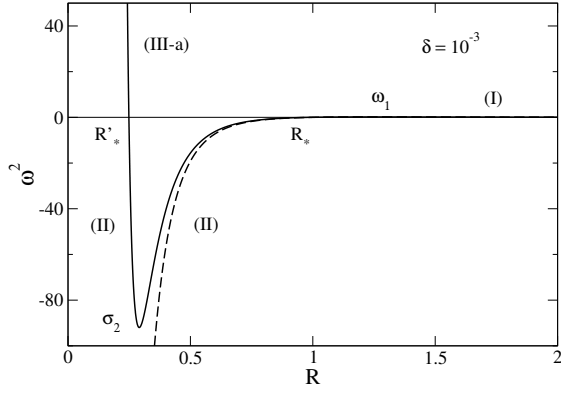


FIG. 15: Complex pulsation as a function of the radius R for axion stars with $\delta = 10^{-3}$. The dashed line corresponds to dilute axion stars with $\delta = 0$.

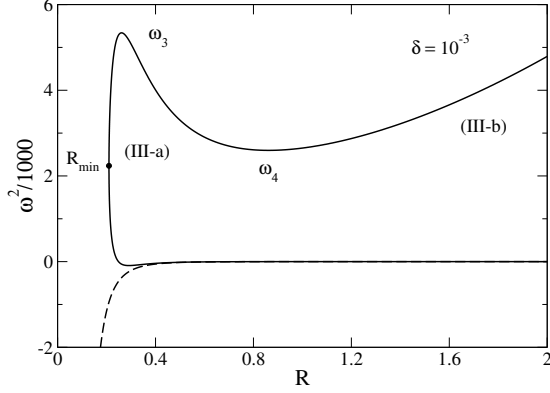


FIG. 16: Same as Fig. 15 showing the branch of dense axion stars with high pulsations (ω^2 has been divided by 1000).

points $(M_{\max}(\delta), R_*(\delta))$ and $(M_{\min}(\delta), R'_*(\delta))$ where a change of stability occurs. The stable branch of dilute axion stars (I) has a positive square pulsation $\omega^2 > 0$. The pulsation achieves a maximum value $\omega_1(\delta)$ at a point $(M_1(\delta), R_1(\delta))$. For $\delta = 0$ this point is characterized analytically in [73] (see also Appendix I). The unstable branch of axion stars (II) has a negative square pulsation $\omega^2 < 0$. The growth rate $\sigma = \sqrt{-\omega^2}$ achieves a maximum value $\sigma_2(\delta)$ at a point $(M_2(\delta), R_2(\delta))$. The stable branch of dense axion stars (III) has a positive square pulsation $\omega^2 > 0$. The pulsation achieves a maximum value $\omega_3(\delta)$ at a point $(M_3(\delta), R_3(\delta))$ and a minimum value $\omega_4(\delta)$ at a point $(M_4(\delta), R_4(\delta))$. This last point is characterized analytically below in the TF approximation.

In the TF approximation, the first term in Eq. (167) can be neglected. Using Eq. (131), the pulsation can be written as

$$\omega^2 = \frac{1 + R^2}{6\delta} \left(5 + \frac{3}{R^2} \right). \quad (168)$$

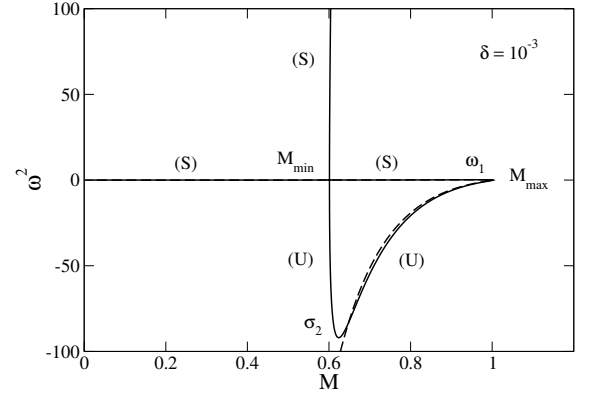


FIG. 17: Complex pulsation as a function of the mass M for axion stars with $\delta = 10^{-3}$. The dashed line corresponds to dilute axion stars with $\delta = 0$.

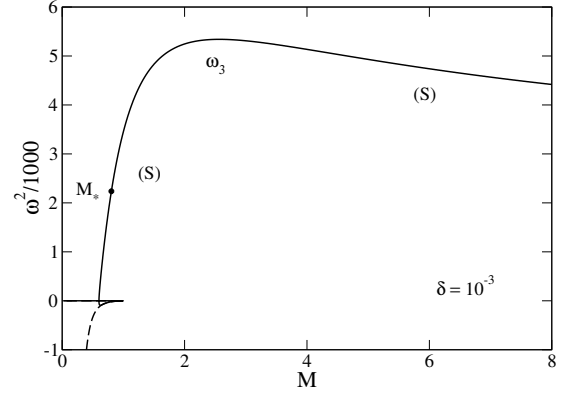


FIG. 18: Same as Fig. 17 showing the branch of dense axion stars with high pulsations (ω^2 has been divided by 1000). The minimum pulsation ω_4 corresponds to a large mass $M_4 = 202$ that is not represented on the figure.

For $R \ll 1$ (nongravitational limit):

$$\omega^2 \sim \frac{1}{2\delta R^2}, \quad \omega^2 \sim \frac{1}{2^{5/3} 3^{2/3} \delta^{5/3} M^{2/3}}. \quad (169)$$

Coming back to dimensional variables, we get

$$\omega = \left(\frac{27}{32\pi} \right)^{1/2} \left(\frac{6\pi\zeta}{\alpha} \right)^{1/2} \frac{c}{R} = 0.463 \frac{c}{R}. \quad (170)$$

This relation can be compared with the exact result (E21).

For $R \gg 1$ (nonattractive limit):

$$\omega^2 \sim \frac{5R^2}{6\delta}, \quad \omega^2 \sim \frac{5M^{2/5}}{(6\delta)^{3/5}}. \quad (171)$$

This is also the asymptotic behavior of the general relations (103) and (167) for $R \rightarrow +\infty$ and $M \rightarrow +\infty$. Using Eq. (136), we find that $\omega^2 \sim 5M/R^3$. Coming back to

dimensional variables, we obtain

$$\omega^2 \sim \frac{5\nu}{\alpha} \frac{GM}{R^3} \sim 1.33 \frac{GM}{R^3}. \quad (172)$$

This relation can be compared with the result (F18) obtained from the Ledoux formula for a polytrope $n = 1/2$.

In the TF approximation, the square pulsation ω^2 has a minimum

$$\omega_4^2 = \frac{5 + \sqrt{15}}{6\delta} \left(1 + \sqrt{\frac{3}{5}} \right) \quad (173)$$

at the point

$$R_4 = \left(\frac{3}{5} \right)^{1/4}, \quad M_4 = \frac{\left(\frac{3}{5} \right)^{3/4} \left(1 + \sqrt{\frac{3}{5}} \right)}{6\delta}. \quad (174)$$

We note that $M_4 \sim M_0$. For such a large mass, general relativity must be taken into account (see Secs. VIC and X) so our Newtonian results (173) and (174) may not be physically relevant.

Remark: We note that dilute axion stars have low pulsations while dense axion stars have very high pulsations. Numerical applications are made in Sec. VIII B for dense axion stars and in Appendix I for dilute axion stars.

D. The turning point argument

In this section, we derive a simplified version of Poincaré's turning point argument based on the Gaussian ansatz. If we differentiate the mass-radius relation (101) with respect to R and use Eq. (104), we obtain

$$V''(R) + \left(-\frac{2}{R^3} + \frac{2M}{R^2} + \frac{2M}{R^4} - 18\delta \frac{M^2}{R^7} \right) \frac{dM}{dR} = 0. \quad (175)$$

Simplifying the term in parenthesis with the aid of Eq. (101), and using Eq. (166), the foregoing equation can be rewritten as

$$\omega^2(R) = -\frac{4R - M(R^2 + 1)}{MR^4} \frac{dM}{dR}. \quad (176)$$

It relates the square of the complex pulsation ω^2 determining the stability of the system to the slope of the mass-radius relation $M(R)$.

It is better to develop the following discussion at a general level. For an arbitrary potential $V(R, M)$, the mass-radius relation $M(R)$ is given in implicit form by

$$\frac{\partial V}{\partial R}(R, M(R)) = 0. \quad (177)$$

Differentiating this relation with respect to R , and using Eq. (166), we get

$$M\omega^2 = \frac{\partial^2 V}{\partial R^2}(R, M) = -\frac{\partial^2 V}{\partial R \partial M}(R, M) \frac{dM}{dR}, \quad (178)$$

which is the generalization of Eq. (175). We first note that a turning point of mass ($M'(R) = 0$) corresponds to $\omega^2 = (1/M)\partial^2 V/\partial R^2 = 0$. On the other hand, a turning point of radius ($R'(M) = 0$ or $M'(R) = \pm\infty$) corresponds to $\partial^2 V/\partial R \partial M = 0$. A change of stability along the series of equilibria takes place when $\omega^2 = (1/M)\partial^2 V/\partial R^2$ changes sign. According to Eq. (178), this happens at a point where $M'(R)$ changes sign while $\partial^2 V/\partial R \partial M$ does not change sign. Therefore, this happens at a turning point of mass, *not* at a turning point of radius. At a turning point of mass, both dM/dR and ω^2 change sign by passing through 0 while $\partial^2 V/\partial R \partial M$ does not change sign. At a turning point of radius, dM/dR changes sign by passing through ∞ and $\partial^2 V/\partial R \partial M$ changes sign by passing through 0 while ω^2 does not change sign (it remains finite and nonzero). In conclusion, a change of stability along the series of equilibria ($\omega^2 = V''(R) = 0$) coincides with a turning point of mass ($M'(R) = 0$). This is a simplified version, for a potential $V(R, M)$, of the turning point argument obtained from Poincaré's theory of linear series of equilibria [143] (see also the $M(R)$ theorem of Wheeler [144] and the theory of catastrophes [145]). We emphasize that the stability of the system is not directly related to the sign of the slope of the mass-radius relation since there is no change of stability after a turning point of radius although the slope changes. A change of slope is a necessary (but not a sufficient) condition for a change of stability.

Coming back to our particular problem, let us explicitly check that the condition of marginal stability $\omega^2 = (1/M)V''(R) = 0$ returns Eq. (119) corresponding to $M'(R) = 0$ and that the condition $\partial^2 V/\partial R \partial M = 0$ returns Eq. (112) corresponding to $R'(M) = 0$.

According to Eq. (104), the condition $V''(R) = 0$ is equivalent to

$$\frac{6M}{R^4} - \frac{2M^2}{R^3} - \frac{4M^2}{R^5} + 42\delta \frac{M^3}{R^8} = 0. \quad (179)$$

Multiplying this equation by $R/7$ and adding the resulting expression to Eq. (101) in order to eliminate δ , we recover Eq. (119).

According to Eq. (91), we have

$$\frac{\partial^2 V}{\partial M \partial R} = -\frac{2}{R^3} + \frac{2M}{R^2} + \frac{2M}{R^4} - 18\delta \frac{M^2}{R^7}. \quad (180)$$

Multiplying Eq. (101) by $-3/M$ and adding the resulting expression to Eq. (180) in order to eliminate δ , we obtain

$$\frac{\partial^2 V}{\partial M \partial R} = \frac{4R - M(R^2 + 1)}{R^4}. \quad (181)$$

These equalities show the equivalence between Eqs. (175), (176) and (178). Furthermore, we can check that the condition $\partial^2 V/\partial R \partial M = 0$ returns Eq. (112).

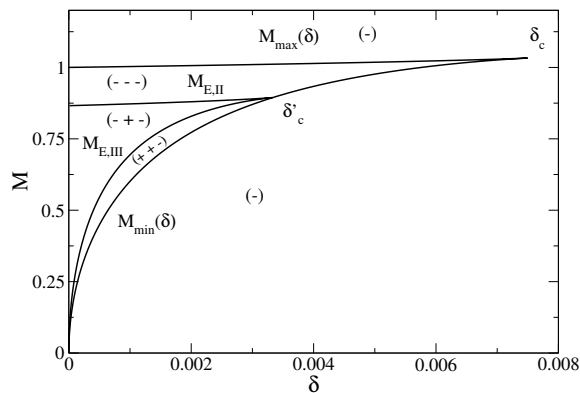


FIG. 19: The mass $M_E(\delta)$ at which the total energy vanishes as a function of δ . The upper branch $M_{E,II}(\delta)$ corresponds to unstable axion stars and the lower branch $M_{E,III}(\delta)$ corresponds to metastable dense axion stars. For comparison, we have also plotted the maximum and minimum mass. Finally, we have indicated the sign of the energy of the different equilibrium states in each domain. For example (+ + -) means that the dense stable axion star (left) has a positive energy, the unstable axion star (middle) has a positive energy and the stable dilute axion (right) star has a negative energy.

E. The sign of the total energy

We have seen that a change of stability in the series of equilibria corresponds to a turning point of mass, or equivalently, to a turning point of total energy. For future discussions (see Sec. IX D), it is useful to determine the points in the series of equilibria where the total energy vanishes. Writing $E_{\text{tot}} = 0$ in Eq. (144) and combining the resulting equation with the mass-radius relation (102), we find after simplification that the mass $M_E(\delta)$ of an equilibrium state (stable or unstable) for which $E_{\text{tot}} = 0$ is determined by the parametric equations

$$M_E = \frac{4R_E}{1 + 5R_E^2}, \quad (182)$$

$$\delta = \frac{1}{48} R_E^2 (1 + 5R_E^2) (1 - 3R_E^2), \quad (183)$$

where the parameter R_E is the radius. The function $M_E(\delta)$ is plotted in Fig. 19. It displays two branches $M_{E,II}(\delta)$ and $M_{E,III}(\delta)$ whose meaning is explained below. From Eqs. (118), (119) and (144), we find that the total energy at the point of maximum mass is always negative, going from $E_{\text{tot}} = -1/3$ at $\delta = 0$ to $E_{\text{tot}} = -(8/27)\sqrt{5/3}$ at $\delta = \delta_c$ (see Fig. 20). From Fig. 12, we conclude that the stable dilute axion stars (branch I) always have a negative energy ($E_{\text{tot}} < 0$). On the other hand, from Eqs. (118), (119), (144), (182) and (183) we find that the total energy at the point of minimum mass is positive for $\delta < \delta'_c = 1/300$ and negative for $\delta > \delta'_c$, going from $E_{\text{tot}} = +\infty$ at $\delta = 0$ to

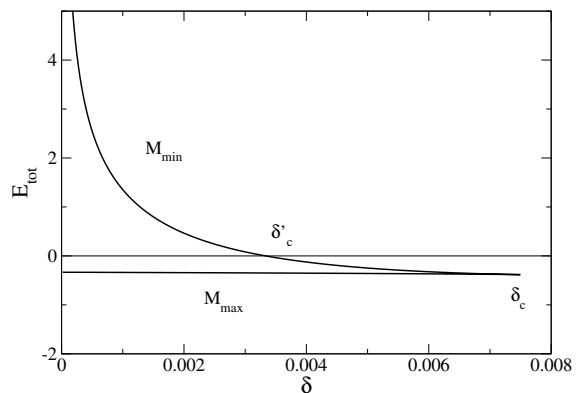


FIG. 20: Total energy at the point of maximum mass (lower branch) and at the point of minimum mass (upper branch) as a function of δ .

$E_{\text{tot}} = -(8/27)\sqrt{5/3}$ at $\delta = \delta_c$ (at the transition point $\delta'_c = 1/300$ we find $M = 2/\sqrt{5}$ and $R = 1/\sqrt{5}$). Considering Fig. 12 again, we come to the following conclusions. When $\delta < \delta'_c$, the unstable axion stars (branch II) have a positive energy for $M_{\text{min}} < M < M_{E,II}$ and a negative energy for $M_{E,II} < M < M_{\text{max}}$ while the metastable dense axion stars (branch III) have a positive energy for $M_{\text{min}} < M < M_{E,III} < M_t$ and a negative energy for $M > M_{E,III}$. When $\delta > \delta'_c$, the unstable axion stars and the stable dense axion stars have a negative energy. For $\delta \rightarrow 0$, we recover the result $(M_{E,II}, R_{E,II}) = (\sqrt{3}/2, 1/\sqrt{3})$ obtained in [73]. We also find that $M_{E,III} \sim 16\sqrt{3}\delta$ and $R_{E,III} \sim 4\sqrt{3}\delta$, so that $(R_{E,III}, M_{E,III})$ approaches the point with the minimum radius (R_{min}, M_*) . More generally, $M_{\text{min}} < M_{E,III} < M_*$ and $R_{\text{min}} < R_{E,III} < R'_*$. Using the preceding results, it is easy to determine the sign of the energy of each equilibrium state as indicated in Fig. 19.

VIII. THE RADIUS OF THE AXION STAR RESULTING FROM A COLLAPSE OR AN EXPLOSION AT A CRITICAL POINT

A. The different solutions as a function of M depending on the value of δ

We are now in a position to discuss the different equilibrium states of axion stars (characterized by their radius R) as a function of their mass M depending on the value of the interaction parameter δ . Specifically, we fix δ and determine the possible radii R as a function of M (see Fig. 10).

(i) We first assume $\delta < \delta_c$. If $M < M_{\text{min}}(\delta)$, there is only one solution: a stable dilute axion star (I). If $M_{\text{min}}(\delta) < M < M_{\text{max}}(\delta)$, there are three solutions: a stable dilute axion star (I), an unstable axion star (II), and a stable dense axion star (III). If $M > M_{\text{max}}(\delta)$, there is only one solution: a stable dense axion star (III).

(ii) We now assume $\delta > \delta_c$. In that case, there is only one solution: a stable dilute axion star (I) if $M < M_*(\delta)$ and a dense axion star (III) if $M > M_*(\delta)$.

B. Collapse when $\delta \ll 1$ and $M \sim M_{\max}^+$

Let us consider the situation where $\delta \ll 1$ and $M \sim M_{\max}(\delta)^+ \sim 1^+$. Physically, we assume that a stable axion star gains mass (for example by accreting matter around it or through its collision with another star) and passes above the critical point. In that case, the dilute axion star collapses and ultimately forms a dense axion star. Since $M_0 \gg 1$ for $\delta \ll 1$, this dense axion star is of type (III-a). We assume that there is no mass loss during the collapse.¹⁶ Using Eq. (132), the radius of the dense axion star is

$$R_{\text{coll}}(\delta) = (6\delta)^{1/3}. \quad (184)$$

We note that the scaling of $R_{\text{coll}}(\delta)$ is different from the scaling of $R_{\text{min}}(\delta)$ given by Eq. (113). Coming back to dimensional variables we get

$$R_{\text{coll}} \sim \left(\frac{96\pi\sigma}{27\nu}\right)^{1/3} \left(\frac{\nu}{6\pi\zeta}\right)^{1/6} \left(\frac{|a_s|\hbar^6}{Gm^7c^4}\right)^{1/6} = 2.30R_d, \quad (185)$$

where the scale R_d is defined in Appendix A 3. This expression can be compared with the exact result from Eq. (E22).

The density of the dense axion star resulting from gravitational collapse is $\rho_{\text{dense}} = 1/(8\pi\delta)$ [see Eq. (133)]. In comparison, the density of the dilute axion star at the point of maximum mass is $\rho_{\text{dilute}} = 3/(4\pi)$. This leads to a ratio

$$\frac{\rho_{\text{dense}}}{\rho_{\text{dilute}}} = \frac{1}{6\delta}. \quad (186)$$

For $\delta \ll 1$, the increase in density is great.

The pulsation of the dense axion star resulting from gravitational collapse is given by [see Eq. (169)]:

$$\omega_{\text{coll}}(\delta) = \frac{1}{2^{5/6}3^{1/3}\delta^{5/6}}. \quad (187)$$

¹⁶ This assumption may not be correct and will have to be revised in future works. Indeed, the collapse of a dilute axion star is generally accompanied by an emission of relativistic axions (bosonova), leaving a dense axion star as the remnant with a mass smaller than the initial one [103]. If the mass loss is not too important, our results should remain qualitatively correct. Similarly, white dwarf stars above the Chandrasekhar mass collapse and form neutron stars. Since the maximum mass of white dwarf stars $M_{\max} = 1.44 M_{\odot}$ [119] is larger than the maximum mass of ideal neutron stars $M_{\max} = 0.710 M_{\odot}$ [120], the collapse is necessarily accompanied by an ejection of mass (note, however, that in more realistic models, the maximum mass of neutron stars, being in the range $2 - 2.4 M_{\odot}$, is larger than the maximum mass of white dwarf stars).

For $\delta \ll 1$, the dense axion star has a very high pulsation. In comparison, the maximum pulsation of a dilute axion star is $\omega_{\text{max}} = 0.424$ (see Appendix I). Coming back to dimensional variables we get

$$\begin{aligned} \omega_{\text{coll}} &= \frac{(\sigma/\alpha)^{1/2}}{2^{5/6}3^{1/3}} \left(\frac{27\nu}{16\pi\sigma}\right)^{5/6} \left(\frac{6\pi\zeta}{\nu}\right)^{2/3} \left(\frac{Gm^7c^{10}}{|a_s|\hbar^6}\right)^{1/6} \\ &= 0.202 \left(\frac{Gm^7c^{10}}{|a_s|\hbar^6}\right)^{1/6}. \end{aligned} \quad (188)$$

This expression can be compared with the exact result from Eq. (E23).

The total energy of the dense axion star resulting from gravitational collapse is given by [see Eq. (148)]:

$$E_{\text{tot}}^{\text{coll}}(\delta) = -\frac{1}{36\delta}. \quad (189)$$

For $\delta \ll 1$, the dense axion star has a very negative energy. In comparison, the energy of a dilute axion star with the critical mass is $E_{\text{tot}}^{\text{dilute}} = -1/3$. Coming back to dimensional variables we get

$$\begin{aligned} E_{\text{tot}}^{\text{coll}} &= -\frac{3\sigma}{64\pi} \left(\frac{6\pi\zeta}{\nu}\right)^{1/2} \frac{\hbar c^2}{(Gm|a_s|)^{1/2}} \\ &= -1.94 \times 10^{-2} \frac{\hbar c^2}{(Gm|a_s|)^{1/2}}. \end{aligned} \quad (190)$$

We note that $E_{\text{tot}}^{\text{coll}} = -(9\zeta/32)M_{\max}c^2 = -1.79 \times 10^{-2} M_{\max}c^2$. These expressions can be compared with the exact results from Eq. (E24).

For QCD axions with $\delta = 8.88 \times 10^{-16}$, assuming $M_{\text{coll}} = M_{\max} = 1$, we get $R_{\text{coll}} = 1.75 \times 10^{-5}$, $\rho_{\text{dense}} = 4.48 \times 10^{13}$, $2\pi/\omega_{\text{coll}} = 4.62 \times 10^{-12}$ and $E_{\text{tot}}^{\text{coll}} = -3.13 \times 10^{13}$. Coming back to original variables, assuming $M_{\text{coll}} = M_{\max} = 6.92 \times 10^{-14} M_{\odot}$, we get $R_{\text{coll}} = 1.80 \times 10^{-9} R_{\odot} = 1.25$ m, $\rho_{\text{dense}} = 1.68 \times 10^{19}$ g/m³, $2\pi/\omega_{\text{coll}} = 5.65 \times 10^{-8}$ s and $E_{\text{tot}}^{\text{coll}} = -2.21 \times 10^{39}$ ergs (in comparison $R_* = 71.5$ km, $\rho_{\text{dilute}} = 8.98 \times 10^4$ g/m³, $2\pi/\omega_{\text{max}} = 50.3$ hrs, $E_{\text{tot}}^{\text{dilute}} = -2.35 \times 10^{25}$ ergs).

For ULAs with $\delta = 1.02 \times 10^{-8}$, assuming $M_{\text{coll}} = M_{\max} = 1$, we get $R_{\text{coll}} = 3.94 \times 10^{-3}$, $\rho_{\text{dense}} = 3.90 \times 10^6$, $2\pi/\omega_{\text{coll}} = 3.54 \times 10^{-6}$ and $E_{\text{tot}}^{\text{coll}} = -2.72 \times 10^6$. Coming back to original variables, assuming $M_{\text{coll}} = M_{\max} = 1.07 \times 10^8 M_{\odot}$, we get $R_{\text{coll}} = 1.23$ pc, $\rho_{\text{dense}} = 9.21 \times 10^{-10}$ g/m³, $2\pi/\omega_{\text{coll}} = 54.8$ yrs and $E_{\text{tot}}^{\text{coll}} = -3.40 \times 10^{60}$ ergs (in comparison $R_* = 0.313$ kpc, $\rho_{\text{dilute}} = 5.63 \times 10^{-17}$ g/m³, $2\pi/\omega_{\text{max}} = 229$ Myrs, $E_{\text{tot}}^{\text{dilute}} = -4.17 \times 10^{53}$ ergs).

C. Explosion when $\delta \ll 1$ and $M \sim M_{\min}^-$

We now consider the situation where $\delta \ll 1$ and $M \sim M_{\min}(\delta)^-$. Physically, we assume that a stable dense axion star loses mass and passes below the critical point. In that case, the dense axion star explodes and ultimately becomes a dilute axion star (I) with a very large

radius.¹⁷ We assume that there is no mass loss during the explosion. Using Eqs. (106) and (120), the radius and the average density of the dilute axion star are

$$R_{\text{exp}}(\delta) \sim \frac{3}{32\sqrt{\delta}}, \quad \rho_{\text{exp}}(\delta) \sim \frac{524288}{27\pi} \delta^2. \quad (191)$$

Coming back to dimensional variables, we get

$$R_{\text{exp}} \sim \frac{3}{128} \left(\frac{27}{\pi\sigma} \right)^{1/2} \frac{(6\pi\zeta)^{3/2} |a_s| \hbar c}{\nu G m^2} = 0.260 R_e, \quad (192)$$

$$\rho_{\text{exp}} \sim \left(\frac{512}{27} \right)^3 \frac{\pi\nu^3 \sigma^3}{(6\pi\zeta)^6} \frac{G^3 m^6}{|a_s|^4 \hbar^2 c^4} = 195 \rho_e, \quad (193)$$

where the scales R_e and ρ_e are defined in Appendix A 4.

The pulsation of the dilute axion star resulting from the explosion is given by

$$\omega_{\text{exp}} \sim \frac{2048}{9\sqrt{2}} \delta = 161 \delta. \quad (194)$$

The total energy of the dilute axion star resulting from the explosion is given by

$$E_{\text{tot}}^{\text{exp}} \sim -\frac{65536}{27} \delta^{3/2} = -2.43 \times 10^3 \delta^{3/2}. \quad (195)$$

In comparison, the total energy of the dense axion star with the minimum mass is

$$E_{\text{tot}}^{\text{dense}} \sim \frac{2}{27\sqrt{\delta}} = \frac{7.41 \times 10^{-2}}{\sqrt{\delta}}. \quad (196)$$

We note that it is positive. This is possible because the dense axion star is metastable, not fully stable (see the Remark at the end of Sec. IX B).

For QCD axions with $\delta = 8.88 \times 10^{-16}$, assuming $M_{\text{exp}} = M_{\text{min}} = 6.36 \times 10^{-7}$, we get $R_{\text{exp}} \sim 3.14 \times 10^6$, $\rho_{\text{exp}} = 4.90 \times 10^{-27}$, $2\pi/\omega_{\text{exp}} = 4.40 \times 10^{13}$ and $E_{\text{tot}}^{\text{exp}} = -6.42 \times 10^{-20}$ (in comparison $E_{\text{tot}}^{\text{dense}} = 2.49 \times 10^6$). Coming back to original variables, assuming $M_{\text{exp}} = M_{\text{min}} = 4.40 \times 10^{-20} M_{\odot}$, we get $R_{\text{exp}} = 323 R_{\odot}$, $\rho_{\text{exp}} = 1.84 \times 10^{-21} \text{ g/m}^3$, $2\pi/\omega_{\text{exp}} = 17.1 \text{ Gyrs}$ and $E_{\text{tot}}^{\text{exp}} = -4.53 \times 10^6 \text{ ergs}$ (in comparison $E_{\text{tot}}^{\text{dense}} = 1.76 \times 10^{32} \text{ ergs}$).

For ULAs with $\delta = 1.02 \times 10^{-8}$, assuming $M_{\text{exp}} = M_{\text{min}} = 2.15 \times 10^{-3}$, we get $R_{\text{exp}} \sim 928$, $\rho_{\text{exp}} = 6.42 \times 10^{-13}$, $2\pi/\omega_{\text{exp}} = 3.83 \times 10^6$ and $E_{\text{tot}}^{\text{exp}} = -2.50 \times 10^{-9}$ (in comparison $E_{\text{tot}}^{\text{dense}} = 733$). Coming back to original variables, assuming $M_{\text{exp}} = M_{\text{min}} = 2.30 \times 10^5 M_{\odot}$, we get $R_{\text{exp}} = 290 \text{ kpc}$, $\rho_{\text{exp}} = 1.52 \times 10^{-28} \text{ g/m}^3$, $2\pi/\omega_{\text{exp}} = 5.93 \times 10^4 \text{ Gyrs}$ and $E_{\text{tot}}^{\text{exp}} = -3.12 \times 10^{45} \text{ ergs}$ (in comparison $E_{\text{tot}}^{\text{dense}} = 9.16 \times 10^{36} \text{ ergs}$).

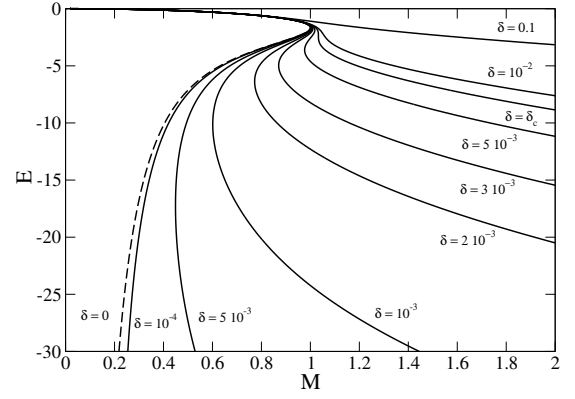


FIG. 21: Series of equilibria $E(M)$ for different values of the interaction parameter δ . The dashed line corresponds to dilute axion stars with $\delta = 0$.

D. Radiation

Since energy is conserved, the collapse of a dilute axion star above the maximum mass towards a dense axion star ($|E_{\text{tot}}^{\text{dense}}| \ll |E_{\text{tot}}^{\text{dilute}}|$) must be accompanied by the emission of a form of radiation that will carry energy (and mass) away. This is similar to the process of gravitational cooling [147] or to the situation investigated by Levkov *et al.* [110]. The final state could be a dense axion star (remnant) with a smaller energy (and usually a smaller mass) than the energy of the dilute axion star, plus a radiation. The same situation occurs for the explosion of dense axion stars below the minimum mass.

Remark: We note that the Gaussian ansatz is not able to describe this complex evolution. For $M > M_{\text{max}}$, we find that the radius $R(t)$ of the star permanently oscillates about the equilibrium state R_{coll} , at fixed energy. An improvement of the model would be to heuristically introduce a source of dissipation (damping) in the GPP equations in order to describe the relaxation process as proposed in [78].

IX. STABILITY ANALYSIS AND PHASE TRANSITIONS IN AXION STARS

In this section we discuss the stability of the different solutions found previously and the nature of phase transitions between dilute axion stars and dense axion stars. This description is similar to the description of phase transitions in the self-gravitating Fermi gas at finite temperature given in Ref. [148].

A. Series of equilibria and stability of the equilibrium states

A stable axion star is a minimum of energy E_{tot} at fixed mass M . To determine the stability of axion

¹⁷ We consider this situation for curiosity and remain brief because it may not be physically relevant. In view of the numerical applications made at the end of this section, the explosion, if it really takes place, is expected to form a dispersed cloud, not a star.

stars, we can use the Poincaré theory of linear series of equilibria (see Appendix D). The variable conjugate to the mass M (conserved quantity) with respect to the energy E_{tot} (quantity to minimize) is the eigenenergy $E = \partial E_{\text{tot}} / \partial M$.¹⁸ To apply the Poincaré theory to the present situation, we have to plot the eigenenergy E as a function of the mass M along the series of equilibria of axion stars.¹⁹ The series of equilibria $E(M)$ depends on the value of the interaction parameter δ as shown in Fig. 21.

In the following, for illustration, we shall consider the series of equilibria $E(M)$ of Fig. 22 corresponding to $\delta = 10^{-3}$. This series of equilibria is multi-valued. It has a Z-shape structure that gives rise to phase transitions. The solutions on the upper branch (I) form the “dilute phase”. They correspond to dilute axion stars. The solutions on the lower branch (III) form the “condensed phase”. They correspond to dense axion stars. As explained below, the system has to cross a barrier of potential, played by the solutions of the intermediate branch (II) corresponding to unstable axion stars, to pass from the dilute phase to the condensed phase (or inversely).

For $M \rightarrow 0$ and $E \rightarrow 0$, an axion star is equivalent to a noninteracting Newtonian boson star in which self-gravity is stabilized by the quantum potential (Heisenberg’s uncertainty principle) [6, 34, 96]. This structure is known to be stable (it is a global minimum of energy E_{tot} at fixed mass M). From the turning point criterion, we conclude that the dilute axion stars on the branch (I) of Fig. 22 are stable (energy minima) until the first turning point of mass. At $M = M_{\text{max}}(\delta)$, the curve $E(M)$ rotates clockwise so that a mode of stability is lost. Therefore, the axion stars on the intermediate branch (II) of Fig. 22 are unstable (maxima or saddle points of energy) until the second turning point of mass. They lie in the region where $dE/dM > 0$ which is inaccessible. This is the analogue of a region of negative specific heats $dE/dT < 0$ in thermodynamics [148]. At $M = M_{\text{min}}(\delta)$, the curve $E(M)$ rotates anti-clockwise so that the mode of stability lost at $M = M_{\text{max}}(\delta)$ is regained. Therefore, the dense axion stars on the branch (III) of Fig. 22 are stable.

Remark: We note that the turning point of radius at (R_{min}, M_*) in the mass-radius relation $M(R)$ of Fig. 4 does not signal a change of stability as noted in Sec. VII D.

¹⁸ As before, we have introduced dimensionless variables. We note that $E = NE/M$ where NE is given by Eq. (155).

¹⁹ As explained in Appendix D, the correct series of equilibria to consider in order to determine the stability of the solutions from the Poincaré theory and study phase transitions is the eigenenergy-mass relation $E(M)$, not the mass-radius relation $M(R)$. In particular, we cannot apply the Maxwell construction (see Appendix J) on the mass-radius relation $M(R)$. The stability of the solutions can nevertheless be obtained from the mass-radius relation by using Wheeler’s theorem [144].

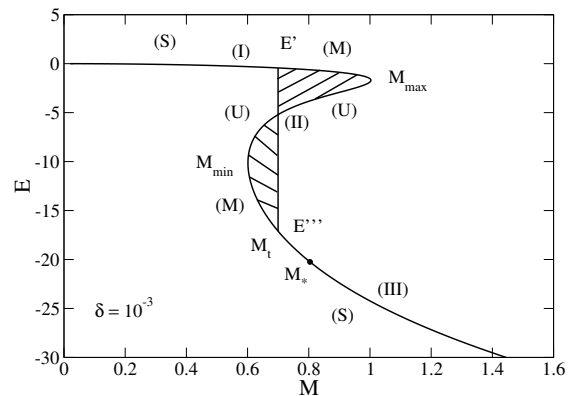


FIG. 22: Stability of the equilibrium states from the Poincaré theory of linear series of equilibria. We have also performed the Maxwell construction. The equilibrium states can be fully stable (S), metastable (M), and unstable (U).

B. Fully stable and metastable states

We must now determine which configurations are fully stable (global minima of energy) and which configurations are metastable (local minima of energy). This can be done by plotting the energy E_{tot} of the two phases as a function of the mass M as done in Fig. 12, comparing their respective values, and determining at which mass $M_t(\delta)$ they become equal. Alternatively, one can perform the Maxwell construction on the curve $E(M)$ as described in Appendix J. The Maxwell construction is illustrated in Fig. 22. The transition mass $M_t(\delta)$ is such that the two hatched areas are equal.

When $M < M_t(\delta)$ the dilute axion stars (I) are fully stable (S) and when $M_t(\delta) < M < M_{\text{max}}(\delta)$ they are metastable (M). Inversely, when $M_{\text{min}}(\delta) < M < M_t(\delta)$ the dense axion stars (III) are metastable (M) and when $M > M_t(\delta)$ they are fully stable (S). The axion stars on the branch (II) are unstable (U). These results are illustrated in Fig. 23. In a strict sense, an equilibrium state corresponds to a fully stable state (S). Therefore, the strict energy-mass and eigenenergy-mass relations are obtained from Figs. 12 and 22 by keeping only the fully stable states (S). From these curves, we expect the occurrence of a first order phase transition at $M = M_t(\delta)$ connecting the dilute phase to the condensed phase. It is accompanied by a discontinuity of $E'_{\text{tot}}(M)$ (the first derivative of $E_{\text{tot}}(M)$) at $M = M_t(\delta)$. Since $E'_{\text{tot}}(M) = E(M)$, this corresponds to a discontinuity of the eigenenergy $E(M)$ at $M_t(\delta)$. As a result, the region where $dE/dM > 0$ is replaced by a phase transition (vertical Maxwell plateau) that connects the dilute phase to the dense phase (see Fig. 22).

Remark: We can check in Fig. 12 that the stable branches (I) and (III) have a lower energy E_{tot} than the unstable branch (II) as it should, since a stable state corresponds to a (local) minimum of energy E_{tot} (see Figs. 3 and 23). We also recall that a necessary (but not suf-

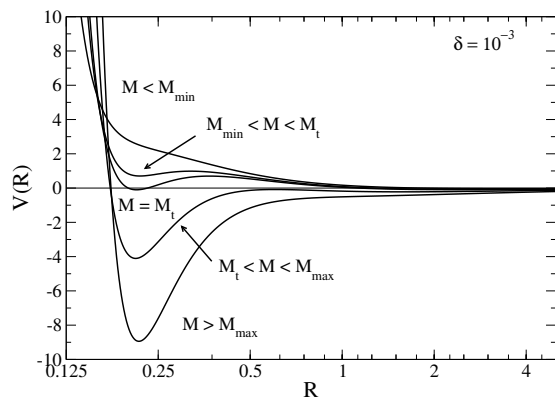


FIG. 23: Effective potential $V(R)$ as a function of the radius for $\delta = 10^{-3}$. For $M < M_{\min} = 0.601$ (here $M = 0.5$), the dilute axion stars are fully stable and the dense axion stars are inexistent. For $M_{\min} = 0.601 < M < M_t = 0.700$ (here $M = 0.65$), the dilute axion stars are fully stable and the dense axion stars are metastable. For $M = M_t = 0.700$, the dense axion stars have the same energy as the dilute axion stars. For $M_t = 0.700 < M < M_{\max} = 1.00$ (here $M = 0.9$), the dense axion stars are fully stable and the dilute axion stars are metastable. For $M > M_{\max} = 1.00$ (here $M = 1.1$), the dense axion stars are fully stable and the dilute axion stars are inexistent.

ficient) condition of nonlinear dynamical stability is that $E_{\text{tot}} < 0$. We can check in Fig. 12 that the configurations on the fully stable branches (S) corresponding to global energy minima satisfy this condition, while this is not necessarily true for the configurations on the metastable branches (M) corresponding to local energy minima since they are only linearly dynamically stable.²⁰ Finally, we note from the inspection of Fig. 22 that the eigenenergy E of an unstable axion star (II) is higher than the eigenenergy of a stable dense axion star (III) but lower than the eigenenergy of a stable dilute axion star (I). There is no paradox, however, since the eigenenergy E represents the chemical potential μ (see Appendix D), not the energy E_{tot} that has to be a (local) minimum at equilibrium.

C. Lifetime of metastable states

The preceding discussion suggests the occurrence of a first order phase transition at $M_t(\delta)$. However, for systems with long-range interactions such as self-gravitating

²⁰ The stable dilute axion stars always have a negative energy while the unstable axion stars and the metastable dense axion stars may have negative or positive energies (see Sec. VII E). The reason why stable dilute axion stars have a negative energy is due to the fact that $V(R) \rightarrow 0^-$ as $R \rightarrow +\infty$ so the energy of the last minimum is necessarily negative.

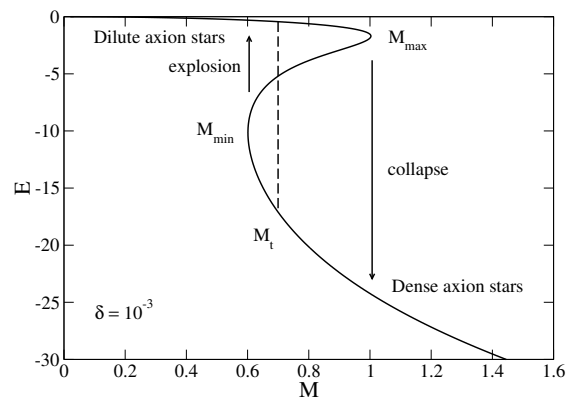


FIG. 24: Series of equilibria illustrating the collapse from a dilute axion star to a dense axion star above M_{\max} (see Sec. VIII B) or the explosion from a dense axion star to a dilute axion star below M_{\min} (see Sec. VIII C).

systems, a first order phase transition does not take place in practice. Indeed, the metastable states are long-lived because the probability of a fluctuation able to trigger the phase transition is extremely low. Indeed, to trigger a phase transition from (I) to (III), or the converse, the system has to cross a barrier of potential played by the solutions on the intermediate branch (II). This energetic barrier is illustrated in Figs. 3 and 23. For $N \gg 1$, this barrier of potential rapidly increases as we depart from the critical point $M_{\max}(\delta)$ and is usually very hard to cross. Since the metastable states are extremely robust, the first order phase transition expected to occur at $M_t(\delta)$ does not take place in practice. The system remains in the metastable phase past the transition point. As a result, the physical energy-mass and eigenenergy-mass relations must take metastable states into account. They are obtained from Figs. 12 and 22 by discarding only the unstable states (U).

The true phase transition from dilute to dense axion stars occurs at the maximum mass $M_{\max}(\delta)$ at which the metastable branch disappears (see Fig. 24). This point is similar to a spinodal point in thermodynamics. It also corresponds to a saddle node bifurcation. If the mass of dilute axion stars increases above $M_{\max}(\delta)$ the system collapses due to the effect of self-gravity and the attractive self-interaction of the bosons. However, when the repulsive self-interaction is taken into account, the core of the system ceases to shrink when it feels the repulsion of the bosons at sufficiently high densities, and a dense axion star is formed. Since this collapse is accompanied by a discontinuous jump of energy E_{tot} (see Fig. 12), this is sometimes called a *zeroth order* phase transition.

For $M > M_t(\delta)$, the condensed states (dense axion stars) are fully stable (S). If their mass decreases, the system remains in the condensed phase past the transition mass $M_t(\delta)$. Indeed, for the same reason as before, the condensed states with $M_{\min}(\delta) < M < M_t(\delta)$ are long-lived metastable states (M) so that the first order

phase transition from the dense phase to the dilute phase does not take place in practice. However, below $M_{\min}(\delta)$ the condensed metastable branch disappears and the system undergoes a discontinuous transition reversed to the collapse at $M_{\max}(\delta)$ (see Fig. 24). This transition can be called an “explosion” since it transforms dense axion stars into dilute axion stars. Since the collapse and the explosion occur at different values of mass, due to the presence of metastable states, we can generate an *hysteresic cycle* by varying the mass between $M_{\min}(\delta)$ and $M_{\max}(\delta)$.

D. The evolution of unstable equilibrium states

It is also interesting to determine the evolution of a slightly perturbed unstable (U) equilibrium state. This evolution will depend on the sign of its energy E_{tot} as determined in Sec. VII E. Recall that for $\delta < \delta_c$ and $M_{\min}(\delta) < M < M_{\max}(\delta)$ the effective potential $V(R)$ has three extrema (see Fig. 3): a minimum corresponding to a stable dense axion star of small radius (left), a maximum corresponding to an unstable axion star of intermediate radius (middle), and another minimum corresponding to a stable dilute axion star of large radius (right). When $\delta'_c < \delta < \delta_c$ or when $\delta < \delta'_c$ and $M_{E,\text{II}}(\delta) < M < M_{\max}(\delta)$ the unstable axion star has a negative total energy $E_{\text{tot}} < 0$ (see Fig. 19). As a result, when slightly perturbed, it either relaxes towards a stable dense axion star with a smaller radius or towards a stable dilute axion star with a larger radius (assuming an efficient dissipation process as explained in Sec. VIII D). When $\delta < \delta'_c$ and $M_{\min}(\delta) < M < M_{E,\text{II}}(\delta)$ the unstable axion star has a positive total energy $E_{\text{tot}} > 0$ (see Fig. 19). As a result, when slightly perturbed, it either relaxes towards a dense axion star with a smaller radius (again assuming dissipation) or explodes and disperses to infinity.

E. Critical points and phase diagram

The deformation of the series of equilibria $E(M)$ as a function of the parameter δ is represented in Fig. 21.

For $\delta = 0$, we recover the mass-eigenenergy relation of dilute axion stars [73] which presents a maximum mass $M_{\max} = 1$ that separates the branch of stable dilute axion stars (I) and the branch of unstable axion stars (II). For $M > M_{\max} = 1$ the system collapses and is expected to form a Dirac peak (see Appendix C).

For $0 < \delta < \delta_c$, a minimum mass $M_{\min}(\delta)$ exists in addition to the maximum mass $M_{\max}(\delta)$. In that case, a new branch appears which corresponds to stable dense axion stars (III). The curve $E(M)$ becomes multi-valued (Z -shape) so that a first order phase transition between dilute and dense axion stars is expected to occur. If we keep only fully stable states (S), the Z -curve has to be

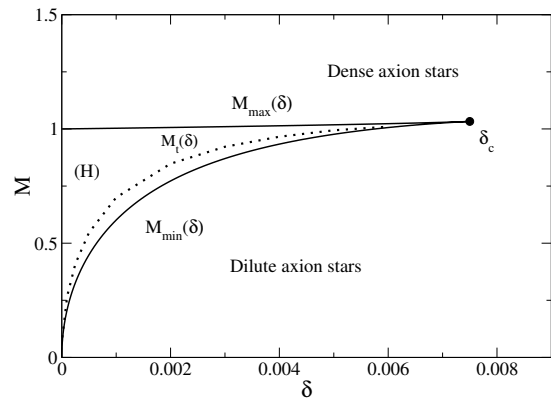


FIG. 25: Phase diagram of Newtonian axion stars. The H -zone corresponds to a hysteretic zone where the actual phase depends on the history of the system. If it is initially prepared in a dilute state, it will remain dilute until the maximum mass M_{\max} at which it will collapse and become dense. Inversely, if the system is initially prepared in a dense state, it will remain dense until the minimum mass M_{\min} at which it will explode and become dilute. We show in Appendix K that the transition mass $M_t(\delta)$, which is by definition in the interval $[M_{\min}(\delta), M_{\max}(\delta)]$, approaches the mass $M_*(\delta)$ corresponding to the minimum radius as $\delta \rightarrow 0$. We recall, however, that the transition mass $M_t(\delta)$ is usually not physically relevant because of the very long lifetime of metastable states (see main text).

replaced by a vertical Maxwell plateau. The extent of the plateau decreases as δ increases towards δ_c .

At the critical point δ_c , the plateau disappears and the series of equilibria $E(M)$ presents an inflexion point. At that point, dE/dM (the equivalent of the specific heats in thermodynamics) is infinite.

For $\delta > \delta_c$, the curve $E(M)$ is univalued so there is no phase transition. There is only one branch of stable axion stars.

In summary, for $\delta = 0$ the system exhibits a collapse towards a Dirac peak at $M_{\max} = 1$; for $0 < \delta < \delta_c$ the system exhibits a first order phase transition at $M_t(\delta)$ characterized by a vertical Maxwell plateau; for $\delta > \delta_c$ there is no phase transition. We recall, however, that because of the presence of long-lived metastable states, the first order phase transition and the Maxwell plateau are usually not physically relevant. Only the zeroth order phase transitions that occur at $M_{\max}(\delta)$ and $M_{\min}(\delta)$ (spinodal points) are physically relevant.

The phase diagram of axion stars can be directly deduced from the properties of the series of equilibria by identifying characteristic masses. We note $M_{\max}(\delta)$ the end point of the metastable dilute phase (first turning point of mass), $M_{\min}(\delta)$ the end point of the metastable condensed phase (last turning point of mass), and $M_t(\delta)$ the mass of transition determined by the equality of the energies of the two phases. The phase diagram is represented in Fig. 25. It displays in particular the critical point $\delta_c = 3/400 = 0.0075$ at which the phase transitions

appear/disappear.

F. The dilute limit $\delta \rightarrow 0$

It is of interest to discuss the limit $\delta \rightarrow 0$ specifically so as to make the connection with the results obtained for dilute axion stars ($\delta = 0$) in [73] when there is no self-repulsion. For $\delta \rightarrow 0$, the transition mass $M_t(\delta) \rightarrow 0$ so that the dilute axion stars on the branch (I) are metastable (M) while the dense axion stars on the branch (III) are fully stable (S). However, the branch (III) is rejected at infinity ($E \rightarrow -\infty$). It is made of Dirac peaks (see Appendix C). Therefore, the $\delta \rightarrow 0$ limit of the series of equilibria $E(M)$ (Fig. 21) is formed by the metastable branch (I) and the unstable branch (II) of the series of equilibria $E(M)$ of dilute axion stars with $\delta = 0$ plus a singular stable branch (III) at $E = -\infty$ made of Dirac peaks. Similarly, the $\delta \rightarrow 0$ limit of the mass-radius relation $M(R)$ (Fig. 10) is formed by the metastable branch (I) and the unstable branch (II) of the mass-radius relation $M(R)$ of dilute axion stars with $\delta = 0$ plus a singular stable branch (III) at $R = 0$ made of Dirac peaks.

Remark: For $\delta \rightarrow 0$ but $\delta \neq 0$, the Dirac peaks on the singular branch (III) are *not* black holes whatever the mass M since the typical mass at which general relativistic effects become important, of the order of $M_0(\delta)$, tends to infinity for $\delta \rightarrow 0$ (see Appendix C).

X. QUALITATIVE DESCRIPTION OF GENERAL RELATIVISTIC EFFECTS

Our Newtonian treatment is valid if the radius of an axion star of mass M satisfies the condition $R \gg R_S = 2GM/c^2$, where R_S is the Schwarzschild radius. In terms of dimensionless variables, this condition can be rewritten as $R \gg R_S$ with $R_S = (81\zeta/4\nu)M\delta = 3.23M\delta$ or, equivalently, as

$$M \ll \frac{4\nu}{81\zeta} \frac{R}{\delta} = 0.310 \frac{R}{\delta} \quad (\text{Newtonian}). \quad (197)$$

When this condition is not satisfied, i.e. when $R \sim R_S$ or, in dimensionless form, when

$$M \sim \frac{4\nu}{81\zeta} \frac{R}{\delta} = 0.310 \frac{R}{\delta} \quad (\text{GR}), \quad (198)$$

general relativistic effects become important. Generalizing the arguments developed in Appendix B of [34], the combination of the Newtonian mass-radius relation $M(R)$ given by Eq. (103) and the relativistic criterion (198), sometimes called the black hole line, gives a qualitative estimate of the general relativistic maximum mass $M_{\text{max,GR}}$ of an axion star (see Fig. 26 for an illustration). Although this method can only give an order of

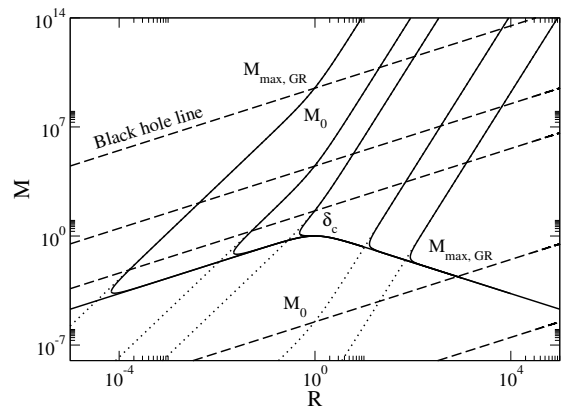


FIG. 26: Mass-radius relationship of Newtonian axion stars for different values of the interaction parameter ($\delta = 10^{-10}, 10^{-5}, \delta_c, 10^5, 10^{10}$). The intersection between the $M(R)$ curve and the black hole line $M = Rc^2/2G$ ($M = 0.310R/\delta$ in dimensionless form) determines the limit of validity of the Newtonian treatment and the order of magnitude of the general relativistic maximum mass of axion stars. The mass-radius relation (solid line) and the black hole line (dashed line) corresponding to the same δ can be easily identified by using the fact that the black hole line and the TF curve intersect each other at $M \sim M_0$ (i.e. when the TF curve presents a change of slope).

magnitude of this maximum mass,²¹ we shall keep all the prefactors from our analysis for future comparison.

A. The general relativistic maximum mass of dilute axion stars

Let us first determine the general relativistic maximum mass of dilute axion stars. Considering the possible intersection between the stable part ($R > 1$) of the Newtonian mass-radius relation (105) and the black hole line (198), we obtain

$$M_{\text{max,GR}}^{\text{dilute}} = \frac{\delta_*}{\delta} \sqrt{\frac{2\delta}{\delta_*} - 1}, \quad (199)$$

$$R_{*,\text{GR}}^{\text{dilute}} = \sqrt{\frac{2\delta}{\delta_*} - 1}, \quad (200)$$

provided that $\delta \geq \delta_*$ with

$$\delta_* = \frac{4\nu}{81\zeta} = 0.310. \quad (201)$$

These results lead to the following conclusions:

(i) If $\delta < \delta_*$ (strongly self-interacting axions), there is no intersection. Therefore, the Newtonian treatment of

²¹ It captures, however, the correct scaling of the maximum mass.

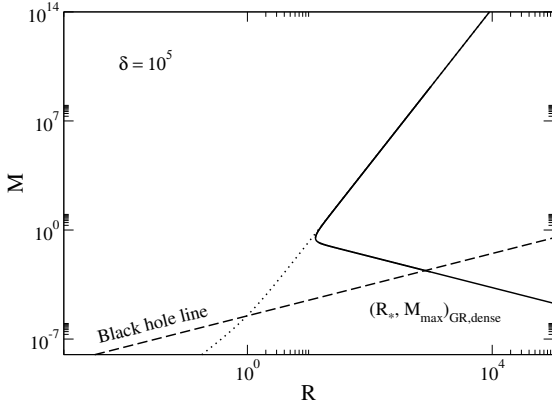


FIG. 27: Mass-radius relation of weakly self-interacting axion stars with $\delta > \delta_*$ (for illustration we have taken $\delta = 10^5$). The Newtonian relation is only valid for $M \ll M_{\max, \text{GR}}^{\text{dilate}}$ and $R \gg R_{*, \text{GR}}^{\text{dilate}}$. Close to $M_{\max, \text{GR}}^{\text{dilate}}$, the real (relativistic) mass-radius relation $M(R)$ should form a spiral like in the case of noninteracting boson stars (see Appendix A 5).

dilute axion stars is always valid. In that case, the maximum mass and the minimum radius of dilute axion stars are given by $M_{\max} = 1$ and $R_* = 1$. We shall write them as $M_{\max, \text{N}}^{\text{dilate}}$ and $R_{*, \text{N}}^{\text{dilate}}$ to emphasize that they have a non-relativistic (Newtonian) origin. We recall that $\delta \ll 1$ for QCD axions and typical ULAs (such as those considered in Sec. IV D) so the Newtonian approximation describes dilute axion stars very well.

(ii) If $\delta > \delta_*$ (weakly self-interacting axions), there is one intersection (see Fig. 27). In that case, the Newtonian treatment is valid for $M \ll M_{\max, \text{GR}}^{\text{dilate}}$ and $R \gg R_{*, \text{GR}}^{\text{dilate}}$ but ceases to be valid as we approach these values.²² When general relativity is taken into account, we expect that the mass-radius relation close to $(M_{\max, \text{GR}}^{\text{dilate}}, R_{*, \text{GR}}^{\text{dilate}})$ forms a spiral (see below). Above $M_{\max, \text{GR}}^{\text{dilate}}$ the system is expected to collapse into a black hole.

If we come back to dimensional variables, we obtain²³

$$M_{\max, \text{GR}}^{\text{dilate}} = \left(\frac{\sigma}{2\nu}\right)^{1/2} \sqrt{2 - \frac{6\pi\zeta}{2\sigma} \frac{2|a_s|}{r_S} \frac{M_P^2}{m}}, \quad (202)$$

$$R_{*, \text{GR}}^{\text{dilate}} = \left(\frac{2\sigma}{\nu}\right)^{1/2} \sqrt{2 - \frac{6\pi\zeta}{2\sigma} \frac{2|a_s|}{r_S}} \lambda_C, \quad (203)$$

provided that $|a_s| \leq |a_s|_*$ with

$$|a_s|_* = \frac{\sigma}{6\pi\zeta} r_S = 0.627 r_S. \quad (204)$$

For $a_s = 0$ (noninteracting limit), we obtain

$$M_{\max, \text{GR}}^{\text{dilate}} = \left(\frac{\sigma}{\nu}\right)^{1/2} \frac{M_P^2}{m} = 1.37 M_c, \quad (205)$$

$$R_{*, \text{GR}}^{\text{dilate}} = 2 \left(\frac{\sigma}{\nu}\right)^{1/2} \lambda_C = 2.74 R_c, \quad (206)$$

where the scales M_c and R_c are defined in Appendix A 5. Our approximate relativistic treatment recovers the Kaup scales of noninteracting boson stars. We know that the mass-radius relation of general relativistic noninteracting boson stars forms a spiral close to the maximum mass (the spiral being made of unstable states), and we expect this property to be preserved for weakly self-interacting axions with $|a_s| \leq |a_s|_*$.

For $|a_s| \geq |a_s|_*$, the maximum mass and the minimum radius of dilute axion stars are given by Eqs. (79) and (80). They can be written as

$$M_{\max, \text{N}}^{\text{dilate}} = \left(\frac{\sigma^2}{6\pi\zeta\nu}\right)^{1/2} \left(\frac{r_S}{2|a_s|}\right)^{1/2} \frac{M_P^2}{m} = 1.085 M_a, \quad (207)$$

$$R_{*, \text{N}}^{\text{dilate}} = \left(\frac{6\pi\zeta}{\nu}\right)^{1/2} \left(\frac{2|a_s|}{r_S}\right)^{1/2} \lambda_C = 1.732 R_a. \quad (208)$$

We note from Eqs. (202)-(206) that the general relativistic maximum mass $M_{\max, \text{GR}}^{\text{dilate}}$ and the general relativistic minimum radius $R_{*, \text{GR}}^{\text{dilate}}$ of dilute axion stars change only weakly with the self-interaction for $|a_s| \leq |a_s|_*$. By contrast, for $|a_s| \geq |a_s|_*$, the Newtonian maximum mass $M_{\max, \text{N}}^{\text{dilate}}$ decrease as $|a_s|^{-1/2}$ and the Newtonian minimum radius $R_{*, \text{N}}^{\text{dilate}}$ increases as $|a_s|^{1/2}$. At the transition $|a_s| = |a_s|_*$, we find that

$$M_{\max, \text{N}}^{\text{dilate}} = M_{\max, \text{GR}}^{\text{dilate}} = \left(\frac{\sigma}{2\nu}\right)^{1/2} \frac{M_P^2}{m} = 0.969 M_c, \quad (209)$$

$$R_{*, \text{N}}^{\text{dilate}} = R_{*, \text{GR}}^{\text{dilate}} = \left(\frac{2\sigma}{\nu}\right)^{1/2} \lambda_C = 1.94 R_c. \quad (210)$$

We note that the value of the scattering length $|a_s|_*$ that separates the weakly self-interacting regime from the strongly self-interacting regime is of the order of the effective Schwarzschild radius r_S of the axion. In Ref. [77], we have obtained a similar result in a cosmological context. For QCD axions with $m = 10^{-4} \text{ eV}/c^2$ and $|a_s| = 5.8 \times 10^{-53} \text{ m}$, we find $|a_s|_* = 1.66 \times 10^{-67} \text{ m}$. For ULAs with $m = 2.19 \times 10^{-22} \text{ eV}/c^2$ and $|a_s| = 1.11 \times 10^{-62} \text{ fm}$, we find $|a_s|_* = 3.64 \times 10^{-85} \text{ m}$. Therefore, these types of axions are in the strongly self-interacting regime since $|a_s| \gg |a_s|_*$.

²² Note that the axion stars become denser and denser when $M \rightarrow M_{\max, \text{GR}}^{\text{dilate}}$ so they should not be called dilute axion stars anymore. However, we keep the notation $M_{\max, \text{GR}}^{\text{dilate}}$ to signify that it corresponds to the general relativistic maximum mass of the branch of dilute axion stars.

²³ These results are in agreement with previous estimates made in Appendix B5 of [34] and in footnote 18 of [73].

The results from Eqs. (202)-(210) can be expressed equivalently in terms of f and λ by using Eq. (72). The critical values of f and λ separating the weakly self-interacting regime from the strongly self-interacting regime are

$$f_* = \left(\frac{6\pi\zeta}{64\pi\sigma} \right)^{1/2} M_P c^2 = 8.91 \times 10^{-2} M_P c^2, \quad (211)$$

$$|\lambda|_* = \frac{16\pi\sigma}{6\pi\zeta} \left(\frac{m}{M_P} \right)^2 = 31.5 \left(\frac{m}{M_P} \right)^2. \quad (212)$$

We note that f_* is independent of the mass of the axion and is of the order of $0.1 M_P c^2$. On the other hand, the value of the dimensionless self-interaction constant $|\lambda|_*$ separating the weakly self-interacting regime from the strongly self-interacting regime is $|\lambda|_* = 2.11 \times 10^{-63}$ for QCD axions with mass $m = 10^{-4} \text{ eV}/c^2$ and $|\lambda|_* = 1.01 \times 10^{-98}$ for ULAs with mass $m = 2.19 \times 10^{-22} \text{ eV}/c^2$. Since QCD axions have $\lambda = -7.39 \times 10^{-49}$ and ULAs have $\lambda = -3.10 \times 10^{-91}$, they are in the strongly self-interacting regime although their values of $|\lambda|$ may seem very small at first sight. This is because the critical parameter $|\lambda|_*$ scales as $(m/M_P)^2$ which is an extraordinarily small quantity.²⁴ It is therefore crucial to take the self-interaction of the axions into account (see the Remark at the end of Sec. IV D 2), although it is oftentimes neglected [52, 72, 75].

If we consider QCD axions with mass $m = 10^{-4} \text{ eV}/c^2$ and neglect their self-interaction (taking $a_s = 0$), we obtain $M_{\text{max,GR}}^{\text{dilute}} = 1.83 \times 10^{-6} M_\odot$ and $R_{*,GR}^{\text{dilute}} = 0.540 \text{ cm}$. The maximum mass set by general relativity $M_{\text{max,GR}}^{\text{dilute}} = 1.83 \times 10^{-6} M_\odot$ is much larger than the Newtonian maximum mass $M_{\text{max,N}}^{\text{dilute}} = 6.92 \times 10^{-14} M_\odot$ obtained when the attractive self-interaction of the axions is taken into account ($a_s = -5.8 \times 10^{-53} \text{ m}$).

If we consider ULAs with mass $m = 2.19 \times 10^{-22} \text{ eV}/c^2$ and neglect their self-interaction (taking $a_s = 0$), we obtain $M_{\text{max,GR}}^{\text{dilute}} = 8.36 \times 10^{11} M_\odot$ and $R_{*,GR}^{\text{dilute}} = 0.0800 \text{ pc}$. The maximum mass set by general relativity $M_{\text{max,GR}}^{\text{dilute}} = 8.36 \times 10^{11} M_\odot$ is much larger than the Newtonian maximum mass $M_{\text{max,N}}^{\text{dilute}} = 1.07 \times 10^8 M_\odot$ obtained when the

²⁴ In particle physics and quantum field theory, one usually considers that the self-interaction is weak when $|\lambda| \ll 1$. In our situation, in which gravity is in action, the self-interaction is weak when $|\lambda| \ll (m/M_P)^2$, which is a very different criterion since the ratio m/M_P is extremely small (see Appendix L). It is therefore relevant to introduce a new dimensionless self-interaction constant $\Lambda = \lambda(M_P/m)^2$ adapted to our problem so that the weakly self-interacting regime corresponds to $|\Lambda| \ll 1$ and the strongly self-interacting regime corresponds to $|\Lambda| \gg 1$. We stress that the conditions $|\lambda| \ll 1$ and $|\Lambda| \ll 1$ have a very different physical meaning. We can be in the strongly self-interacting regime $|\Lambda| \gg 1$ for our problem, even if we are in the weakly self-interacting regime of quantum field theory $|\lambda| \ll 1$ (we have reached a similar conclusion in Sec. III.H. of [77] in a cosmological context).

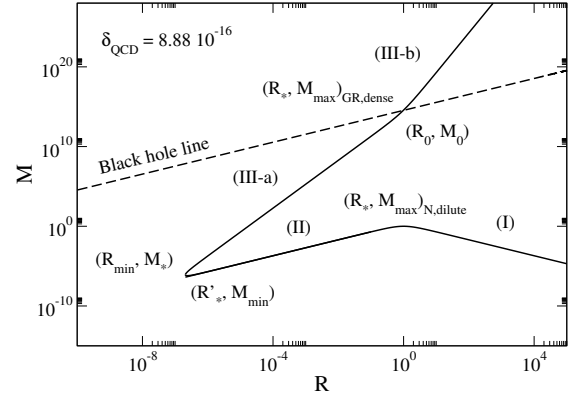


FIG. 28: Mass-radius relation of strongly self-interacting axion stars with $\delta < \delta_*$ (for illustration we have taken $\delta_{\text{QCD}} = 8.88 \times 10^{-16}$). The Newtonian relation is only valid for $M < M_{\text{max,GR}}^{\text{dense}}$. Close to $M_{\text{max,GR}}^{\text{dense}}$, the exact (general relativistic) mass-radius relation $M(R)$ may form a spiral or stop suddenly (see footnote 25).

attractive self-interaction of the axions is taken into account ($a_s = -1.11 \times 10^{-62} \text{ fm}$).

In this sense, an attractive self-interaction substantially reduces the maximum mass of axion stars and make it nonrelativistic instead of relativistic.

B. The general relativistic maximum mass of dense axion stars

We now consider the general relativistic maximum mass of dense axion stars. Considering the intersection between the Newtonian mass-radius relation (131) in the TF limit and the black hole line (198) we obtain

$$M_{\text{max,GR}}^{\text{dense}} = \frac{\sqrt{-1 + \sqrt{1 + 24\delta_*}}}{\sqrt{2}} \frac{\delta_*}{\delta} = 0.976 \frac{\delta_*}{\delta}, \quad (213)$$

$$R_{*,GR}^{\text{dense}} = \frac{\sqrt{-1 + \sqrt{1 + 24\delta_*}}}{\sqrt{2}} = 0.976... \quad (214)$$

These results lead to the following conclusions:

(i) If $\delta > \delta_*$ (weakly self-interacting axions) there is no intersection in the physical part of the TF curve (the part that correctly approximates the Newtonian mass-radius relation of dense axion stars) because $R_{*,GR}^{\text{dense}} < R_{\text{min}}$. In that case, the maximum mass is $M_{\text{max,GR}}^{\text{dilute}}$, the general relativistic maximum mass of dilute axion stars, and we are led back to the discussion of point (ii) in Sec. X A. Above $M_{\text{max,GR}}^{\text{dilute}}$, the collapse of a dilute axion star is expected to form a black hole, not a dense axion star.

(ii) If $\delta < \delta_*$ (strongly self-interacting axions) there is one intersection in the physical part of the TF curve since $R_{*,GR}^{\text{dense}} > R_{\text{min}}$ (see Fig. 28). We can now refine the discussion of point (i) in Sec. X A. If $M < M_{\text{max,N}}^{\text{dilute}} = 1$

and $R > R_{*,N}^{\text{dilute}} = 1$ the dilute axion stars are stable and they can be treated by Newtonian gravity. If $M_{\text{max},N}^{\text{dilute}} < M < M_{\text{max},GR}^{\text{dense}}$, the system collapses into a dense axion star which can again be treated by Newtonian gravity. If $M > M_{\text{max},GR}^{\text{dense}}$ the system collapses into a black hole. When general relativity is taken into account, we expect that the mass-radius relation close to $(M_{\text{max},GR}^{\text{dense}}, R_{*,GR}^{\text{dense}})$ forms a spiral or stops suddenly.²⁵ We recall that $\delta \ll 1$ for QCD axions and typical ULAs (such as those considered in Sec. IV D) so that $M_{\text{max},GR}^{\text{dense}} \gg 1$ according to Eq. (213). Therefore, there is a wide range of masses $[M_{\text{max},N}^{\text{dilute}}, M_{\text{max},GR}^{\text{dense}}]$ in which a dilute axion star can collapse into a Newtonian dense axion star without forming a black hole.

If we come back to dimensional variables, we obtain

$$M_{\text{max},GR}^{\text{dense}} = 0.976 \left(\frac{6\pi\zeta}{4\nu} \right)^{1/2} \left(\frac{2|a_s|}{r_S} \right)^{1/2} \frac{M_P^2}{m} = 0.845 M_r, \quad (215)$$

$$R_{*,GR}^{\text{dense}} = 0.976 \left(\frac{6\pi\zeta}{\nu} \right)^{1/2} \left(\frac{2|a_s|}{r_S} \right)^{1/2} \lambda_C = 1.69 R_r, \quad (216)$$

provided that $|a_s| \geq |a_{s,*}|$. We note that these scales are similar to the scales characterizing the maximum mass and the minimum radius of boson stars with a purely repulsive $|\varphi|^4$ self-interaction ($a_s > 0$) (see Appendix A 6). However, as far as we know, these scales are new in the case of axion stars with an attractive $|\varphi|^4$ self-interaction ($a_s < 0$) and a repulsive $|\varphi|^6$ self-interaction.

For QCD axions with $m = 10^{-4} \text{ eV}/c^2$ and $a_s = -5.8 \times 10^{-53} \text{ m}$, we obtain $M_{\text{max},GR}^{\text{dense}} = 23.6 M_\odot$ and $R_{*,GR}^{\text{dense}} = 69.8 \text{ km}$, corresponding to an average density $\rho = 3.30 \times 10^{19} \text{ g/m}^3$.

For ULAs with $m = 2.19 \times 10^{-22} \text{ eV}/c^2$ and $a_s = -1.11 \times 10^{-62} \text{ fm}$, we obtain $M_{\text{max},GR}^{\text{dense}} = 3.19 \times 10^{15} M_\odot$ and $R_{*,GR}^{\text{dense}} = 305 \text{ pc}$, corresponding to an average density $\rho = 1.82 \times 10^{-9} \text{ g/m}^3$.

Remark: We note that the relativistic limit point $(M_{\text{max},GR}^{\text{dense}}, R_{*,GR}^{\text{dense}})$ is close to the point (M_0, R_0) separating nongravitational dense axion stars of type (III-a) and nonattractive dense axion stars of type (III-b) in the TF regime. Therefore, we conclude that dense axion stars of type (III-a) can be treated with a Newtonian approach (up to about the end of this branch) while dense axion stars of type (III-b) are always relativistic and cannot

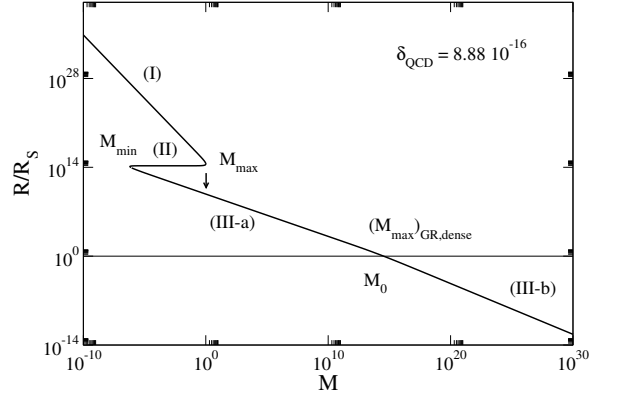


FIG. 29: Compactness $R/R_S = 0.310R/(M\delta)$ as a function of the mass M for QCD axion stars ($\delta = 8.88 \times 10^{-16}$). For $\delta \rightarrow 0$, we find that $(R/R_S)(M_{\text{max}}) \sim 0.310/\delta$, $(R/R_S)(M_{\text{min}}) \sim 0.116/\delta$, and $(R/R_S)_{\text{coll}} \sim 0.563/\delta^{2/3}$. We note that R/R_S is constant ($R/R_S = 0.155/\delta$) on the part of the branch (II) corresponding to unstable axion stars where $M \sim 2R$ (non-gravitational limit). The axion stars are Newtonian when $M \ll M_{\text{max},GR}^{\text{dense}}$ (i.e. $R/R_S \gg 1$) and general relativistic otherwise.

be treated with a Newtonian approach. Therefore, the Newtonian branch of type (III-b) is not physically relevant, except, possibly, at its very beginning. We also note that $M_{\text{max},GR}^{\text{dense}} \sim M_0 \gg M_{\text{max},N}^{\text{dilute}}$ when $\delta \ll 1$. Therefore, we conclude that the collapse of a dilute axion star with mass $M \gtrsim M_{\text{max},N}^{\text{dilute}}$ leads to a dense axion star of type (III-b), not to a black hole. Black holes are formed from the collapse of much heavier stars with a mass $M > M_{\text{max},GR}^{\text{dense}} \sim M_0 \gg M_{\text{max},N}^{\text{dilute}}$. To make things clear, we have plotted the mass-compactness relation of axion stars in Fig. 29.

C. Phase diagrams

We can summarize the previous results on synthetic phase diagrams.

Figure 30 shows the phase diagram in terms of dimensionless variables. It exhibits a triple point at $(\delta_*, M_{\text{max},N}^{\text{dilute}})$ separating three regions: dilute axion stars, dense axion stars of type (III-a), and black holes.²⁶ We recall that the formation of dense axion stars is usually accompanied by the emission of relativistic axions (radiation), so we have added the term “bosenova” in the phase diagram.

²⁵ If the dense axion stars are described by a polytropic equation of state, as in Appendix F, the relativistic mass-radius relation is expected to form a spiral because polytropic spheres become unstable above a maximum central density corresponding to the maximum mass point. Alternatively, if the dense axion stars are described by uniform density spheres, as in Appendix E, the relativistic mass-radius relation is expected to stop suddenly at the point of maximum mass without forming a spiral because uniform density spheres, when they exist, are always stable. We will study this problem further in a specific paper.

²⁶ We have represented the most natural phase diagram, obtained by assuming that we start from a stable dilute axion star and that we progressively increase its mass. As reported in Fig. 25, in the hysteretic zone (H), both dilute and dense axion stars are possible. However, a dilute axion star is more natural.

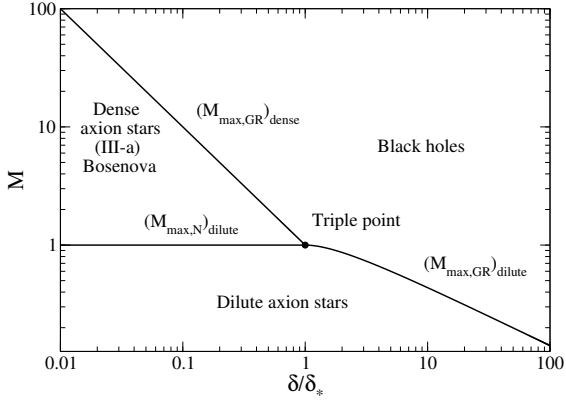


FIG. 30: Phase diagram of axion stars using dimensionless variables.

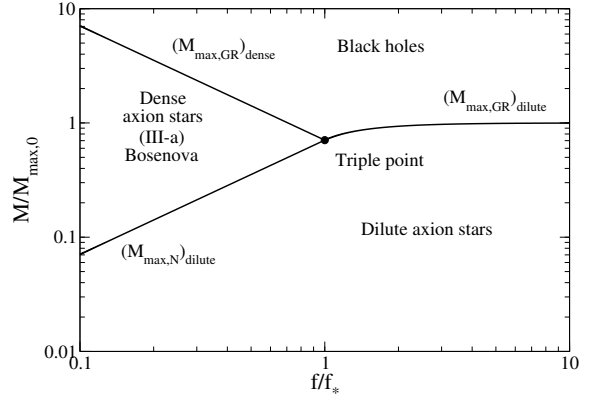


FIG. 32: Phase diagram of axion stars in terms of the axion decay constant f .

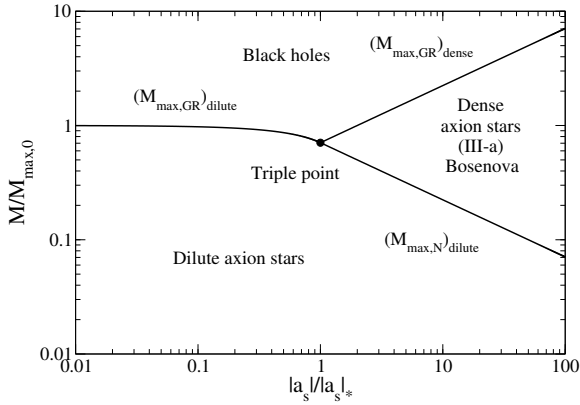


FIG. 31: Phase diagram of axion stars in terms of the scattering length $|a_s|$.

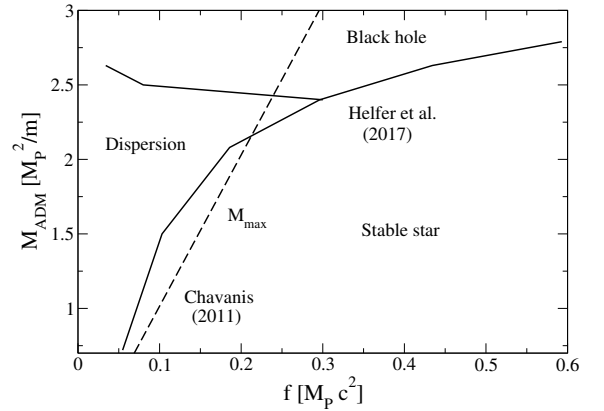


FIG. 33: Sketch of the phase diagram of axion stars obtained by Helfer *et al.* [112]. It can be compared with the phase diagram of Fig. 32 obtained from our analytical study.

When $\delta > \delta_*$ (weakly self-interacting regime), we expect to observe dilute axion stars for $M < M_{\max,GR}^{\text{dilute}}$ and black holes for $M > M_{\max,GR}^{\text{dilute}}$.

When $\delta < \delta_*$ (strongly self-interacting regime), we expect to observe dilute axion stars for $M < M_{\max,N}^{\text{dilute}}$, dense axion stars for $M_{\max,N}^{\text{dilute}} < M < M_{\max,GR}^{\text{dense}}$, and black holes for $M > M_{\max,GR}^{\text{dense}}$.

Figure 31 shows the phase diagram in terms of the scattering length $|a_s|$. In order to present a phase diagram that is not too sensitive on our approximations, we have normalized the scattering length by its transition value $|a_s|_*$ from Eq. (204) and we have normalized the mass by the maximum general relativistic mass $M_{\max,GR}^{\text{dilute}}(0)$ corresponding to noninteracting axion stars ($a_s = 0$), that we call $M_{\max,0}$ for brevity. It is given by Eq. (205). In this way, the phase diagram is relatively universal while the exact values of $|a_s|_*$ and $M_{\max,0}$ are expected to differ from the values (204) and (205) obtained with our qualitative approach. They should be obtained from a rigorous calculation in general relativity. This will be considered in a future work.

Using the relation

$$\frac{\delta_*}{\delta} = \frac{|a_s|}{|a_s|_*} = \left(\frac{f_*}{f}\right)^2 = \frac{|\lambda|}{|\lambda|_*}, \quad (217)$$

we can easily obtain the phase diagrams in terms of f and λ . The normalized phase diagram in terms of $|\lambda|/|\lambda|_*$ coincides with Fig. 31. The phase diagram in terms of the axion decay constant f is presented in Fig. 32.

Remark: the triple point that we have obtained from our analytical study is probably related to the one found numerically by Helfer *et al.* [112]. This is illustrated in Figs. 32 and 33 that have a similar qualitative behavior. We find that the triple point is located at $(f_*/M_P c^2, M_*/(M_P^2/m)) = (0.0891, 0.969)$ while the exact values obtained by Helfer *et al.* [112] are $(f_*/M_P c^2, M_*/(M_P^2/m))_{\text{exact}} = (0.3, 2.4)$. One reason for this quantitative difference is due to the approximations inherent to our analytical study: Gaussian ansatz (see Sec. V) and qualitative treatment of relativistic effects (see Sec. X). Another reason for this discrepancy,

that we believe to be more important, is due to the fact that we are not using the same axionic potential. Helfer *et al.* [112] solve the KGE equations for a real SF described by the instantonic potential (28) while we consider a complex SF described by the polynomial potential (37) involving an attractive $|\psi|^4$ term and a repulsive $|\psi|^6$ term. As an example of this intrinsic difference, we note that, in our model, the maximum mass of dilute axion stars, if it were calculated exactly, would be always smaller than the Kaup mass $M_{\text{Kaup}} = 0.633M_P^2/m$ (see Appendix A 5), and would tend to the Kaup mass in the noninteracting limit $f/M_P c^2 \rightarrow +\infty$ (see Fig. 32). By contrast, the maximum mass obtained by Helfer *et al.* [112] is always larger than the Kaup mass for the values of $f/M_P c^2$ considered, and apparently does not tend to the Kaup mass when $f/M_P c^2 \rightarrow +\infty$ (see Fig. 33).²⁷ This may be an effect of the periodicity and anharmonicity of the instantonic axion potential that is not captured in our polynomial approximation.

XI. SUMMARY

In this section, we summarize the main results of our study, and express the physical quantities of axion stars (mass, radius, density) in terms of dimensional variables. We give the prefactors when we know their exact values. Otherwise, we just give the scaling of the physical quantities when the prefactor is uncertain (the prefactors obtained from the Gaussian ansatz can be found in the main text if needed).

A. Weakly self-interacting axions

We first consider weakly self-interacting axions with $|\lambda| < |\lambda|_* \sim (m/M_P)^2$. For $M \ll M_{\text{max,GR}}^{\text{dilute}} \sim M_P^2/m$ and $R \gg R_{*,\text{GR}}^{\text{dilute}} \sim \lambda_C$, we are on the branch (I) of the mass-radius relation corresponding to stable dilute axion stars. They can be described by Newtonian gravity. Suppose that we increase their mass M (physically, this can happen if the axion stars accrete matter from the surrounding or collide with other stars). As we approach the general relativistic maximum mass $M_{\text{max,GR}}^{\text{dilute}}$, the axion stars become more and more relativistic (they also become denser and denser). Close to $M_{\text{max,GR}}^{\text{dilute}}$, the mass-radius relation forms a spiral. For $M > M_{\text{max,GR}}^{\text{dilute}}$ there is no equilibrium state and the axion star collapses into a black hole. For noninteracting complex boson stars ($\lambda = 0$), the maximum mass and the minimum radius are $M_{\text{max,GR}}^{\text{dilute}} = 0.633M_P^2/m$ and $R_{*,\text{GR}}^{\text{dilute}} = 6.03\lambda_C$ [95, 96]. For self-interacting axion stars, the maximum mass and

the minimum radius are not expected to change appreciably with $|\lambda|$ when $\lambda < |\lambda|_* \sim (m/M_P)^2$ (see Sec. X A).

B. Strongly self-interacting axions

We now consider strongly self-interacting axions with $|\lambda| > |\lambda|_* \sim (m/M_P)^2$. This is the regime of physical interest for QCD axions and ULAs. For $M < M_{\text{max,N}}^{\text{dilute}} = 5.073M_P/\sqrt{|\lambda|}$ and $R_{99} > R_{*,\text{N}}^{\text{dilute}} = 1.1\sqrt{|\lambda|}(M_P/m)\lambda_C$ [34, 35], we are on the branch (I) of the mass-radius relation corresponding to stable dilute axion stars. They can be described by Newtonian gravity up to the maximum mass $M_{\text{max,N}}^{\text{dilute}}$. Let us assume that the mass progressively increases. For $M > M_{\text{max,N}}^{\text{dilute}}$ the axion stars collapse and become denser and denser until the collapse is stopped by the repulsive self-interaction. In that case, the system reaches an equilibrium state corresponding to a dense axion star located on the branch (III-a) of the mass-radius relation on which self-gravity is weak. As discussed in [110], this collapse may be associated with an emission of relativistic axions (bosenova phenomenon). The star may also undergo a series of implosions and explosions. Assuming that the mass is approximately conserved during the collapse, the resulting dense axion star has a radius $R_{\text{coll}} = 0.812|\lambda|^{1/6}(M_P/m)^{1/3}\lambda_C$. For sufficiently small masses and sufficiently small radii, the dense axion stars on the branch (III-a) of the mass-radius relation can be described by Newtonian gravity. They have a constant density $\rho_{\text{dense}} = 2.25|\lambda|^{-1}m/\lambda_C^3$, independent of their mass. As their mass increases further and approaches $M_{\text{max,GR}}^{\text{dense}} \sim |\lambda|^{1/2}M_P^3/m^2$ (which is of the order of M_0) corresponding to a radius $R_{*,\text{GR}}^{\text{dense}} \sim |\lambda|^{1/2}(M_P/m)\lambda_C$, the dense axion stars become relativistic.²⁸ Close to $M_{\text{max,GR}}^{\text{dense}}$, the mass-radius relation forms a spiral or stops suddenly (see footnote 25). For $M > M_{\text{max,GR}}^{\text{dense}}$, there is no equilibrium state and the axion star collapses into a black hole. Let us now assume that the mass decreases along the branch (III-a) of the mass radius relation. When $M < M_{\text{min,N}}^{\text{dense}} \sim m/|\lambda|$ and $R < R_{*,\text{N}}^{\text{dense}} \sim \lambda_C$, the dense axion star explodes and forms a dilute axion star of radius $R_{\text{exp}} \sim |\lambda|(M_P/m)^2\lambda_C$ or, more realistically, disperses to infinity.

It is interesting to see that the mass scales $M_{\text{max,GR}}^{\text{dilute}} \sim M_c \sim M_P^2/m$, $M_{\text{max,N}}^{\text{dilute}} \sim M_a \sim M_P/\sqrt{|\lambda|}$, $M_{\text{max,GR}}^{\text{dense}} \sim M_r \sim \sqrt{|\lambda|}M_P^3/m^2$ and $M_{\text{min,N}}^{\text{dense}} \sim M_i \sim m/|\lambda|$ representing the scalings M_P^2/m , $M_P/\sqrt{|\lambda|}$, $\sqrt{|\lambda|}M_P^3/m^2$ and $m/|\lambda|$ play a fundamental role in the problem.

²⁷ Helfer *et al.* [112] do not consider the noninteracting limit $f/M_P c^2 \rightarrow +\infty$ because they mention that high-particle physics generically imposes $f < M_P c^2$.

²⁸ Depending on the exact values of $M_{\text{max,GR}}^{\text{dense}}$ and M_0 , the dense axion stars may be in a Newtonian regime for $M_0 < M < M_{\text{max,GR}}^{\text{dense}}$ corresponding to the beginning of the branch (III-b) of the mass-radius relation where the self-attraction of the bosons is negligible, before becoming relativistic for $M \sim M_{\text{max,GR}}^{\text{dense}}$.

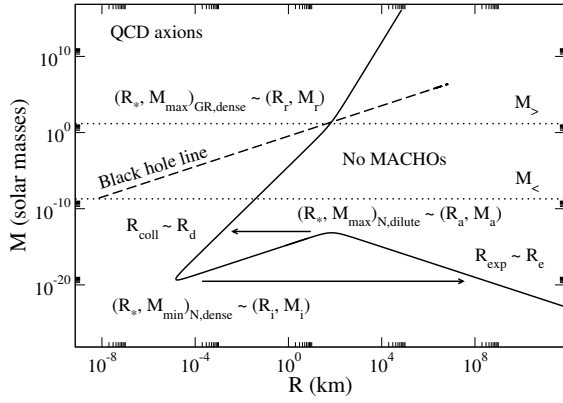


FIG. 34: Mass-radius relation of QCD axion stars with dimensional variables obtained from the Gaussian ansatz. The Newtonian maximum mass and the corresponding radius of dilute axion stars are $M_{\max,N}^{\text{dilute}} = 6.92 \times 10^{-14} M_{\odot}$ and $R_{*,N}^{\text{dilute}} = 71.5 \text{ km}$. The radius of the dense axion star resulting from the collapse of a dilute axion star with the maximum mass is $R_{\text{coll}} = 1.25 \text{ m}$. The general relativistic maximum mass and the corresponding radius of dense axion stars are $M_{\max,GR}^{\text{dense}} = 23.6 M_{\odot}$ and $R_{*,GR}^{\text{dense}} = 69.8 \text{ km}$. Close to $M_{\max,GR}^{\text{dense}}$, the mass-radius relation $M(R)$ may form a spiral or stop suddenly. The Newtonian minimum mass and the corresponding radius of dense axion stars are $M_{\min,N}^{\text{dense}} = 4.40 \times 10^{-20} M_{\odot}$ and $R_{*,N}^{\text{dense}} = 1.70 \text{ cm}$. The radius of the dilute axion star resulting from the explosion of a dense axion star with the minimum mass is $R_{\text{exp}} = 2.25 \times 10^8 \text{ km}$ suggesting that the star is dispersed away. From the exact results of [35], we get $M_{\max,N}^{\text{dilute}} = 6.46 \times 10^{-14} M_{\odot}$ and $R_{*,99,N}^{\text{dilute}} = 227 \text{ km}$. From the exact results of [103], we get $M_{\min,N}^{\text{dense}} = 1.2 \times 10^{-20} M_{\odot}$ and $R_{*,N}^{\text{dense}} = 1.81 \text{ cm}$. The authors of [103] find no solution with $M_{\max,N}^{\text{dense}} = 1.9 M_{\odot}$ (see Appendix E 2). From the exact result of Appendix E, we get $R_{\text{coll}} = 0.756 \text{ m}$. We have also plotted the lines $M_{<} = 2 \times 10^{-9} M_{\odot}$ and $M_{>} = 15 M_{\odot}$ between which MACHOs are excluded from observations [115, 116]. We see that axionic DM can be in the form of gases of axions, or dilute axion stars, or dense axion stars with $M < 2 \times 10^{-9} M_{\odot}$, or dense axion stars (or axionic black holes) with $M > 15 M_{\odot}$.

C. Analogy with white dwarfs, neutron stars and black holes

We have represented the mass-radius relations of QCD axion stars and ULA clusters in Figs. 34 and 35 using dimensional variables. Numerical values of the characteristic masses and radii are given in the captions. We note that the mass-radius relation of QCD axion stars reported in Fig. 34, and obtained analytically in our approximate study, is in good agreement with the exact mass-radius relation of QCD axion stars obtained numerically by Braaten *et al.* [103] (see their Fig. 1). We also note that Figs. 34 and 35 look the same except for a change of scales. However, this impression is misleading in the sense that there is no scale-invariance in the general mass-radius relation (103) of axion stars: the self-interaction parameter δ cannot be eliminated from this

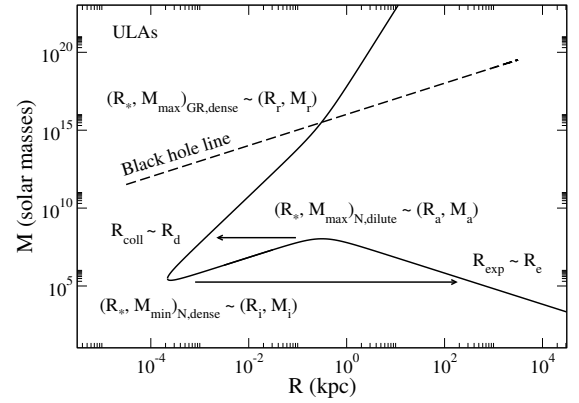


FIG. 35: Mass-radius relation of ULA clusters (this concerns more precisely their solitonic core) with dimensional variables obtained from the Gaussian ansatz. The Newtonian maximum mass and the corresponding radius of dilute clusters are $M_{\max,N}^{\text{dilute}} = 1.07 \times 10^8 M_{\odot}$ and $R_{*,N}^{\text{dilute}} = 0.313 \text{ kpc}$. The radius of the dense cluster resulting from the collapse of a dilute cluster with the maximum mass is $R_{\text{coll}} = 1.23 \text{ pc}$. The general relativistic maximum mass and corresponding radius of dense clusters are $M_{\max,GR}^{\text{dense}} = 3.19 \times 10^{15} M_{\odot}$ and $R_{*,GR}^{\text{dense}} = 0.305 \text{ kpc}$. Close to $M_{\max,GR}^{\text{dense}}$, the mass-radius relation $M(R)$ may form a spiral or stop suddenly. However, the general relativistic maximum mass $M_{\max,GR}^{\text{dense}} = 3.19 \times 10^{15} M_{\odot}$ is too large to describe the solitonic core of ULA clusters suggesting that ULA clusters never form black holes. The Newtonian minimum mass and corresponding radius of dense clusters are $M_{\min,N}^{\text{dense}} = 2.30 \times 10^5 M_{\odot}$ and $R_{*,N}^{\text{dense}} = 0.253 \text{ pc}$. The radius of the dilute cluster resulting from the explosion of a dense cluster with the minimum mass is $R_{\text{exp}} = 290 \text{ kpc}$ suggesting that the cluster is dispersed away. From the exact results of [35], we get $M_{\max,N}^{\text{dilute}} = 10^8 M_{\odot}$ and $R_{*,N}^{\text{dilute}} = 1 \text{ kpc}$. From the exact result of Appendix E, we find $R_{\text{coll}} = 0.745 \text{ pc}$.

relation by a simple rescaling. Only the branch of dilute axion stars is invariant for sufficiently small values of δ (see footnote 14).

The mass-radius relation of axion stars shares some analogies with the mass-radius relation of fermion stars at $T = 0$ such as white dwarf stars and neutron stars based on the Harrison-Wakano-Wheeler (HWW) equation of state (compare Figs. 34 and 35 with Fig. 7 of [144], Fig. 2 of [149], or Fig. 11.2 of [150]). For sufficiently small masses and sufficiently large radii, a star at $T = 0$ (more properly at $T \ll T_F$ where T_F is the Fermi temperature) is in a Newtonian nonrelativistic white dwarf stage where the gravitational attraction is balanced by the quantum pressure of the degenerate electron gas on account of the Pauli exclusion principle. As we approach the Newtonian Chandrasekhar maximum mass $M_{\max,N}^{\text{WD}} = 0.776 M_P^3 / H^2 = 1.44 M_{\odot}$ (where H is the proton mass), special relativistic effects come into play

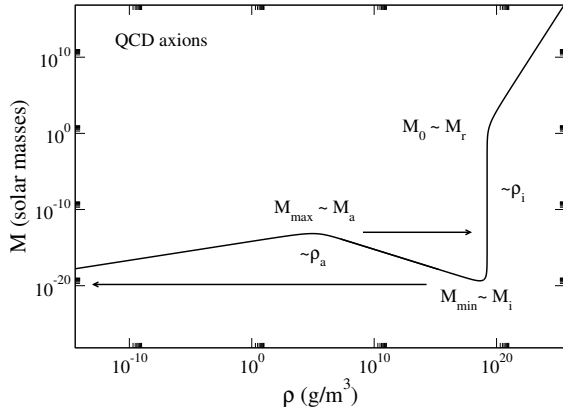


FIG. 36: Mass-density relation of QCD axion stars with dimensional variables obtained from the Gaussian ansatz. The density of dilute axion stars at the Newtonian maximum mass is $\rho = 8.98 \times 10^4 \text{ g/m}^3$ (the exact value obtained from the results of [35] is $\rho = 2.62 \times 10^3 \text{ g/m}^3$). The constant density of dense axion stars in the TF + nongravitational regime, which includes the dense axion star resulting from the collapse of a dilute axion star with the maximum mass, is $\rho_{\text{dense}} = 1.68 \times 10^{19} \text{ g/m}^3$ (the exact value obtained from the results of Appendix E is $\rho_{\text{dense}} = 7.07 \times 10^{19} \text{ g/m}^3$). The density of dense axion stars at the general relativistic maximum mass is $\rho = 3.30 \times 10^{19} \text{ g/m}^3$. The density of dense axion stars at the Newtonian minimum mass is $\rho = 4.21 \times 10^{18} \text{ g/m}^3$ (the exact value obtained from the results of [103] is $\rho = 9.61 \times 10^{17} \text{ g/m}^3$). The density of the dilute axion star resulting from the explosion of a dense axion star with the minimum mass is $\rho = 1.84 \times 10^{-21} \text{ g/m}^3$ suggesting that the star is dispersed away.

and the radius $R_{*,N}^{\text{WD}}$ tends to zero.²⁹ Above the Chandrasekhar maximum mass, white dwarf stars collapse, the electrons and the protons combine together to form neutrons, and the system becomes a neutron star in which the gravitational attraction is balanced by the quantum pressure of the degenerate neutron gas (some mass is ejected during the collapse). Above the Oppenheimer-Volkoff general relativistic maximum mass $M_{\text{max,GR}}^{\text{NS}} = 0.384 M_P^3 / m^2 = 0.710 M_\odot$ (where m is the neutron mass), corresponding to a radius $R_{*,GR}^{\text{NS}} = 9.18 \text{ km}$, the neutron star collapses into a black hole.

In the analogy between axion stars and fermion stars, the dilute axion stars are the counterpart of the white dwarf stars and the dense axion stars are the counterpart of the neutron stars. Similarly, the Newtonian maximum mass of dilute axion stars $M_{\text{max,N}}^{\text{dilute}}$ is the counterpart of the Newtonian Chandrasekhar maximum mass of white dwarf stars $M_{\text{max,N}}^{\text{WD}}$ and the general relativistic maximum mass of dense axion stars $M_{\text{max,GR}}^{\text{dense}}$ is the counterpart of

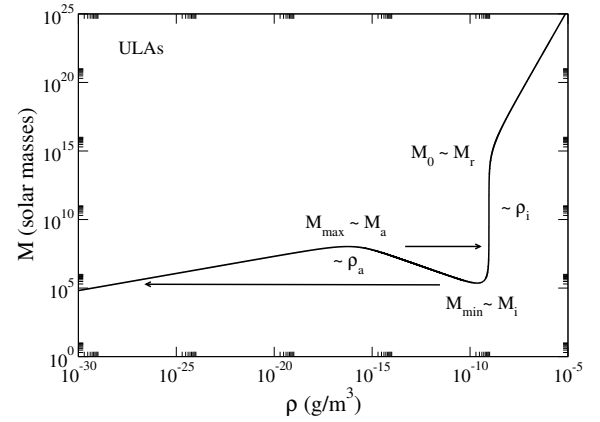


FIG. 37: Mass-density relation of ULAs clusters (this concerns more precisely their solitonic core) with dimensional variables obtained from the Gaussian ansatz. The density of dilute axionic clusters at the Newtonian maximum mass is $\rho = 5.63 \times 10^{-17} \text{ g/m}^3$ (the exact value obtained from the results of [35] is $\rho = 1.62 \times 10^{-18} \text{ g/m}^3$). The constant density of dense axionic clusters in the TF + nongravitational regime, which includes the dense axionic cluster resulting from the collapse of a dilute axionic cluster with the maximum mass, is $\rho = 9.21 \times 10^{-10} \text{ g/m}^3$ (the exact value obtained from the results of Appendix E is $\rho = 3.88 \times 10^{-9} \text{ g/m}^3$). The density of dense axionic clusters at the general relativistic maximum mass is $\rho = 1.82 \times 10^{-9} \text{ g/m}^3$. The density of dense axion stars at the Newtonian minimum mass is $\rho = 2.30 \times 10^{-10} \text{ g/m}^3$. The density of the dilute axionic clusters resulting from the explosion of a dense axionic cluster with the minimum mass is $\rho = 1.52 \times 10^{-28} \text{ g/m}^3$ suggesting that the cluster is dispersed away.

the general relativistic Oppenheimer-Volkoff maximum mass of neutron stars $M_{\text{max,GR}}^{\text{NS}}$. Close to the general relativistic maximum mass, the mass-radius relation of dense axion stars is expected to form a spiral (see footnote 25 for more details) similarly to the mass-radius relation of neutron stars.

There is, however, a difference in the sense that the Chandrasekhar mass is larger than the Oppenheimer-Volkoff maximum mass while, in the present context, the Newtonian maximum mass of dilute axion stars is smaller than the general relativistic maximum mass of dense axion stars. In this sense, the mass-radius relation of axion stars is more similar to the mass-radius relation of compact stars obtained with the Skyrme-Cameron-Saakyan (SCS) equation of state (see Fig. 3 of [149]). Indeed, in more realistic models of neutron stars, the maximum mass is substantially larger than the ideal Oppenheimer-Volkoff limit, being in the range $2 - 2.4 M_\odot$, and overcomes the Chandrasekhar limiting mass of white dwarf stars. This is why Shapiro and Teukolsky [151] draw a mass-radius relation (see their Fig. 6.3) in which the maximum mass of neutron stars is larger than the maximum mass of white dwarf stars. This figure, which can be seen as a synthesis of Figs. 2 and 3 of [149] is similar

²⁹ If we take general relativity into account, we obtain a minimum radius $R_{*,GR}^{\text{WD}} = 102 \text{ km}$.

to Figs. 34 and 35 of axion stars.

We finally note that we can determine the stability of the different configurations of fermion stars represented in Fig. 7 of [144], in Figs. 2 and 3 of [149], in Fig. 11.2 of [150] and in Fig. 6.3 of [151] by using the Poincaré theory of linear series of equilibria, as shown here in the case of axion stars. The Poincaré theory provides an alternative, and a generalization, of the $M(R)$ theorem devised by Wheeler [144] in the physics of compact objects (white dwarfs and neutron stars) and used in [149–151].

For completeness, we have also represented the mass-density relations of QCD axion stars and ULA clusters in Figs. 36 and 37 using dimensional variables. Again, they present analogies with the mass-central density relations of fermion stars (compare Figs. 36 and 37 with Fig. 5 of [144] or Figs. 6.2 and 9.1 of [151]). If the mass-radius relation of dense axion stars forms a spiral close to $M_{\max, \text{GR}}^{\text{dense}}$ (for the reason explained previously), then the mass-density relation will display damped oscillations as in the case of neutron stars (see the previous references and Fig. 1 of [152]).

D. Analogy with self-gravitating fermions at finite temperature

We have seen that axion stars are expected to undergo a phase transition between a dilute phase and a dense phase when the self-interaction parameter δ is below a critical value $\delta_c = 0.0075$.

This phase transition is similar to the Van der Waals phase transition between a gas and a liquid when the temperature T is below a critical value T_c . However, in our case, the phase transition is not of thermodynamical origin since we work at $T = 0$. On the other hand, the metastable axionic stars generally have very long lifetimes so that the first order phase transition that is expected to occur at M_t does not take place in practice. Only the zeroth order phase transitions at M_{\max} and M_{\min} are physical. By contrast, in the Van der Waals fluid, the metastable states are less robust and the liquid/gas coexistence usually exists at a unique pressure P_t determined by the Maxwell construction. Therefore, a first order phase transition really occurs in that case.

The nature of phase transitions in axion stars at $T = 0$ is also similar to the nature of phase transitions in the Newtonian self-gravitating Fermi gas at finite temperature studied in [148]. Above a critical size, self-gravitating fermions³⁰ are expected to display a first order phase transition between a gaseous phase and a condensed phase with a core-halo structure. In the gaseous phase, the gravitational attraction is equilibrated by the thermal pressure. In the condensed phase, the gravi-

tational attraction is counterbalanced by the quantum pressure of the degenerate Fermi gas arising from the Pauli exclusion principle. In the self-gravitating Fermi gas at finite temperature, metastable states have very long lifetimes so that the predicted first order phase transition does not take place in practice, like in the case of axion stars. Only the zeroth order phase transitions at the spinodal points take place. The mass-radius relations of Fig. 10 can be compared with the caloric curves of Fig. 14 in [148] and the phase diagram of Fig. 25 can be compared with the phase diagrams of Figs. 34 and 35 in [148]. The phenomenology of the phase transitions in the self-gravitating Fermi gas at finite temperature is, however, richer than the phenomenology of the phase transitions in axion stars because this system displays two critical points, one in each statistical ensembles (microcanonical and canonical). This is related to the phenomenon of ensembles inequivalence that characterizes the thermodynamics of systems with long-range interactions like self-gravitating systems [148, 153].

XII. CONCLUSION

In this paper, we have studied the mass-radius relation of dilute and dense axion stars by using an analytical approach based on a Gaussian ansatz like in our previous works [34, 73, 78]. Our results are in good qualitative, and even quantitative, agreement with the exact results of Chavanis and Delfini [35] for dilute axion stars, and the exact results of Braaten *et al.* [103] for dense axion stars, obtained by solving the GPP equations numerically (see the caption of Fig. 34 for a comparison between our approximate analytical results and the exact numerical ones). An interest of our analytical study is that it allows us to vary more easily the parameters and to isolate characteristic mass, length and density scales that play an important role in the problem.

We have also taken into account relativistic effects in a qualitative manner and obtained an estimate of the maximum mass of axion stars set by general relativity. Above that mass, the axion star is expected to collapse into a black hole. We have obtained a phase diagram presenting a triple point separating dilute axion stars, dense axion stars (that may be the remnants of a bosonova) and axionic black holes. This phase diagram is in qualitative agreement with the phase diagram obtained numerically by Helfer *et al.* [112] by solving the KGE equations. The quantitative disagreement in the position of the triple point may be due to our approximations or to the fact that we use a different potential. Indeed, Helfer *et al.* [112] solve the KGE equations for a real SF described by the instantonic potential (28) while we consider a complex SF described by a polynomial potential (37) involving an attractive $|\psi|^4$ term and a repulsive $|\psi|^6$ term.

The evolution of axion stars above the maximum mass is still unclear and deserves further research. As we have

³⁰ They may represent electrons in white dwarf stars, neutrons in neutron stars, or massive neutrinos in DM models.

indicated, the collapse of a dilute axion star can lead to a dense axion star (possibly associated with an emission of relativistic axions - bosenova) when $M \gtrsim M_{\max}$, or to a black hole when $M \gg M_{\max}$. The mass of the dense axion star, or the mass of the black hole, that results from the collapse of a dilute axion star is not precisely known and should be studied in detail through numerical simulations. As shown by Levkov [110], the collapse of a dilute axion star with $M \gtrsim M_{\max}$ may be accompanied by an important emission of radiation (bosenova) that carries away a large part of the initial mass (about 30%).

A first domain of application of these ideas concerns the formation and the evolution of mini QCD axion stars. Dilute QCD axion stars have a maximum mass $M_{\max}^{\text{exact}} = 6.46 \times 10^{-14} M_{\odot}$ [see Eq. (47)], a minimum radius $(R_{99}^*)^{\text{exact}} = 227 \text{ km}$ [see Eq. (48)], a maximum density $\rho_{\text{dilute}}^{\text{exact}} = 2.62 \times 10^3 \text{ g/m}^3$ [see Eq. (50)], and a typical minimum energy $E_{\text{tot}} \sim -2.35 \times 10^{25} \text{ erg}$ [see Eq. (146)] while dense QCD axion stars that result from the collapse of a dilute QCD axion star with the maximum mass $M_{\max}^{\text{exact}} = 6.46 \times 10^{-14} M_{\odot}$ have a radius $R_{\text{coll}}^{\text{exact}} = 0.756 \text{ m}$ [see Eq. (E22)] and a density $\rho_{\text{dense}}^{\text{exact}} = 7.07 \times 10^{19} \text{ g/m}^3$ [see Eq. (E4)]. They are far from the black hole limit since $R/R_S = 3.96 \times 10^9 \gg 1$. They have a low pulsation period $2\pi/\omega_{\text{coll}}^{\text{exact}} = 6.70 \times 10^{-9} \text{ s}$ [see Eq. (E23)], and a very negative energy $(E_{\text{tot}}^{\text{coll}})_{\text{exact}} = -3.25 \times 10^{40} \text{ erg}$ [see Eq. (E24)]. We can check that self-gravity is weak in dense QCD axion stars since $GM^2/R = 1.46 \times 10^{31} \text{ ergs} \ll |(E_{\text{tot}}^{\text{coll}})_{\text{exact}}|$. The formation time of a dense QCD axion star (collapse time) is $t_{\text{coll}} = 2.90\gamma^{-1/4}t_D = 9.86\gamma^{-1/4} \text{ hrs}$ where $\gamma = M/M_{\max} - 1$ (see Eq. (185) of [73]). For $\gamma = 10^{-4}$ this gives $t_{\text{coll}} = 98.6 \text{ hrs}$. Both dilute and dense QCD axion stars could be the constituents of DM in the form of MACHOs. Axionic black holes with a mass larger than $15M_{\odot}$ could possibly exist (see Fig. 34) but their mechanism of formation (if relevant) is uncertain and remains to be established.

On the other hand, the collisions between dilute axion stars and neutron stars possessing a strong magnetic field [130–132, 134], the collisions between dilute axion stars and the magnetized accretion disk of a black hole [133], or the collapse of dilute axion stars above their maximum mass [110], can produce a radiation (of different origin). If the mass of the axion star is rapidly transformed into electromagnetic radiation, for example during the collision with a neutron star (magnetar) or an accretion disk, this radiation should be detectable. Interestingly, as noted by [130–134], the characteristics of mini QCD axion stars are consistent with the observed properties of recently detected unusual radio pulses known as FRBs: The observed frequency of the bursts ($\sim 1.4 \text{ GHz}$) is comparable to the proper frequency $mc^2/(2\pi\hbar)$ of the QCD axion with a mass $m \sim 10^{-5} \text{ eV}/c^2$, the observed rate of the bursts in a galaxy ($\sim 10^{-3}$ per year) gives a mass of axion stars $\sim 10^{-12} M_{\odot}$ which is comparable to

their maximum mass,³¹ the size of the emitting source must be less than 300 km which is consistent with the radius of axion stars R_{99}^* , and the large amount of radiation energy of the bursts ($\sim 10^{38} - 10^{40} \text{ erg}$) is of the order of $M_{\max}c^2$. Therefore, FRBs can be matched in a model which assumes an explosive decay of axion stars as a result of collisions with neutron stars and accretion disks. In the case of a collapse above the maximum mass, the spectrum obtained in [110] may serve as a distinctive signature of the axion star collapse.

Another domain of application of these ideas concerns the formation and the evolution of DM halos. It has been proposed that DM halos could be giant BECs made of ULAs. In this context, an important issue is whether the DM particle has a self-interaction or not. In many works, the self-interaction of the boson is neglected because the self-interaction parameter $|\lambda| \sim 10^{-91}$ is extremely small. However, we have shown in this paper and in previous ones [35, 73, 77] that even for apparently small values of $|\lambda|$ we can be in a regime of strong self-interaction. This is because, for the self-interaction to be weak in the context of DM halos, $|\lambda|$ has to be small with respect to $(M_P/m)^2$, not with respect to 1. Now, for ULAs, $(M_P/m)^2$ is a very small quantity of the order of 10^{-98} . Therefore, we claim that the self-interaction of the axions has to be taken into account, and that ULAs are actually in a strong self-interaction regime (see Appendix L for a more detailed discussion).

The sign of the scattering length is also of crucial importance. A repulsive self-interaction has the tendency to stabilize a DM halo. In that case, the mass of the ULA can be substantially larger than the value it should have to account for the observations if it were noninteracting (see Appendix D of [77]). For example, a fiducial model of self-repulsive bosons corresponds to a mass $m = 3 \times 10^{-21} \text{ eV}/c^2$ and a self-interaction constant $\lambda/8\pi = 1.69 \times 10^{-87}$ [54, 77]. The boson mass is about one order of magnitude larger than the value $m = 2.92 \times 10^{-22} \text{ eV}/c^2$ required in the absence of self-interaction. This is precisely what we need to alleviate some tensions with the observations of the Lyman- α forest [75] or some tensions with the observations of the abundance of ultrafaint lensed galaxies at redshift $z \simeq 6$ in the Hubble Frontier Fields (HFF) [154]. Therefore, a repulsive self-interaction may solve these problems (see the Remark at the end of Appendix D.4 of [77]). We also note that cosmological constraints from CMB and big bang nucleosynthesis (BBN) exclude the possibility that the bosons are noninteracting [54, 77]. In these models, which are based on a complex SF, a repulsive self-interaction between the bosons ($a_s > 0$) seems to be the most likely in order to account for the observations.

³¹ Iwazaki [131] identifies this mass with the mass of axitons $M_{\text{axiton}} \sim 10^{-12} M_{\odot}$ [94] while it would be more relevant to identify it with the maximum mass $M_{\max} = 6.46 \times 10^{-14} M_{\odot}$ of dilute axion stars [34, 35].

However, if the DM particle is an axion (a real SF), the self-interaction is generally attractive ($a_s < 0$). Now, an attractive self-interaction has the tendency to destabilize a DM halo. A DM halo can be stable only below a maximum mass [34, 35]. Recently, Diez-Tejedor and Marsh [155] have obtained some constraints on the value of the axion decay constant. They argue that if the axion mass is temperature-independent, then $m \sim 10^{-22} \text{ eV}/c^2$ and $f \gtrsim 10^{16} \text{ GeV}$. They also consider the possibility that the axion mass is temperature-dependent and discuss the case where $m \sim 10^{-22} \text{ eV}/c^2$ and $f \sim 10^{15} \text{ GeV}$, corresponding to $a_s = -1.96 \times 10^{-64} \text{ fm}$ and $\lambda = -2.50 \times 10^{-93}$. This leads to dilute axion stars with a maximum mass $M_{\text{max}}^{\text{exact}} = 1.11 \times 10^9 (f/m) M_{\odot}$ [see Eq. (47)], a minimum radius $(R_{99}^*)^{\text{exact}} = 428/(fm) \text{ pc}$ [see Eq. (48)], a maximum density $\rho_{\text{dilute}}^{\text{exact}} = 2.29 \times 10^{-16} (f^4 m^2) \text{ g}/\text{m}^3$ [see Eq. (50)], and a typical minimum energy $E_{\text{tot}} \sim -1.19 \times 10^{56} (f^3/m) \text{ ergs}$ [see Eq. (146)], where the axion mass m is measured in units of $10^{-22} \text{ eV}/c^2$ and the axion decay constant f is measured in units of 10^{15} GeV . We should regard $M_{\text{max}}^{\text{exact}} = 1.11 \times 10^9 (f/m) M_{\odot}$ as the maximum mass of the solitonic core of the DM halo, not the maximum mass of the DM halo itself (see footnote 1). If some DM halos have an axionic solitonic core of mass $M_{\text{core}} > M_{\text{max}}^{\text{exact}} = 1.11 \times 10^9 (f/m) M_{\odot}$, they should undergo core collapse. One possibility is that they form a dense axionic nucleus (axion star) of mass $M_{\text{max}}^{\text{exact}} = 1.11 \times 10^9 (f/m) M_{\odot}$, radius $R_{\text{coll}}^{\text{exact}} = 0.949/(mf^{1/3}) \text{ pc}$ [see Eq. (E22)], and density $\rho_{\text{dense}}^{\text{exact}} = 2.10 \times 10^{-8} (m^2 f^2) \text{ g}/\text{m}^3$ [see Eq. (E4)]. This nucleus is not a black hole, not even a relativistic object, because $R/R_S = 8930 f^{-4/3} \gg 1$. This dense nucleus has a very low pulsation period $2\pi/\omega_{\text{coll}}^{\text{exact}} = 8.24/(mf^{1/3}) \text{ yrs}$ [see Eq. (E23)] and a very negative energy $(E_{\text{tot}}^{\text{coll}})_{\text{exact}} = -5.59 \times 10^{62} (f/m) \text{ ergs}$ [see Eq. (E24)]. Note that this energy is not of gravitational origin since $GM^2/R \sim 1.11 \times 10^{59} (f^{7/3}/m) \text{ ergs} \ll |E_{\text{tot}}^{\text{coll}}|_{\text{exact}}$ for $f \lesssim 1$. The formation time of a dense axionic nucleus (collapse time) is $t_{\text{coll}} = 2.90 \gamma^{-1/4} t_D = 3.80/(\gamma^{1/4} m f^2) \text{ Myrs}$ where $\gamma = M/M_{\text{max}} - 1$ [see Eq. (185) of [73]]. For $\gamma = 10^{-4}$ this gives $t_{\text{coll}} = 38.0/(mf^2) \text{ Myrs}$.

We therefore suggest that DM halos may harbor a dense axionic nucleus (supermassive axion star). We note that part (or all?) of the mass and energy of the dilute axionic solitonic core may be lost during the collapse and could be converted in a radiation as studied by Levkov *et al.* [110]. Indeed, the unstable solitonic core of a DM halo with a mass $M_{\text{core}} > M_{\text{max}}$ could undergo a series of collapses and explosions and emit waves with a very characteristic spectrum [see Fig 3(a) of [110]]. In that case, the dense axionic nucleus would be the remnant of a bosonova. It would have a mass $\sim 10^9 M_{\odot}$ if there is no mass loss during the collapse or smaller if there is mass loss (e.g. by radiation) during the collapse.

Interestingly, the mass $\sim 10^9 M_{\odot}$ is of the order of the maximum mass of the dark objects that are reported to exist at the center of the galaxies. It is also interesting to note that certain characteristics of dense ax-

ionic nuclei are similar to the characteristics of quasistellar radio sources (quasars and active galactic nuclei) in strong radio galaxies. They both present large energies $\sim 10^{60} \text{ ergs}$ and cyclic variations with periods of the order of 10 years. At present, it is believed that a quasar consists of a supermassive black hole with a mass $\sim 10^6 - 10^9 M_{\odot}$ surrounded by an accretion disk of gas. Their source of energy and their large luminosity is the result of the immense friction caused by the gas falling towards the black hole. The energy is released in the form of electromagnetic radiation. The active galactic nucleus radiates in the direction of a jet directed by the lines of a magnetic field. The jet velocity is close to the speed of light. Quasars cease to shine when the supermassive black hole has consumed all the gas and dust around it. Our galaxy may have been active in the past but is now quiet since its central black hole has nothing to “eat” to produce radiation.

Instead of a central black hole, other possibilities have been contemplated. In a first attempt to understand the source of the energy emitted by the radio galaxies, Hoyle and Fowler [156] suggested the possibility that a mass of the order of $10^8 M_{\odot}$ has condensed in the galactic nucleus into a supermassive star in which nuclear-energy generation takes place. Such an object would be supported in hydrostatic equilibrium almost entirely by radiation pressure. In the Hoyle-Fowler theory, the energy corresponds to the gravitational energy of the supermassive star. Assuming a radius $\sim 10^{-3} \text{ pc}$ (corresponding to a superstar with a density $\sim 1 \text{ g}/\text{m}^3$ and $R/R_S \sim 104$), this gives a gravitational energy $GM^2/R \sim 10^{60} \text{ ergs}$. The gravitational energy GM^2/R may be made available for external dissipation necessary to transfer angular momentum from the supermassive star to the surrounding material. Hoyle and Fowler [156] imagined a magnetized field torroidally wound between the central star and a surrounding disk and argued that the energy stored in the magnetic field could be of the order of GM^2/R . This powerful field may explode throwing jets from the center of galaxies. The superstars of mass $10^8 M_{\odot}$ imagined by Hoyle and Fowler [156] were found to be unstable from the viewpoint of general relativity, but Fowler [157] showed that stability is gained if they are rotating.

More recently, it has been proposed that a supermassive neutrino star (fermion ball) may form at the center of a galaxy. It may arise through a phase transition in a self-gravitating gas of neutrinos with mass $17.2 \text{ keV}/c^2$ from a dilute gaseous phase to a condensed phase when the temperature passes below a critical value [148, 158–161]. These compact dark objects with a mass $10^6 - 10^9 M_{\odot}$ and a radius $\sim 10^{-3} - 10^{-2} \text{ pc}$ could mimic the effect of a supermassive black hole purported to exist in the core of galaxies to power active galactic nuclei and quasars.

Similarly, we could consider the possibility that the central dark object in a galaxy is a boson star [162, 163] or a supermassive dense axion star. Realistic models should take into account the formation of an accretion disc around the boson star. An important difference be-

tween dense axion stars and black holes resides in the fact that dense axion stars (like certain types of fermion balls and boson stars) are nonrelativistic objects.³² Still they can have a huge mass $M \sim 10^9 M_\odot$ and a huge energy $E_{\text{tot}} \sim -Mc^2 \sim -10^{60}$ ergs.

In conclusion, the formation of dense axion stars, the radiation emitted during the collapse of a dilute axion star above the maximum mass (bosenova), or the electromagnetic radiation created during the collision of a dilute axion star with a neutron star or an accretion disk, may have different applications of great astrophysical interest such as FRBs and, possibly, the formation of super-massive galactic nuclei accompanied by intense radiation. These topics will be the object of future research.

Appendix A: Characteristic scales

1. The scales associated with self-interacting nonrelativistic self-gravitating BECs

We introduce the mass and length scales associated with nonrelativistic self-gravitating BECs with a $|\psi|^4$ self-interaction:

$$M_a = \left(\frac{\hbar^2}{Gm|a_s|} \right)^{1/2}, \quad R_a = \left(\frac{|a_s|\hbar^2}{Gm^3} \right)^{1/2}. \quad (\text{A1})$$

In the context of our paper, these scales characterize the maximum mass $M_{\text{max},N}^{\text{dilute}}$ and the minimum radius $R_{*,N}^{\text{dilute}}$ of nonrelativistic dilute axion stars. We also introduce the density scale

$$\rho_a = \frac{M_a}{R_a^3} = \frac{Gm^4}{\hbar^2 a_s^2}, \quad (\text{A2})$$

the timescale

$$t_a = \frac{1}{\sqrt{G\rho_a}} = \frac{|a_s|\hbar}{Gm^2}, \quad (\text{A3})$$

the global energy scale

$$E_a = \frac{GM_a^2}{R_a} = \left(\frac{Gm\hbar^2}{|a_s|^3} \right)^{1/2}, \quad (\text{A4})$$

the individual energy scale³³

$$\frac{E_a}{N_a} = \frac{Gm^2}{|a_s|}, \quad (\text{A5})$$

where $N_a = M_a/m$, and the pressure scale

$$P_a = \frac{G^2 m^5}{|a_s|^3 \hbar^2}. \quad (\text{A6})$$

These scales can be expressed in terms of f and λ as

$$M_a = \left(\frac{32\pi f^2 \hbar}{Gm^2 c^3} \right)^{1/2} = \left(\frac{8\pi \hbar c}{|\lambda| G} \right)^{1/2}, \quad (\text{A7})$$

$$R_a = \left(\frac{\hbar^3 c^3}{32\pi f^2 Gm^2} \right)^{1/2} = \left(\frac{|\lambda| \hbar^3}{8\pi Gm^4 c} \right)^{1/2}, \quad (\text{A8})$$

$$\rho_a = \frac{(32\pi f^2)^2 Gm^2}{\hbar^4 c^6} = \frac{(8\pi)^2 Gm^6 c^2}{\lambda^2 \hbar^4}, \quad (\text{A9})$$

$$t_a = \frac{\hbar^2 c^3}{32\pi f^2 Gm} = \frac{|\lambda| \hbar^2}{8\pi Gm^3 c}, \quad (\text{A10})$$

$$E_a = (32\pi f^2)^{3/2} \left(\frac{G}{\hbar m^2 c^9} \right)^{1/2} = \left(\frac{8\pi}{|\lambda|} \right)^{3/2} \left(\frac{Gm^4 c^3}{\hbar} \right)^{1/2}, \quad (\text{A11})$$

$$\frac{E_a}{N_a} = 32\pi f^2 \frac{Gm}{\hbar c^3} = \frac{8\pi}{|\lambda|} \frac{Gm^3 c}{\hbar}, \quad (\text{A12})$$

$$P_a = (32\pi f^2)^3 \frac{G^2 m^2}{\hbar^5 c^9} = \left(\frac{8\pi}{|\lambda|} \right)^3 \frac{G^2 m^8 c^3}{\hbar^5}. \quad (\text{A13})$$

They can also be written as

$$M_a = \left(\frac{r_S}{2|a_s|} \right)^{1/2} \frac{M_P^2}{m} = \sqrt{32\pi} \frac{f}{M_P c^2} \frac{M_P^2}{m} \\ = \left(\frac{8\pi}{|\lambda|} \right)^{1/2} M_P, \quad (\text{A14})$$

$$R_a = \left(\frac{2|a_s|}{r_S} \right)^{1/2} \lambda_C = \frac{1}{\sqrt{32\pi}} \frac{M_P c^2}{f} \lambda_C \\ = \left(\frac{|\lambda|}{8\pi} \right)^{1/2} \frac{M_P}{m} \lambda_C, \quad (\text{A15})$$

$$\rho_a = \left(\frac{r_S}{2|a_s|} \right)^2 \frac{M_P^2}{m \lambda_C^3} = 1024\pi^2 \left(\frac{f}{M_P c^2} \right)^4 \frac{M_P^2}{m \lambda_C^3} \\ = \left(\frac{8\pi}{|\lambda|} \right)^2 \left(\frac{m}{M_P} \right)^4 \frac{M_P^2}{m \lambda_C^3} = \left(\frac{8\pi}{|\lambda|} \right)^2 \frac{m^3}{M_P^2 \lambda_C^3}, \quad (\text{A16})$$

$$t_a = \frac{2|a_s|}{r_S} \frac{\lambda_C}{c} = \frac{1}{32\pi} \left(\frac{M_P c^2}{f} \right)^2 \frac{\lambda_C}{c} \\ = \frac{|\lambda|}{8\pi} \left(\frac{M_P}{m} \right)^2 \frac{\lambda_C}{c}, \quad (\text{A17})$$

³² We note that the compact object associated with Sagittarius A* has a mass $M = 4.31 \times 10^6 M_\odot$ and a radius $R \leq 10^{10}$ km implying $R/R_S \leq 785$. Therefore, this object is not necessarily a black hole unless its radius is much smaller than $R \leq 10^{10}$ km.

³³ Dimensionally, the eigenenergy scale is equal to the gravitational energy of two bosons separated by a distance equal to their scattering length. This is also the gravitational energy of a boson of “size” $|a_s|$.

$$\begin{aligned}
E_a &= \left(\frac{r_S}{2|a_s|} \right)^{3/2} \frac{M_P^2 c^2}{m} = (32\pi)^{3/2} \left(\frac{f}{M_P c^2} \right)^3 \frac{M_P^2 c^2}{m} \\
&= \left(\frac{8\pi}{|\lambda|} \right)^{3/2} \left(\frac{m}{M_P} \right)^3 \frac{M_P^2 c^2}{m} = \left(\frac{8\pi}{|\lambda|} \right)^{3/2} \frac{m^2 c^2}{M_P},
\end{aligned} \tag{A18}$$

$$\begin{aligned}
\frac{E_a}{N_a} &= \frac{r_S}{2|a_s|} m c^2 = 32\pi \left(\frac{f}{M_P c^2} \right)^2 m c^2 \\
&= \frac{8\pi}{|\lambda|} \left(\frac{m}{M_P} \right)^3 M_P c^2 = \frac{8\pi}{|\lambda|} \frac{m^3 c^2}{M_P^2},
\end{aligned} \tag{A19}$$

$$\begin{aligned}
P_a &= \left(\frac{r_S}{2|a_s|} \right)^3 \frac{M_P^2 c^2}{m \lambda_C^3} = (32\pi)^3 \left(\frac{f}{M_P c^2} \right)^6 \frac{M_P^2 c^2}{m \lambda_C^3} \\
&= \left(\frac{8\pi}{|\lambda|} \right)^3 \left(\frac{m}{M_P} \right)^6 \frac{M_P^2 c^2}{m \lambda_C^3} = \left(\frac{8\pi}{|\lambda|} \right)^3 \frac{m^5 c^2}{M_P^4 \lambda_C^3}.
\end{aligned} \tag{A20}$$

These scales appear in our works [34, 35, 73] on self-gravitating BECs with attractive or repulsive self-interactions. For a repulsive self-interaction ($a_s > 0$), they determine the transition between the noninteracting limit and the TF limit. For an attractive self-interaction ($a_s < 0$), M_a is of the order of the maximum mass of a self-gravitating BEC and R_a is of the order of the corresponding radius. The mass-radius relation $M(R)$ (parametrized by the central density ρ_0) of nonrelativistic self-gravitating BECs with a repulsive self-interaction is represented in Fig. 4 of [35]. In the noninteracting limit, the mass-radius relation is given by Eq. (51). In the TF limit, the radius of the system is independent of its mass and given by Eq. (53). At the transition, combining Eqs. (51) and (53), we obtain the scalings of Eq. (A1). The mass-radius relation $M(R)$ (parametrized by the central density ρ_0) of nonrelativistic self-gravitating BECs with an attractive self-interaction is represented in Fig. 6 of [35]. In the noninteracting limit, the mass-radius relation is given by Eq. (51). In the nongravitational limit, the mass-radius relation is given by Eq. (52).³⁴ At the transition, combining Eqs. (51) and (52), we obtain the scalings of Eqs. (A1). They determine the maximum mass of Newtonian self-attracting boson stars above which there is no equilibrium state. By numerically solving the GPP equations, or the equivalent hydrodynamic equations, one gets the exact values $M_{\max} = 1.012M_a$, $R_{\min} = 5.5\lambda_a$ and $(\rho_0)_{\max} = 0.5\rho_a$ [35].

³⁴ We recall that these configurations are unstable.

2. The scales associated with self-attractive and self-repulsive nongravitational BECs

We introduce the mass and length scales associated with nongravitational BECs with an attractive $|\psi|^4$ self-interaction ($a_s < 0$) and a repulsive $|\psi|^6$ self-interaction:

$$M_i = \frac{\hbar}{|a_s|c}, \quad R_i = \frac{\hbar}{mc}. \tag{A21}$$

We note that R_i coincides with the Compton wavelength λ_C of the bosons. To our knowledge, these scales have not been introduced previously. In the context of our paper, they characterize the minimum mass $M_{\min, N}^{\text{dense}}$ and the corresponding radius $R_{*, N}^{\text{dense}}$ of dense axion stars, as well as their minimum radius $R_{\min, N}^{\text{dense}}$ and the corresponding mass $M_{*, N}^{\text{dense}}$. We also introduce the density scale

$$\rho_i = \frac{M_i}{R_i^3} = \frac{m^3 c^2}{|a_s| \hbar^2}. \tag{A22}$$

It characterizes the constant density ρ^{dense} of nongravitational dense axion stars in the TF limit. These scales can be expressed in terms of f and λ as

$$M_i = \frac{32\pi f^2}{m c^4} = \frac{8\pi m}{|\lambda|}, \tag{A23}$$

$$\rho_i = \frac{32\pi m^2 f^2}{\hbar^3 c} = \frac{8\pi m^4 c^3}{|\lambda| \hbar^3}. \tag{A24}$$

They can also be written as

$$\begin{aligned}
M_i &= \frac{r_S}{2|a_s|} \frac{M_P^2}{m} = 32\pi \left(\frac{f}{M_P c^2} \right)^2 \frac{M_P^2}{m} \\
&= \frac{8\pi}{|\lambda|} \left(\frac{m}{M_P} \right)^2 \frac{M_P^2}{m} = \frac{8\pi m}{|\lambda|},
\end{aligned} \tag{A25}$$

$$R_i = \lambda_C, \tag{A26}$$

$$\begin{aligned}
\rho_i &= \frac{r_S}{2|a_s|} \frac{M_P^2}{m \lambda_C^3} = 32\pi \left(\frac{f}{M_P c^2} \right)^2 \frac{M_P^2}{m \lambda_C^3} \\
&= \frac{8\pi}{|\lambda|} \left(\frac{m}{M_P} \right)^2 \frac{M_P^2}{m \lambda_C^3} = \frac{8\pi}{|\lambda|} \frac{m}{\lambda_C^3}.
\end{aligned} \tag{A27}$$

3. The scales associated with dense axion stars resulting from a collapse at $M_{\max, N}^{\text{dilute}}$

We introduce the mass and length scales associated with dense axion stars resulting from the collapse of dilute axion stars at the critical point:

$$M_d = \frac{\hbar}{\sqrt{Gm|a_s|}}, \quad R_d = \left(\frac{|a_s| \hbar^6}{Gm^7 c^4} \right)^{1/6}. \tag{A28}$$

They characterize $M_{\max, N}^{\text{dilute}}$ and R_{coll} . We also introduce the density scale

$$\rho_d = \frac{M_d}{R_d^3} = \frac{m^3 c^2}{|a_s| \hbar^2}. \quad (\text{A29})$$

We note that

$$M_d = M_a, \quad \rho_d = \rho_i. \quad (\text{A30})$$

These scales can be expressed in terms of f and λ as in Eqs. (A7), (A24) and

$$R_d = \left(\frac{\hbar^7}{32\pi G f^2 m^6 c} \right)^{1/6} = \left(\frac{|\lambda| \hbar^7}{8\pi G m^8 c^5} \right)^{1/6}. \quad (\text{A31})$$

They can also be written as in Eqs. (A14), (A27) and

$$\begin{aligned} R_d &= \left(\frac{2|a_s|}{r_S} \right)^{1/6} \lambda_C = \frac{1}{(32\pi)^{1/6}} \left(\frac{M_P c^2}{f} \right)^{1/3} \lambda_C \\ &= \left(\frac{|\lambda|}{8\pi} \right)^{1/6} \left(\frac{M_P}{m} \right)^{1/3} \lambda_C. \end{aligned} \quad (\text{A32})$$

4. The scales associated with dilute axion stars resulting from an explosion at $M_{\min, N}^{\text{dense}}$

We introduce the mass and length scales associated with dilute axion stars resulting from the explosion of dense axion stars at the critical point:

$$M_e = \frac{\hbar}{|a_s| c}, \quad R_e = \frac{|a_s| \hbar c}{G m^2}. \quad (\text{A33})$$

They characterize $M_{\min, N}^{\text{dense}}$ and R_{exp} . We also introduce the density scale

$$\rho_e = \frac{M_e}{R_e^3} = \frac{G^3 m^6}{|a_s|^4 \hbar^2 c^4}. \quad (\text{A34})$$

We note that

$$M_e = M_i. \quad (\text{A35})$$

These scales can be expressed in terms of f and λ as in Eq. (A23) and

$$R_e = \frac{\hbar^2 c^4}{32\pi f^2 G m} = \frac{|\lambda| \hbar^2}{8\pi G m^3}, \quad (\text{A36})$$

$$\rho_e = \frac{(32\pi f^2)^4 G^3 m^2}{\hbar^6 c^{16}} = \frac{(8\pi)^4 G^3 m^{10}}{\lambda^4 \hbar^6}. \quad (\text{A37})$$

They can also be written as in Eq. (A25) and

$$\begin{aligned} R_e &= \frac{2|a_s|}{r_S} \lambda_C = \frac{1}{32\pi} \left(\frac{M_P c^2}{f} \right)^2 \lambda_C \\ &= \frac{|\lambda|}{8\pi} \left(\frac{M_P}{m} \right)^2 \lambda_C, \end{aligned} \quad (\text{A38})$$

$$\begin{aligned} \rho_e &= \left(\frac{r_S}{2|a_s|} \right)^4 \frac{M_P^2}{m \lambda_C^3} = (32\pi)^4 \left(\frac{f}{M_P c^2} \right)^8 \frac{M_P^2}{m \lambda_C^3} \\ &= \left(\frac{8\pi}{|\lambda|} \right)^4 \left(\frac{m}{M_P} \right)^8 \frac{M_P^2}{m \lambda_C^3} = \left(\frac{8\pi}{|\lambda|} \right)^4 \frac{m^7}{M_P^6 \lambda_C^3}. \end{aligned} \quad (\text{A39})$$

5. The scales associated with noninteracting relativistic self-gravitating BECs

We introduce the mass and length scales associated with noninteracting relativistic self-gravitating BECs:

$$M_c = \frac{\hbar c}{G m}, \quad R_c = \frac{\hbar}{m c}. \quad (\text{A40})$$

They are connected to each other by the relativistic scaling $M_c = c^2 R_c / G$. We note that R_c coincides with the Compton wavelength λ_C of the bosons. In the context of our paper, these scales characterize the maximum mass $M_{\max, \text{GR}}^{\text{dilute}}$ and the corresponding radius $R_{*, \text{GR}}^{\text{dilute}}$ of relativistic dilute axion stars. We also introduce the density scale

$$\rho_c = \frac{M_c}{R_c^3} = \frac{m^2 c^4}{G \hbar^2}. \quad (\text{A41})$$

These scales can be rewritten as

$$M_c = \frac{M_P^2}{m}, \quad R_c = \lambda_C, \quad \rho_c = \frac{M_P^2}{m \lambda_C^3}. \quad (\text{A42})$$

These scales appear in the works of Kaup [95] and Ruffini and Bonazzola [96] on boson stars. M_c is of the order of the maximum mass of a noninteracting relativistic self-gravitating BEC and R_c is of the order of the corresponding radius. The mass-radius relation $M(R)$ of noninteracting self-gravitating BECs in the context of general relativity is represented in Fig. 3 of [164]. In the nonrelativistic limit, the mass-radius relation is given by Eq. (51). This relation is obtained by balancing the repulsive quantum pressure against the attractive gravitational force (see Sec. II. G of [34]). The radius of the system is of the order of the particle's de Broglie wavelength $R \sim \hbar/mv$ associated with the virial velocity $v \sim (GM/R)^{1/2}$. The system becomes relativistic when its radius R approaches the Schwarzschild radius R_S . Combining Eqs. (51) and (67) we obtain the scalings of Eq. (A40) (see Appendix B of [34]). They determine the maximum mass and minimum radius of noninteracting boson stars beyond which there is no equilibrium state. By numerically solving the KGE equations, one gets the exact values $M_{\max} = 0.633 M_c$ and $(R_{95})_{\min} = 6.03 R_c$ (leading to $R_{95}/R_S = 4.76$) [95, 96]. The mass-radius relation forms a spiral but the configurations with a central density $\epsilon_0 \geq (\epsilon_0)_{\max}$ where $(\epsilon_0)_{\max}$ is the density corresponding to the configuration with the maximum mass are unstable.

6. The scales associated with self-attractive and self-repulsive relativistic self-gravitating BECs

We introduce the mass and length scales associated with relativistic self-gravitating BECs with an attractive $|\psi|^4$ self-interaction ($a_s < 0$) and a repulsive $|\psi|^6$ self-interaction:

$$M_r = \left(\frac{|a_s| \hbar^2 c^4}{G^3 m^3} \right)^{1/2}, \quad R_r = \left(\frac{|a_s| \hbar^2}{G m^3} \right)^{1/2}. \quad (\text{A43})$$

They are connected to each other by the relativistic scaling $M_r = c^2 R_r / G$. In the context of our paper, these scales characterize the maximum mass $M_{\text{max,GR}}^{\text{dense}}$ and the corresponding radius $R_{\text{max,GR}}^{\text{dense}}$ of general relativistic dense axion stars as well as the mass M_0 and the corresponding radius R_0 marking the transition between nongravitational and nonattractive Newtonian dense axion stars. We also introduce the density scale

$$\rho_r = \frac{M_r}{R_r^3} = \frac{m^3 c^2}{|a_s| \hbar^2}. \quad (\text{A44})$$

We note that

$$R_r = R_a, \quad \rho_r = \rho_i \quad (\text{A45})$$

These scales can be expressed in terms of f and λ as in Eqs. (A8), (A24) and

$$M_r = \left(\frac{\hbar^3 c^7}{32\pi f^2 G^3 m^2} \right)^{1/2} = \left(\frac{|\lambda| \hbar^3 c^3}{8\pi G^3 m^4} \right)^{1/2}. \quad (\text{A46})$$

They can also be written as in Eqs. (A15), (A27) and

$$\begin{aligned} M_r &= \left(\frac{2|a_s|}{r_S} \right)^{1/2} \frac{M_P^2}{m} = \frac{1}{\sqrt{32\pi}} \frac{M_P c^2}{f} \frac{M_P^2}{m} \\ &= \left(\frac{|\lambda|}{8\pi} \right)^{1/2} \frac{M_P^3}{m^2}. \end{aligned} \quad (\text{A47})$$

To the best of our knowledge, these scales have not been introduced previously. However, apart from the presence of the absolute value, R_r and M_r have the same expressions as the scales associated with relativistic BECs with a purely repulsive $|\psi|^4$ self-interaction ($a_s > 0$). These scales appear in the works of Colpi *et al.* [97] and Tkachev [98] on boson stars and in the work of Chavanis and Harko [99] on neutron stars with a superfluid core (BEC stars). In that context, M_r is of the order of the maximum mass of a relativistic self-gravitating BEC in the TF limit and R_r is of the order of the corresponding radius. The mass-radius relation $M(R)$ (parametrized by the central density ϵ_0) of self-gravitating BECs with a repulsive self-interaction in the context of general relativity is represented in Fig. 9 of [99]. In the nonrelativistic limit, the radius of the system is independent of its mass and given by Eq. (53). It is obtained by balancing the repulsive pressure force coming from the self-interaction

against the attractive gravitational force (see Sec. II. G of [34]). The system becomes relativistic when its radius R approaches the Schwarzschild radius R_S . Combining Eqs. (53) and (67), we obtain the scalings of Eq. (A43) (see Appendix B of [34]). They determine the maximum mass and the minimum radius of self-repulsive boson stars beyond which there is no equilibrium state. By numerically solving the KGE equations [97] or the equivalent hydrodynamic equations [99], one gets the exact values $M_{\text{max}} = 0.307 M_r$, $R_{\text{min}} = 1.92 R_r$ and $(\epsilon_0)_{\text{max}} = 1.19 \rho_r c^2$ (leading to $R/R_S = 3.13$). Chavanis and Harko [99] have argued that, because of their superfluid core, neutron stars could actually be BEC stars. Indeed, the neutrons could form Cooper pairs and behave as bosons of mass $2m_n$ (where $m_n = 0.940 \text{ GeV}/c^2$ is the mass of the neutron). By adjusting the value of the self-interaction constant, the maximum mass of these BEC stars could account for the abnormal mass (in the range $2 - 2.4 M_\odot$) of certain neutron stars [165–170] that is much larger than the Oppenheimer-Volkoff limit $M_{\text{OV}} = 0.384 M_P^3/m^2 = 0.709 M_\odot$ based on the assumption that neutron stars are ideal fermion stars [120].

Appendix B: On the collapse time of axion stars

When the self-interaction is purely attractive, the collapse time $t_{\text{coll}}(M, R_0)$ of a dilute axion star with mass $M > M_{\text{max}}$ and initial radius R_0 towards a singular state of vanishing radius ($R = 0$) has been studied in detail in our previous paper [73] within the Gaussian ansatz. Eby *et al.* [108] used our formalism to study the collapse time of a dilute axion star towards a dense axion star, taking into account the fact that the dense axion star has a nonzero radius $R > 0$. We show below that this refinement is not necessary. Since the radius of a dense axion star is extremely small, the same result for $t_{\text{coll}}(M, R_0)$ is obtained by taking $R = 0$ as in [73] instead of $R = 0^+$ as in [108]. The results obtained in [73] are also relevant if, instead of forming a dense axion star, the collapse of a dilute axion star is followed by an explosion and an emission of relativistic axions as in the simulations of Levkov *et al.* [110]. For a purely attractive self-interaction, $t_{\text{coll}}(M, R_0)$ represents the moment at which the self-similar collapse leads to a finite time singularity. When collisions between axions are taken into account, it gives a good estimate of the time at which the explosion takes place. Again, the value of t_{coll} is not expected to be very sensitive on the exact value of R_e at which the explosion takes place as long as $R_e \ll R_0$.

Within the Gaussian ansatz, the equation of motion of a self-gravitating BEC with mass M and initial radius R_0 is given by [73]:

$$\int_{R_0}^{R(t)} \frac{dR}{\sqrt{E_{\text{tot}} - V(R)}} = \pm \left(\frac{2}{M} \right)^{1/2} t, \quad (\text{B1})$$

where the sign $+$ corresponds to an explosion/expansion

and the sign $-$ to a collapse/contraction. In the following, we assume $\delta < \delta_c$ and $M > M_{\max}(\delta)$ so that a collapse takes place. If the BEC starts from R_0 without initial velocity ($\dot{R}_0 = 0$), its total energy is given by $E_{\text{tot}} = V(R_0)$. In the case where the collapse is stopped by the self-repulsion of the bosons, the collapse time is given by

$$t_{\text{coll}} = \left(\frac{M}{2}\right)^{1/2} \int_R^{R_0} \frac{dR'}{\sqrt{V(R_0) - V(R')}}, \quad (\text{B2})$$

where R is the radius of the resulting dense axion star with mass M . It is given by Eq. (101), which can be rewritten in the more convenient form

$$\delta = \frac{R^3(1 + R^2)M - 2R^4}{6M^2}. \quad (\text{B3})$$

For $\delta \ll 1$, we have in good approximation

$$R \sim (6M\delta)^{1/3}. \quad (\text{B4})$$

For given M and R_0 , we can plot $t_{\text{coll}}(\delta)$ by proceeding as follows (for simplicity, we do not explicitly write M and R_0 in the function $t_{\text{coll}}(M, R_0, \delta)$). Instead of prescribing δ , we prescribe R and calculate $\delta(R)$ from Eq. (B3). We can then determine $t_{\text{coll}}(R)$ from Eq. (B2). By running R between 0 and 1, we can obtain $t_{\text{coll}}(\delta)$ in parametric form, with parameter R . The result of this calculation is reported in Fig. 38 for $M = 2$ and $R_0 = 1$.

This “exact” result can be compared with the “approximate” expression of t_{coll} obtained in [73] which amounts to taking $\delta = R = 0$ in Eq. (B2). For $M = 2$ and $R_0 = 1$, we have found that $t_{\text{coll}} = 0.676301\dots$ [73]. As expected, this “approximate” result provides an excellent approximation of the “exact” result for the values of δ corresponding to QCD axions and ULAs.

For QCD axions with $\delta = 8.88 \times 10^{-16}$, we obtain $R = 2.20 \times 10^{-5}$ and $t_{\text{coll}} = 0.676$ (in terms of dimensional variables, this corresponds to $R_{\min} = 1.57$ m and $t_{\text{coll}} = 2.30$ hrs).

For ULAs with $\delta = 1.02 \times 10^{-8}$, we obtain $R = 4.96 \times 10^{-3}$ and $t_{\text{coll}} = 0.676$ (in terms of dimensional variables, this corresponds to $R = 1.55$ pc and $t_{\text{coll}} = 10.5$ Myrs).

Appendix C: Dirac peaks and black holes

1. Absence of global minimum of energy in the case of a purely attractive self-interaction

Let us consider a self-gravitating BEC with a purely attractive $|\psi|^4$ self-interaction as in [73]. The energy functional $E_{\text{tot}}[\rho]$ is given by Eq. (D1), where $V(\rho)$ is given by the first term of Eq. (44). To show the absence of a global energy minimum E_{tot} at fixed mass M , it is sufficient to construct a particular family of distributions $\rho_\epsilon(\vec{x})$, depending on a parameter ϵ , that conserve the mass M , and for which the energy $E_{\text{tot}}[\rho_\epsilon]$ tends to

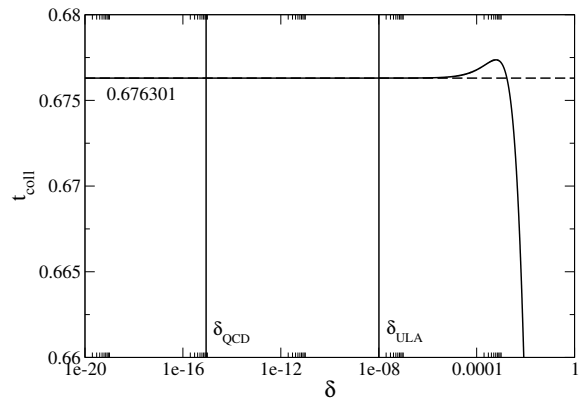


FIG. 38: Collapse time of axion stars as a function of δ for $M = 2$ and $R_0 = 1$. We note that it presents a small maximum at $\delta = 6.16 \times 10^{-4}$ before decreasing. The dashed line corresponds to the result obtained in [73] by taking $\delta = 0$. It provides an excellent approximation of the collapse time of QCD axions ($\delta_{\text{QCD}} = 8.88 \times 10^{-16}$) and ULAs ($\delta_{\text{ULA}} = 1.02 \times 10^{-8}$).

$-\infty$ when $\epsilon \rightarrow 0$ (we use a strategy similar to the one developed in Appendixes A and B of [124] in relation to the thermodynamics of self-gravitating systems). In the present context, it is convenient to take a Gaussian density profile of size $R = \epsilon$ [34, 73, 78]. We also take $\mathbf{u} = \mathbf{0}$ since we are interested in equilibrium states. In that case, the total energy $E_{\text{tot}} = V(R) = V(\epsilon)$ is given by Eq. (77) without the last term (corresponding to a repulsive self-interaction). For $R = \epsilon \rightarrow 0$, the total energy clearly goes to $-\infty$ implying the absence of a global minimum of energy for any mass M .

The previous argument proves the absence of a global minimum of energy at fixed mass. However, it says nothing about the possible existence of local energy minima (metastable states). As we have seen, for $M < M_{\max}$, there exists a local energy minimum corresponding to a dilute axion star [34]. As discussed in Sec. IX C, this metastable state can have a very long lifetime so it is physically relevant. However, for $M > M_{\max}$ there is no equilibrium state at all and the system is expected to collapse.³⁵

The family of distributions constructed above forms a Dirac peak $\rho(\vec{x}) = M\delta(\vec{x})$ when $R = \epsilon \rightarrow 0$. This Dirac peak has an infinitely negative energy ($E_{\text{tot}} \rightarrow -\infty$). Therefore, we expect that a self-gravitating BEC with a purely attractive $|\psi|^4$ self-interaction will ultimately form a Dirac peak if $M > M_{\max}$. As discussed in the Introduction, this Dirac peak may appear in the post-collapse regime of the dynamics. Since a Dirac peak has

³⁵ This assumes that the system remains compact. If not, a star of mass $M > M_{\max}$ can break into different pieces of mass $M' < M_{\max}$ and form a stable system [105].

a finite mass and a vanishing radius, it may be regarded as a form of “extreme” black hole. However, to make things rigorous, and prove that a self-gravitating BEC with a purely attractive self-interaction really collapses into a black hole, one must take general relativity into account and study the KGE equations.

2. The case of self-gravitating BECs with attractive and repulsive self-interactions

We now consider a self-gravitating BEC with an attractive $|\psi|^4$ self-interaction and a repulsive $|\psi|^6$ self-interaction. In that case, we have seen that there exists a global minimum of energy for any mass M . There also exists a local minimum of energy for $M_{\min} < M < M_{\max}$ as described in Sec. IX. In the limit $\delta \rightarrow 0$, it seems that the general mass-radius relation (103) reduces to the mass-radius relation (105) of dilute axion stars, suggesting that above M_{\max} the system forms a Dirac peak according to the arguments given in Appendix C 1. However, when repulsive interactions are included, we have shown that dense axion stars with $M_{\max} < M < M_0$ are *not* black holes, whatever the value of $\delta > 0$. We note furthermore that $M_0 \rightarrow +\infty$ when $\delta \rightarrow 0$ implying that this result is true for any mass M . How can we solve this apparent paradox?

We must be careful that the limit $\delta \rightarrow 0$ is not equivalent to $\delta = 0$. Indeed, for $\delta \rightarrow 0$ the mass-radius relation tends to the mass-radius relation of dilute axion stars only for sufficiently large radii. At very small radii we recover the branch of dense axion stars that is pushed towards the vertical axis $R = 0$ as $\delta \rightarrow 0$. To be specific, let us consider a dense axion star with a mass $M \in [M_{\max}, M_0]$ resulting from the collapse of a dilute axion star. It is a global minimum of energy (fully stable state). For a fixed mass M and $\delta \rightarrow 0$ its radius tends to zero as $R \sim (6\delta M)^{1/3}$ [see Eq. (142)] and its energy tends to $-\infty$ as $E_{\text{tot}} \sim -M/(36\delta)$ [see Eq. (148)]. Therefore, in the limit $\delta \rightarrow 0$, a dense axion star tends towards a Dirac peak $\rho(\vec{x}) \rightarrow M\delta(\vec{x})$. This is compatible with the case $\delta = 0$ considered in Appendix C 1. However, for $\delta > 0$, the dense axion star is never a black hole, whatever small δ may be (the reason is that, in dimensionless variables, the Schwarzschild radius depends on δ). Indeed, it would be a black hole if $R \sim R_S$. Since $R \sim (6\delta M)^{1/3}$ [see Eq. (142)] and $R_S = 3.23M\delta$ [see Eq. (197)], we find that $R \gg R_S$ for $\delta \rightarrow 0$ (assuming $M \ll M_0 = 1/6\delta$). Therefore, the black hole criterion is never satisfied for dense axion stars although they tend to Dirac peaks as $\delta \rightarrow 0$. On the contrary, such structures are highly nonrelativistic. In conclusion, for $\delta \rightarrow 0$ the dense axion star tends towards a Dirac peak, but it is never a black hole.

Another way to resolve this apparent paradox is to notice that the limit $\delta \rightarrow 0$ corresponds to $c \rightarrow +\infty$ [see Eq. (92)], the other parameters being fixed. In this limit, the Schwarzschild radius $R_S = 2GM/c^2$ tends to

zero as $1/c^2$ while, according to Eq. (134), the radius of the dense axion star tends to zero as $1/c^{2/3}$. Therefore, $R \gg R_S$ implying that the dense axion star is not a black hole.

Remark: Things would be different if the coefficient of the repulsive term in Eq. (45) involved a new parameter χ , independent of the other parameters, measuring the strength of the repulsive self-interaction. In that case, when $\chi \rightarrow 0$, the radius of the star would tend to zero ($R \rightarrow 0$) and, at some point, R would be of the order of R_S implying that the star is a black hole. This situation does not occur for axion stars because the coefficient of the repulsive term in Eq. (45) depends on a_s , m , c and \hbar so that it is completely constrained.

Appendix D: The Poincaré theory of linear series of equilibria

In this Appendix, we briefly explain how one can apply the Poincaré [143] theory of linear series of equilibria to our problem in order to determine the stability of axion stars.

In a static Universe ($a = 1$ and $H = 0$), the GPP equations (9) and (10), or the equivalent quantum EP equations (15)-(18), conserve the total energy

$$E_{\text{tot}} = \int \rho \frac{\mathbf{u}^2}{2} d\mathbf{x} + \frac{1}{m} \int \rho Q d\mathbf{x} + \int V(\rho) d\mathbf{x} + \frac{1}{2} \int \rho \Phi d\mathbf{x} \quad (\text{D1})$$

and the mass

$$M = \int \rho d\mathbf{x}, \quad (\text{D2})$$

where we have expressed these functionals in terms of the hydrodynamic variables ρ and \mathbf{u} (see Ref. [78] for details). As a result, a stable equilibrium state is a (local) minimum of energy E_{tot} at fixed mass M .³⁶ We therefore have to consider the minimization problem

$$E_{\text{tot}}(M) = \min_{\rho, \mathbf{u}} \{E_{\text{tot}}[\rho, \mathbf{u}] \mid M \text{ fixed}\}. \quad (\text{D3})$$

An equilibrium state, being a critical point of energy at fixed mass, is determined by the variational principle

$$\delta E_{\text{tot}} - \frac{\mu}{m} \delta M = 0, \quad (\text{D4})$$

where μ is a Lagrange multiplier that takes into account the mass constraint. Using the results of [78], this variational problem gives $\mathbf{u} = \mathbf{0}$ (the equilibrium state is

³⁶ From general considerations, one can show that a global minimum of energy at fixed mass is nonlinearly dynamically stable [171]. However, we shall also be interested in local minima of energy at fixed mass that are linearly dynamically stable. These states are metastable but they have very long lifetimes (see Sec. IX C) so they are fully relevant for our problem.

static) and the eigenvalue equation

$$m\Phi + mh(\rho) + Q = \mu, \quad (\text{D5})$$

where we recall that $Q = -(\hbar^2/2m)\Delta\sqrt{\rho}/\sqrt{\rho}$ and $\Phi(\mathbf{r}) = -G \int \rho(\mathbf{r}')|\mathbf{r} - \mathbf{r}'|^{-1} d\mathbf{r}'$. The density can be written formally as

$$\rho = h^{-1} \left(\frac{\mu}{m} - \frac{Q}{m} - \Phi \right). \quad (\text{D6})$$

We note, however, that Eq. (D6) is an integrodifferential equation. Taking the gradient of Eq. (D5), and using Eq. (20), we obtain the condition of hydrostatic equilibrium

$$\nabla P + \rho \nabla \Phi + \frac{\rho}{m} \nabla Q = \mathbf{0}. \quad (\text{D7})$$

This returns the steady state of the quantum Euler equation (17). Equation (D5) is also equivalent to the time-independent GP equation obtained by substituting into Eq. (9) a wavefunction of the form $\psi(\mathbf{r}, t) = \phi(\mathbf{r})e^{-iEt/\hbar}$ and making the identification

$$\mu = E. \quad (\text{D8})$$

This shows that the Lagrange multiplier (chemical potential) in the variational problem associated with Eq. (D3) is equal to the eigenenergy E . Inversely, the eigenenergy E may be interpreted as a chemical potential.

We call critical point (or equilibrium state) any solution of the variational principle (D4). The ensemble of these critical points forms a series of equilibria. An equilibrium state is determined by the differential equation (D5). This equation is equivalent to the fundamental equation of hydrostatic equilibrium obtained by coupling Eq. (D7) to the Poisson equation (18). There can be several equilibrium states with the same mass M because the variational problem (D4) can have several solutions: a global minimum of energy (fully stable state), a local minimum of energy (metastable state), and a maximum or saddle point of energy (unstable state). It is convenient to represent all these solutions on the series of equilibria (see, e.g., Fig. 22) in order to see its global structure and apply the Poincaré theory (see below). On the other hand, as already indicated, local minima of energy (metastable states) can be as much physical, or even more physical, than global minima of energy for the timescales achieved in astrophysics (see Sec. IX C and Refs. [148, 172] in the context of stellar systems).

Stable equilibrium states correspond to (local or global) minima of energy at fixed mass. The stability of an equilibrium state can be determined by studying the sign of the second order variations of the energy functional E_{tot} whose general expression is given in Ref. [78]. An equilibrium state is stable if $\delta^2 E_{\text{tot}} > 0$ for all perturbations that conserve mass. In general, it is difficult to study the sign of $\delta^2 E_{\text{tot}}$ because we have to solve a complicated eigenvalue equation. Fortunately, the stability of the system can be directly deduced from topological properties of continuous series of equilibria. This

graphical method just requires to solve the first order variational problem (D4). This is the so-called Poincaré theory of linear series of equilibria. It works as follows. According to Eqs. (D4) and (D8), the eigenenergy $E/m = \partial E_{\text{tot}}/\partial M$ is the variable conjugate to the mass M (constraint) with respect to the total energy E_{tot} (potential to minimize). Therefore, if we plot E as a function of M along the series of equilibria, we have the following results:

(i) A change of stability can occur only at a turning point of mass.

(ii) One mode of stability is lost if the curve $E(M)$ turns clockwise and one mode of stability is gained if the curve $E(M)$ rotates anti-clockwise.

Therefore, if we know a limit in which the configuration is stable, we can use the Poincaré theory to deduce the stability of the whole series of equilibria.

This theory does not tell us if an equilibrium state is fully stable (global minimum of E_{tot} at fixed M) or metastable (local minimum of E_{tot} at fixed M). To settle this issue we can plot $E_{\text{tot}}(M)$ along the series of equilibria and compare the total energy of the different equilibrium states for the same mass M . Alternatively, we can perform a Maxwell construction (see Fig. 22) as explained in Appendix J.

A general property can be noted. According to Eq. (D4), the total energy E_{tot} and the mass M reach their extrema along the series of equilibria at the same points since

$$\delta M = 0 \Leftrightarrow \delta E_{\text{tot}} = 0. \quad (\text{D9})$$

This implies that the curve $E_{\text{tot}}(M)$ presents cusps at these extrema. This is illustrated in Fig. 12.

The Poincaré theory of linear series of equilibria is very general. For example, it was applied by Lynden-Bell and Woods [173] and Katz [174] in relation to the thermodynamics of classical self-gravitating systems and by Chavanis [148] in relation to the thermodynamics of fermionic self-gravitating systems. In that context, the role of E_{tot} is played by the entropy S in the microcanonical ensemble (MCE) and by the free energy F in the canonical ensemble (CE); the role of M is played by the energy E and the mass M in MCE and by the mass M in CE; the role of $\mu/m = E/m$ is played by the inverse temperature β and the chemical potential μ/m in MCE and by the chemical potential μ/m in CE. An interesting feature of the statistical mechanics of self-gravitating systems is the notion of ensembles inequivalence [153] leading to various types of phase transitions [148]. The Poincaré theory of linear series of equilibria was also applied to dilute axion stars in [34, 35, 73] and to general relativistic white dwarf stars and neutron stars. In the present paper, it has been applied to dense axion stars.

Remark: An alternative to the Poincaré theory of linear series of equilibria is the $M(R)$ theorem devised by Wheeler in the physics of compact objects [144]. To apply it, one plots the mass-radius relation $M(R)$ parametrized by the central density ρ_0 . We know from classical theory

that the configurations of very low central density are stable. As we move along the series of equilibria $M(R)$ in the direction of increasing central density all configurations remain stable until the first extremal value (maximum or minimum) of M is reached. At the first extremal point the fundamental mode of radial oscillation becomes unstable. All configurations between the first extremal point and the second have one unstable radial mode. At the second extremal point (and also at each succeeding extremal point) one more mode of radial oscillation changes stability. The direction of stability change is determined by the way in which the $M(R)$ -curve bends as it passes through the extremal point. If the direction of bend is counterclockwise, then one previously stable radial mode becomes unstable at the turning point; if the direction bend is clockwise, then one previously unstable mode becomes stable at the turning point. This method is illustrated in Fig. 7 of [144], in Figs. 2 and 3 of [149], in Fig. 11.2 of [150] and in Fig. 6.3 of [151]. We note that the $M(R)$ theorem of Wheeler is less general than the Poincaré theory. For example, it cannot be directly applied in the context of the thermodynamics of self-gravitating systems [148, 173, 174].

Appendix E: Nongravitational dense axion stars in the TF limit

We have seen that dense axion stars are described by a mixed polytropic equation of state (45) involving an attractive self-interaction (first term with $a_s < 0$) and a repulsive self-interaction (second term). More generally, let us consider a system described by a mixed polytropic equation of state of the form

$$P(\rho) = K_1 \rho^{\gamma_1} + K_2 \rho^{\gamma_2}, \quad (\text{E1})$$

where the first term is attractive ($K_1 < 0$) and the second term is repulsive ($K_2 > 0$).³⁷ We consider the situation in which the quantum potential and the self-gravity are negligible (TF + nongravitational limit). For the equation of state (45), this corresponds to the branch (III-a) of the mass-radius relation of dense axion stars.

1. Constant density

In the TF + nongravitational limit, the equilibrium state of the system results from the balance between the attractive self-interaction and the repulsive self-interaction. This is a situation where the system is spatially homogeneous and the total pressure is equal to zero ($P = 0$):

$$-|K_1| \rho^{\gamma_1} + K_2 \rho^{\gamma_2} = 0. \quad (\text{E2})$$

The resulting density is

$$\rho = \left(\frac{|K_1|}{K_2} \right)^{1/(\gamma_2 - \gamma_1)}. \quad (\text{E3})$$

Specializing on the equation of state (45), we find that the axion star has a constant density

$$\rho_{\text{dense}} = \frac{9m^3 c^2}{32\pi |a_s| \hbar^2} = 8.95 \times 10^{-2} \rho_i. \quad (\text{E4})$$

For QCD axions with $m = 10^{-4} \text{ eV}/c^2$ and $a_s = -5.8 \times 10^{-53} \text{ m}$, we obtain $\rho_{\text{dense}} = 7.07 \times 10^{19} \text{ g/m}^3$.

For ULAs with $m = 2.19 \times 10^{-22} \text{ eV}/c^2$ and $a_s = -1.11 \times 10^{-62} \text{ fm}$, we obtain $\rho_{\text{dense}} = 3.88 \times 10^{-9} \text{ g/m}^3$.

Remark: we note that ρ_{dense} given by Eq. (E4) corresponds to the density scale appearing in the potential of Eq. (39). As a result, we directly recover the fact that the dilute limit corresponds to $\rho \ll \rho_{\text{dense}}$. The scaling of Eq. (E4) can also be obtained from the KG equation (2) by equating the rest-mass term ($m^2 c^2 / \hbar^2$) φ^2 and the self-interaction term ($m^2 c^3 / f^2 \hbar$) φ^4 [see Eq. (30)], or by equating the self-interaction terms ($m^2 c^3 / f^2 \hbar$) φ^4 and ($m^2 c^4 / f^4$) φ^6 . In the dilute limit, one has ($m^2 c^2 / \hbar^2$) $\varphi^2 \ll$ ($m^2 c^3 / f^2 \hbar$) $\varphi^4 \ll$ ($m^2 c^4 / f^4$) φ^6 . Finally, we note that ρ_{dense} depends only on $|a_s|/m^3$ which is fixed for QCD axions (see the Remark at the end of Sec. IV D 1).

2. Mass-radius relation

Since the density is uniform, the mass-radius relation is

$$M = \frac{3m^3 c^2}{8\hbar^2 |a_s|} R^3. \quad (\text{E5})$$

For QCD axions, we obtain

$$\frac{R}{R_\odot} = 2.72 \times 10^{-5} \left(\frac{M}{M_\odot} \right)^{1/3}. \quad (\text{E6})$$

This relation can be compared with the exact expression $R/R_\odot = 2.1 \times 10^{-5} (M/M_\odot)^{0.305}$ found numerically by Braaten *et al.* [103]. The exponent 0.305 instead of 1/3 takes into account the fact that the density is not exactly constant on the branch (III-a), implying that self-gravity plays a certain role on this branch. Indeed, the pressure cannot be exactly zero otherwise the dense axion star would collapse under its own gravity. Therefore, the star must be (slightly) inhomogeneous so that the pressure gradient arising from the self-interaction can equilibrate the self-gravity. Its exact structure can be obtained by solving the generalized Lane-Emden equation of Appendix H. However, gravitational effects are subdominant on the branch (III-a) so we expect that even if the density profile of the dense axion stars is not uniform, their central (or average) density should be almost

³⁷ We assume that $\gamma_1 > 0$ and $\gamma_2 > 0$.

independent of the mass and approximately given by Eq. (E4). On the other hand, the different value of the prefactor comes in part from the different axionic potential considered. Braaten *et al.* [103] use the effective potential (33) while we use the polynomial potential (37). The value of the density at which the pressure P given by Eq. (40) vanishes is $\rho = 0.3025 m^3 c^2 / |a_s| \hbar^2$ instead of $\rho = 8.95 \times 10^{-2} m^3 c^2 / |a_s| \hbar^2$ corresponding to the vanishing of the pressure P given by Eq. (45). Assuming that the density is uniform (with the warning made previously), we obtain a mass-radius relation of the form of Eq. (E6) with a prefactor 1.81×10^{-5} which is closer to the value found by Braaten *et al.* [103], showing that the exact form of the potential has some importance. Another consequence of using the polynomial potential (37) instead of the effective potential (33) is that we find solutions for any mass M in the Newtonian approximation while Braaten *et al.* [103] find solutions only for $M < 1.9 M_\odot$. This is because, with the effective potential (33), new (secondary) branches appear at high densities as explained in Sec. III B. There are no such branches in our simplified model based on the polynomial potential (37). It is easy to show from simple scaling arguments that the maximum mass found in [103] scales as $A(|a_s| \hbar^2 c^4 / G^3 m^3)^{1/2}$. Using their numerical value $1.9 M_\odot$ obtained for QCD axions, we obtain the general value of the prefactor: $A = 0.0679$. It is about one order of magnitude smaller than the prefactor of M_0 and $M_{\max, \text{GR}}^{\text{dense}}$ found in our approach. This means that for certain potentials, such as the one considered by Braaten *et al.* [103], the fundamental Newtonian branch of dense axion stars may end before general relativistic effects come into play.

3. Energy

In the TF + nongravitational limit, the virial theorem, the total energy and the eigenenergy of a system described by the equation of state (E1) are [see Eqs. (169)-(171) of [78]]:

$$3(\gamma_1 - 1)U_1 + 3(\gamma_2 - 1)U_2 = 0, \quad (\text{E7})$$

$$E_{\text{tot}} = U_1 + U_2, \quad (\text{E8})$$

$$NE = \gamma_1 U_1 + \gamma_2 U_2, \quad (\text{E9})$$

where $U = [K/(\gamma - 1)] \int \rho^\gamma d\mathbf{r}$ is the internal energy of a polytrope of index γ . From these equations we obtain

$$E_{\text{tot}} = NE. \quad (\text{E10})$$

Since this relation has been derived without having to evaluate the functionals explicitly, the same exact relation can be obtained from the Gaussian ansatz (see Sec. VII B) since the formulae obtained with the Gaussian ansatz are consistent with Eqs. (E7)-(E9) [78].

If we now evaluate the functionals for a spatially homogeneous system (see Sec. E 1), using $U = [K/(\gamma - 1)]\rho^\gamma V$ where $V = (4/3)\pi R^3$ is the volume of the system, we first note that the virial theorem (E7) returns Eq. (E2). On the other hand, Eqs. (E8) and (E9) become

$$E_{\text{tot}} = \left(\frac{K_1}{\gamma_1 - 1} \rho^{\gamma_1} + \frac{K_2}{\gamma_2 - 1} \rho^{\gamma_2} \right) V, \quad (\text{E11})$$

$$NE = \left(\frac{\gamma_1 K_1}{\gamma_1 - 1} \rho^{\gamma_1} + \frac{\gamma_2 K_2}{\gamma_2 - 1} \rho^{\gamma_2} \right) V. \quad (\text{E12})$$

Using Eq. (E2), we obtain

$$E_{\text{tot}} = NE = -\frac{\gamma_2 - \gamma_1}{(\gamma_1 - 1)(\gamma_2 - 1)} |K_1| \rho^{\gamma_1} V, \quad (\text{E13})$$

where ρ is given by Eq. (E3). Specializing on the equation of state (45), and using Eqs. (E4) and (E5), we get

$$E_{\text{tot}} = NE = -\frac{27m^3 c^4}{256\hbar^2 |a_s|} R^3 = -\frac{9}{32} M c^2. \quad (\text{E14})$$

4. Pulsation

The pulsation of a nongravitational dense axion star in the TF limit can be obtained as follows. If we neglect the self-gravity and the quantum potential, the hydrodynamic equations (15) and (17) reduce to

$$\frac{\partial \rho}{\partial t} + \vec{\nabla} \cdot (\rho \vec{v}) = 0, \quad (\text{E15})$$

$$\frac{\partial \vec{v}}{\partial t} + (\vec{v} \cdot \vec{\nabla}) \vec{v} = -\frac{1}{\rho} \vec{\nabla} P. \quad (\text{E16})$$

Linearizing these equations about an homogeneous sphere of density ρ given by Eq. (E4) and writing the time evolution of the perturbation under the form $\delta\rho \sim e^{-i\omega t}$, we obtain the eigenvalue equation

$$\Delta \delta\rho + \frac{\omega^2}{c_s^2} \delta\rho = 0, \quad (\text{E17})$$

where $c_s^2 = P'(\rho)$ is the square of the speed of sound. For radial perturbations, the solution of Eq. (E17) that is regular at the origin is

$$\delta\rho = A \frac{\sin\left(\frac{\omega}{c_s} r\right)}{r}. \quad (\text{E18})$$

The boundary condition $\delta\rho = 0$ at $r = R$ implies

$$\omega = \pi \frac{c_s}{R}. \quad (\text{E19})$$

From the equation of state (45), we find that

$$c_s = \frac{3}{4}c. \quad (\text{E20})$$

Therefore, the pulsation of the axion star is

$$\omega = \frac{3\pi c}{4R}. \quad (\text{E21})$$

The pulsation period $2\pi/\omega$ is of the order of the time taken by a photon to cross the axion star.

Remark: For a dense axion star of radius $R \sim R_{\min}$ [see Eq. (115)], we find that $\omega \sim mc^2/\hbar$, corresponding to the proper pulsation $\omega_{\text{proper}} = mc^2/\hbar$ of the axion. More generally, we can write $\omega/\omega_{\text{proper}} = R_{\min}/R$ so the pulsation of the axion stars is smaller than the proper pulsation of the axion.

5. The dense axion star resulting from the collapse of a dilute axion star at the critical point

The dense axion star resulting from the collapse of a dilute axion star with mass $M_{\text{max,N}}^{\text{dilute}}$ has a radius

$$R_{\text{coll}} = 1.39 \left(\frac{|a_s| \hbar^6}{Gm^7 c^4} \right)^{1/6} = 1.39 R_d, \quad (\text{E22})$$

a pulsation³⁸

$$\omega_{\text{coll}} = 1.70 \left(\frac{Gm^7 c^{10}}{|a_s| \hbar^6} \right)^{1/6}, \quad (\text{E23})$$

and an energy³⁹

$$E_{\text{tot}}^{\text{coll}} = -\frac{9}{32} M_{\text{max}} c^2 = -0.285 \frac{\hbar c^2}{\sqrt{Gm|a_s|}}. \quad (\text{E24})$$

For QCD axions with $m = 10^{-4} \text{ eV}/c^2$ and $a_s = -5.8 \times 10^{-53} \text{ m}$, we obtain $M_{\text{max,N}}^{\text{dilute}} = 6.46 \times 10^{-14} M_{\odot}$, $R_{\text{coll}} = 75.6 \text{ cm}$, $\rho_{\text{coll}} = 7.07 \times 10^{19} \text{ g/m}^3$, $2\pi/\omega_{\text{coll}} =$

$6.70 \times 10^{-9} \text{ s}$, and $E_{\text{tot}}^{\text{coll}} = -3.25 \times 10^{40} \text{ erg}$ (for comparison $2\pi/\omega_{\text{proper}} = 4.13 \times 10^{-11} \text{ s}$).

For ULAs with $m = 2.19 \times 10^{-22} \text{ eV}/c^2$ and $a_s = -1.11 \times 10^{-62} \text{ fm}$, we obtain $M_{\text{max,N}}^{\text{dilute}} = 10^8 M_{\odot}$, $R_{\text{coll}} = 0.745 \text{ pc}$, $\rho_{\text{coll}} = 3.88 \times 10^{-9} \text{ g/m}^3$, $2\pi/\omega_{\text{coll}} = 6.47 \text{ yrs}$, and $E_{\text{tot}}^{\text{coll}} = -5.03 \times 10^{51} \text{ erg}$ (for comparison $2\pi/\omega_{\text{proper}} = 0.599 \text{ yrs}$).

Remark: These results can be compared with the minimum period of white dwarfs and neutron stars (see the Remark at the end of Appendix I). We stress that the pulsation period of dense axion stars resulting from the collapse of a dilute axion star with the maximum mass is very small. We also note that the density of dense QCD axion stars is comparable to the maximum density of neutron stars, but their mass and radius are smaller.

6. The dense axion star resulting from the collapse of an axion minicluster

As recalled in the Introduction, QCD axion stars are expected to result from the gravitational collapse of axion miniclusters (axitons) [98, 100]. However, the mass of axitons $M_{\text{axiton}} \sim 10^{-12} M_{\odot}$ is larger than the maximum mass $M_{\text{max}}^{\text{exact}} = 6.46 \times 10^{-14} M_{\odot}$ of dilute axion stars [34]. Therefore, when axion miniclusters gravitationally collapse, they can either (i) form a dilute axion star of mass $M < M_{\text{max}}$ by shedding mass, (ii) fragment into several axion drops with mass $M' < M_{\text{max}}$ (this is possible because the size of axion miniclusters, $R_{\text{axiton}} \sim 10^6 \text{ km}$, is significantly larger than the size $(R_{99}^*)^{\text{exact}} = 227 \text{ km}$ of dilute axion stars), or (iii) directly form a dense axion star of mass M_{axiton} . Let us consider this third possibility. For QCD axions with $m = 10^{-4} \text{ eV}/c^2$ and $a_s = -5.8 \times 10^{-53} \text{ m}$, using the foregoing results and assuming $M_{\text{coll}} = M_{\text{axiton}} = 10^{-12} M_{\odot}$, we get $R_{\text{coll}} = 1.89 \text{ m}$, $\rho_{\text{dense}} = 7.07 \times 10^{19} \text{ g/m}^3$, $2\pi/\omega_{\text{coll}} = 1.68 \times 10^{-8} \text{ s}$, and $E_{\text{tot}}^{\text{coll}} = -5.03 \times 10^{41} \text{ ergs}$ (in comparison $R_{\text{axiton}} \sim 10^6 \text{ km}$ and $\rho_{\text{axiton}} = 4.75 \times 10^{-7} \text{ g/m}^3$). On the other hand, using the results of [73], we find that a minicluster of mass $M_{\text{axiton}}/M_{\text{max}}^{\text{exact}} = 15.5$ and radius $R_{\text{axiton}}/(R_{99}^*)^{\text{exact}} = 4405$ collapses towards a dense axion star on a time $t_{\text{coll}} = 82483t_D = 32.0 \text{ yrs}$.

7. The maximum mass of general relativistic dense axion stars

We have seen that nongravitational dense axion stars in the TF limit, corresponding to the branch (III-a) of the general mass-radius relation, have a constant density given by Eq. (E4) and a vanishing pressure ($P = 0$). When the mass M of the star approaches the value M_0 (see Appendix G), self-gravity starts to become important but we may still assume that the density approximately keeps its value given by Eq. (E4). On the other hand, general relativity must be taken into account (see Sec. XB). In that case, we have to deal with a uniform

³⁸ We note that the pulsation satisfies the relation $\omega_{\text{coll}}/\omega_{\text{proper}} = 1.99 \delta^{1/6}$. Since the exponent 1/6 is small, ω_{coll} is relatively close to ω_{proper} . This may question the validity of the fast oscillation approximation made in Sec. IIB.

³⁹ It is interesting to note that the energy $|E_{\text{tot}}^{\text{coll}}|$ of the dense axion star that results from gravitational collapse is of the order of the rest-mass energy $M_{\text{max}} c^2$ of the dilute axion star that collapses. This is rather coincidental since we are using purely Newtonian gravity in conformity with the fact that $R \gg R_S$ so there is no rest-mass energy in our problem. We obtain this result because we have kept relativistic contributions in the self-interaction potential (see footnote 9). Indeed, the speed of light occurs in the repulsive self-interaction term. In this connection, we note that Tkachev [130] argues that the energy of FRBs is of the order of $M_{\text{max}} c^2$ [see his Eq. (3)]. This is consistent with our results if we assume that $|E_{\text{tot}}^{\text{coll}}|$ corresponds to the energy released during the collapse - possibly in the form of radiation (see Sec. VIII D).

sphere of energy density $\epsilon = \rho c^2$ in general relativity. We know that the radius of a uniform sphere of mass M is restricted by the inequality⁴⁰

$$R \geq \frac{9}{8} \frac{2GM}{c^2}. \quad (\text{E25})$$

Combining Eqs. (E5) and (E25), we obtain the following expressions for the general relativistic maximum mass and corresponding radius of dense axion stars

$$M_{\text{max,GR}}^{\text{dense}} = \frac{16}{27} \sqrt{\frac{2}{3}} \left(\frac{|a_s| \hbar^2 c^4}{G^3 m^3} \right)^{1/2} = 0.484 M_r, \quad (\text{E26})$$

$$R_{*,GR}^{\text{dense}} = \frac{4}{3} \sqrt{\frac{2}{3}} \left(\frac{|a_s| \hbar^2}{G m^3} \right)^{1/2} = 1.09 R_r. \quad (\text{E27})$$

If we use the qualitative argument of Sec. X, which amounts to replacing Eq. (E25) by $R > 2GM/c^2$, we get

$$M_{\text{max,GR}}^{\text{dense}} = \frac{1}{\sqrt{3}} \left(\frac{|a_s| \hbar^2 c^4}{G^3 m^3} \right)^{1/2} = 0.577 M_r, \quad (\text{E28})$$

$$R_{*,GR}^{\text{dense}} = \frac{2}{\sqrt{3}} \left(\frac{|a_s| \hbar^2}{G m^3} \right)^{1/2} = 1.15 R_r. \quad (\text{E29})$$

For QCD axions with $m = 10^{-4} \text{ eV}/c^2$ and $a_s = -5.8 \times 10^{-53} \text{ m}$, we obtain $M_{\text{max,GR}}^{\text{dense}} = 13.5 M_\odot$ and $R_{*,GR}^{\text{dense}} = 45.0 \text{ km}$ (with the qualitative argument of Sec. X, we get $M_{\text{max,GR}}^{\text{dense}} = 16.1 M_\odot$ and $R_{*,GR}^{\text{dense}} = 47.5 \text{ km}$).

For ULAs with $m = 2.19 \times 10^{-22} \text{ eV}/c^2$ and $a_s = -1.11 \times 10^{-62} \text{ fm}$, we obtain $M_{\text{max,GR}}^{\text{dense}} = 1.83 \times 10^{15} M_\odot$ and $R_{*,GR}^{\text{dense}} = 197 \text{ pc}$ (with the qualitative argument of Sec. X, we get $M_{\text{max,GR}}^{\text{dense}} = 2.18 \times 10^{15} M_\odot$ and $R_{*,GR}^{\text{dense}} = 208 \text{ pc}$).

Appendix F: Nonattractive dense axion stars in the TF limit

We consider dense axion stars for which the quantum potential and the attractive self-interaction can be neglected (TF + nonattractive limit). This corresponds to

⁴⁰ Uniform spheres exist for any $R \geq (9/8)R_S$ and they are stable. Buchdahl [175] has shown that the lower limit to R set by the inequality (E25) is absolute in the sense that it is satisfied by any star, whatever its equation of state. However, such a lower bound is usually not reached. The radius of a star is usually substantially larger than $(9/8)R_S$. For example, the minimum radius of ideal ${}^4_2\text{He}$ white dwarfs satisfies $R_{\text{min}} = 247 R_S$ (corresponding to $M = 1.39 M_\odot$, $R_{\text{min}} = 1.02 \times 10^3 \text{ km}$, and $\rho_0 = 2.35 \times 10^{16} \text{ g/m}^3$) and the minimum radius of ideal neutron stars satisfies $R = 4.37 R_S$ (corresponding to $M = 0.710 M_\odot$, $R = 9.16 \text{ km}$, and $\rho_0 = 3.54 \times 10^{21} \text{ g/m}^3$).

the branch (III-b) of the mass-radius relation of Newtonian dense axion stars. We recall that only the beginning of this branch is valid (in the best case) because the value M_0 of the mass at which this branch appears is precisely of the order of the maximum mass $M_{\text{max,GR}}^{\text{dense}}$ set by general relativity (see Sec. XB).

1. Polytrope $n = 1/2$

In the TF + nonattractive limit, the axion star is equivalent to a barotropic star with an equation of state

$$P = \frac{64\pi^2 \hbar^4 a_s^2}{9m^6 c^2} \rho^3. \quad (\text{F1})$$

This is the equation of state of a polytrope with polytropic constant $K = 64\pi^2 \hbar^4 a_s^2 / 9m^6 c^2$ and polytropic index $\gamma = 3$ (i.e. $n = 1/2$).

2. Mass-radius relation

The general mass-radius relation of polytropic spheres is [176]:

$$M^{(n-1)/n} R^{(3-n)/n} = \frac{K(1+n)}{(4\pi)^{1/n} G} \omega_n^{(n-1)/n}, \quad (\text{F2})$$

where ω_n is a constant that can be obtained from the Lane-Emden equation (some values of ω_n are tabulated in [176]). Specializing on the equation of state (F1), we obtain

$$M = \frac{3Gm^6 c^2}{2\hbar^4 a_s^2} \omega_{1/2} R^5 = 0.0323 \frac{Gm^6 c^2}{\hbar^4 a_s^2} R^5, \quad (\text{F3})$$

where we have used $\omega_{1/2} = 0.02156\dots$

3. Energy

In the TF limit, the virial theorem, the total energy and the eigenenergy of a polytrope are [see Eqs. (169)-(171) of [78]]:

$$3(\gamma - 1)U + W = 0, \quad (\text{F4})$$

$$E_{\text{tot}} = U + W, \quad (\text{F5})$$

$$NE = \gamma U + 2W. \quad (\text{F6})$$

From these equations we obtain

$$E_{\text{tot}} = \left(1 - \frac{n}{3}\right) W, \quad (\text{F7})$$

$$U = -\frac{n}{3} W, \quad (\text{F8})$$

$$NE = \frac{1}{3}(5-n)W. \quad (\text{F9})$$

Eliminating the gravitational energy W from these relations, we get

$$E_{\text{tot}} = \frac{3-n}{5-n}NE. \quad (\text{F10})$$

This relation shows that the total energy E_{tot} is not equal to N times the eigenenergy E , as one might naively expect. Specializing on the polytrope $n = 1/2$, we obtain

$$E_{\text{tot}} = \frac{5}{9}NE. \quad (\text{F11})$$

Since this relation has been derived without having to evaluate the functionals explicitly, the same exact relation can be obtained from the Gaussian ansatz (see Sec. VII B) since the formulae obtained with the Gaussian ansatz are consistent with Eqs. (F4)-(F6) [78].

In the TF limit, the gravitational energy of a polytropic sphere of index $n < 5$ is given by the Betti-Ritter formula [176]:

$$W = -\frac{3}{5-n} \frac{GM^2}{R}. \quad (\text{F12})$$

Substituting for W from Eq. (F12) into Eqs. (F7)-(F9), we obtain

$$E_{\text{tot}} = -\frac{3-n}{5-n} \frac{GM^2}{R}, \quad (\text{F13})$$

$$U = \frac{n}{5-n} \frac{GM^2}{R}, \quad (\text{F14})$$

$$NE = -\frac{GM^2}{R}. \quad (\text{F15})$$

For a polytrope of index $n = 1/2$, the first two equations become

$$E_{\text{tot}} = -\frac{5}{9} \frac{GM^2}{R}, \quad U = \frac{1}{9} \frac{GM^2}{R}. \quad (\text{F16})$$

On the other hand, we note that the third relation is independent of the index of the polytrope. Actually, in the TF limit, this relation is valid for an arbitrary equation of state provided that the enthalpy vanishes on the boundary of the star. It can be directly obtained from Eqs. (D5) and (D8) by applying this relation at $r = R$ and using $h(R) = 0$ and $\Phi(R) = -GM/R$.

4. Pulsation

An approximate expression of the complex pulsation of a polytrope is given by the Ledoux formula [177]:

$$\omega^2 = (4 - 3\gamma) \frac{W}{I}, \quad (\text{F17})$$

where I is the moment of inertia of the star. For a polytrope $n = 1/2$, we have $I = 0.489 MR^2$ and $W = -(2/3)GM^2/R$, giving

$$\omega^2 = 6.82 \frac{GM}{R^3}. \quad (\text{F18})$$

Specializing on the equation of state (F1), the pulsation is given by Eq. (F18), the mass and the radius being related to each other by Eq. (F3).

Remark: It can be shown that polytropes of index $0 < n < 3$ are dynamically stable while polytropes of index $3 < n < 5$ are dynamically unstable. In particular, the polytrope $n = 1/2$ is stable. We note that stable polytropes have a negative energy ($E_{\text{tot}} < 0$) while unstable polytropes have a positive energy ($E_{\text{tot}} > 0$).

5. The maximum mass of general relativistic dense axion stars

An estimate of the maximum mass of general relativistic dense axion stars is obtained by combining the Newtonian mass-radius relation (F3) with the constraint $R \geq R_S$, where R_S is the Schwarzschild radius defined in Eq. (67).⁴¹ This gives a maximum general relativistic mass

$$M_{\text{max,GR}}^{\text{dense}} = \frac{1}{2(3\omega_{1/2})^{1/4}} \left(\frac{|a_s| \hbar^2 c^4}{G^3 m^3} \right)^{1/2} = 0.991 M_r \quad (\text{F19})$$

and a corresponding radius

$$R_{*,\text{GR}}^{\text{dense}} = \frac{1}{(3\omega_{1/2})^{1/4}} \left(\frac{|a_s| \hbar^2}{G m^3} \right)^{1/2} = 1.98 R_r. \quad (\text{F20})$$

As expected, these values are of the same order of magnitude as those obtained in Appendix E 7. This is because general relativistic effects set in precisely at the transition between nongravitational and nonattractive dense axion stars (see Sec. X B).

For QCD axions with $m = 10^{-4} \text{ eV}/c^2$ and $a_s = -5.8 \times 10^{-53} \text{ m}$, we obtain $M_{\text{max,GR}}^{\text{dense}} = 27.7 M_\odot$ and $R_{*,\text{GR}}^{\text{dense}} = 81.9 \text{ km}$.

For ULAs with $m = 2.19 \times 10^{-22} \text{ eV}/c^2$ and $a_s = -1.11 \times 10^{-62} \text{ fm}$, we obtain $M_{\text{max,GR}}^{\text{dense}} = 3.74 \times 10^{15} M_\odot$ and $R_{*,\text{GR}}^{\text{dense}} = 358 \text{ pc}$.

⁴¹ We could also use the Buchdahl inequality $R \geq (9/8)R_S$ [175] but this refinement is not necessary since our procedure can only give a rough estimate of the maximum mass anyway. A more detailed calculation of the maximum mass of general relativistic dense axion stars will be reported elsewhere.

Appendix G: Transition between nongravitational and nonattractive dense axion stars in the TF limit

We have seen that nongravitational dense axion stars in the TF limit, corresponding to the branch (III-a), have a constant density given by Eq. (E4) and a mass-radius relation given by Eq. (E5). On the other hand, nonattractive dense axion stars in the TF limit, corresponding to the branch (III-b), are equivalent to polytropes of index $n = 1/2$ with a mass-radius relation given by Eq. (F3). From these results, we find that the transition between nongravitational and nonattractive dense axion stars in the TF limit corresponds to

$$M_0 = \frac{3}{64\omega_{1/2}^{3/2}} \left(\frac{|a_s|\hbar^2 c^4}{G^3 m^3} \right)^{1/2} = 14.8M_r, \quad (\text{G1})$$

$$R_0 = \frac{1}{2(\omega_{1/2})^{1/2}} \left(\frac{|a_s|\hbar^2}{Gm^3} \right)^{1/2} = 3.41R_r. \quad (\text{G2})$$

For QCD axions with $m = 10^{-4} \text{ eV}/c^2$ and $a_s = -5.8 \times 10^{-53} \text{ m}$, we obtain $M_0 = 414 M_\odot$ and $R_0 = 141 \text{ km}$.

For ULAs with $m = 2.19 \times 10^{-22} \text{ eV}/c^2$ and $a_s = -1.11 \times 10^{-62} \text{ fm}$, we obtain $M_0 = 5.60 \times 10^{16} M_\odot$ and $R_0 = 615 \text{ pc}$.

Remark: We note that the value of M_0 given by Eq. (G1) is substantially larger than the value of $M_{\text{max,GR}}^{\text{dense}}$ given by Eqs. (E26) and (F19). This suggests that the Newtonian branch (III-b) is not physically relevant, even marginally. However, since our approach is qualitative, we should remain cautious about this claim.

Appendix H: Generalized Lane-Emden equation

We have seen that dense axion stars are described by an equation of state of the form of Eq. (46) which is the sum of two polytropic equations of state of index $\gamma = 2$ and $\gamma = 3$ and polytropic constants $K_2 < 0$ and $K_3 > 0$. More generally, we consider a self-gravitating system described by an equation of state of the form

$$P = K\rho^\gamma + K_*\rho^{\gamma_*}, \quad (\text{H1})$$

which is the sum of two polytropic equations of state of index $\gamma = 1 + 1/n$ and $\gamma_* = 1 + 1/n_*$ and polytropic constants K and K_* . The fundamental differential equation of hydrostatic equilibrium for a spherically symmetric barotropic self-gravitating system writes [176]:

$$\frac{1}{r^2} \frac{d}{dr} \left(\frac{r^2}{\rho} \frac{dP}{dr} \right) = -4\pi G\rho. \quad (\text{H2})$$

Substituting Eq. (H1) into Eq. (H2), and rearranging some terms, we obtain

$$\frac{1}{r^2} \frac{d}{dr} \left(r^2 \frac{d}{dr} \left[\frac{K(n+1)}{4\pi G} \rho^{\frac{1}{n}} + \frac{K_*(n_*+1)}{4\pi G} \rho^{\frac{1}{n_*}} \right] \right) = -\rho. \quad (\text{H3})$$

Defining θ and ξ through the relations

$$\rho = \rho_0 \theta^n, \quad \xi = \left[\frac{4\pi G \rho_0^{1-1/n}}{K(n+1)} \right]^{1/2} r, \quad (\text{H4})$$

where ρ_0 is the central density, we can rewrite the foregoing equation under the form

$$\frac{1}{\xi^2} \frac{d}{d\xi} \left[\xi^2 \frac{d}{d\xi} (\theta + \chi \theta^q) \right] = -\theta^n, \quad (\text{H5})$$

where we have introduced the abbreviations

$$\chi = \frac{K_*(n_*+1)}{K(n+1)} \rho_0^{1/n_*-1/n}, \quad q = \frac{n}{n_*}. \quad (\text{H6})$$

Equation (H5) must be solved with the boundary conditions at the origin

$$\theta(0) = 1, \quad \theta'(0) = 0. \quad (\text{H7})$$

The differential equation (H5) is a generalization of the Lane-Emden equation for a spherically symmetric self-gravitating system described by a polytropic equation of state $P = K\rho^\gamma$ [176]. The traditional Lane-Emden equation is recovered from Eq. (H5) by setting $\chi = 0$.

The generalized Lane-Emden equation (H5) describes dense axion stars with the equation of state (46) in the TF limit (in that case $\gamma = 2$, $K = K_2 < 0$, $\gamma = 3$, and $K_* = K_3 > 0$). This corresponds to the configurations forming the branch (III) of the general mass-radius relation of axion stars. The nongravitational limit, corresponding to the branch (III-a), is described by the constant density solution $\theta = 1$ studied in Appendix E.⁴² The nonattractive limit, corresponding to the branch (III-b), is described by the standard Lane-Emden equation associated with a polytrope of index $n = 1/2$.

Appendix I: The maximum pulsation of dilute axion stars

Using the Gaussian ansatz, we have shown in Ref. [73] that the pulsation of stable dilute axion stars with $\delta = 0$ presents a maximum

$$\omega_{\text{max}} = \frac{\sqrt{8}(\sqrt{5}-1)^{1/2}}{(\sqrt{5}+3)^{1/2}(1+\sqrt{5})} = 0.4246\dots \quad (\text{I1})$$

⁴² We note that a constant density profile is not an exact solution of the generalized Lane-Emden equation (H5) as discussed after Eq. (E6). However, we expect that on the the branch (III-a) the typical (central or average) density is independent of the mass, as for a uniform sphere, so the results of Appendix E should provide correct orders of magnitude. A detailed study of Eq. (H5) will be reported elsewhere.

at

$$R = \left(\frac{1 + \sqrt{5}}{2} \right)^{1/2} = 1.272... \quad (I2)$$

$$M = \frac{[8(1 + \sqrt{5})]^{1/2}}{3 + \sqrt{5}} = 0.9717... \quad (I3)$$

Coming back to dimensional variables, we get

$$\omega_{\max} = 0.425 \frac{\nu}{6\pi\zeta} \left(\frac{\sigma}{\alpha} \right)^{1/2} \frac{Gm^2}{|a_s|\hbar} = 0.100 \omega_a, \quad (I4)$$

where $\omega_a = 1/t_a$ (see Appendix A 1).

For QCD axions with $m = 10^{-4} \text{ eV}/c^2$ and $a_s = -5.8 \times 10^{-53} \text{ m}$, we obtain a minimum period $2\pi/\omega_{\max} = 50.3 \text{ hrs}$ (it corresponds to an axion star with $R = 90.9 \text{ km}$, $M = 6.72 \times 10^{-14} M_\odot$, and $\rho = 4.25 \times 10^4 \text{ g/m}^3$).

For ULAs with $m = 2.19 \times 10^{-22} \text{ eV}/c^2$ and $a_s = -1.11 \times 10^{-62} \text{ fm}$, we obtain a minimum period $2\pi/\omega_{\max} = 229 \text{ Myrs}$ (it corresponds to an axionic DM halo with $R = 0.398 \text{ kpc}$, $M = 1.04 \times 10^8 M_\odot$, and $\rho = 2.67 \times 10^{-17} \text{ g/m}^3$).

Remark: These results can be compared with the minimum period $T_{\min} = 2.13 \text{ s}$ of ideal ${}^4_2\text{He}$ white dwarfs (corresponding to $R = 1.47 \times 10^3 \text{ km}$, $M = 1.39 M_\odot$, and $\rho_0 = 6.58 \times 10^{15} \text{ g/m}^3$) and with the minimum period $T_{\min} = 9.00 \times 10^{-4} \text{ s}$ of ideal neutron stars (corresponding to $R = 11.5 \text{ km}$, $M = 0.670 M_\odot$, and $\rho_0 = 1.48 \times 10^{21} \text{ g/m}^3$).

Appendix J: Maxwell construction

In a first order phase transition, the point of transition where the two phases have the same probability can be determined by the Maxwell construction. Applied to our problem, the Maxwell construction tells us that the transition mass M_t at which the two phases (dilute and dense axion stars) have the same energy E_{tot} is such that the two hatched areas in Fig. 22 are equal. This result can be proven as follows.

The equal area Maxwell condition $A_1 = A_2$ can be expressed as

$$\int_{E'}^{E'''} (M - M_t) dE = 0, \quad (J1)$$

where E' is the eigenenergy of the dilute axion star and E''' is the eigenenergy of the dense axion star at the transition mass M_t . We introduce the grand potential

$$G = E_{\text{tot}} - \frac{E}{m} M = E_{\text{tot}} - NE \quad (J2)$$

which is the Legendre transform of the energy E_{tot} with respect to the mass M , with conjugate parameter E/m .

From Eq. (D4), we get

$$\begin{aligned} \delta G &= \delta E_{\text{tot}} - \frac{E}{m} \delta M - \frac{\delta E}{m} M \\ &= \frac{E}{m} \delta M - \frac{E}{m} \delta M - \frac{\delta E}{m} M \\ &= -\frac{\delta E}{m} M. \end{aligned} \quad (J3)$$

Using this relation, we can integrate Eq. (J1), thereby obtaining

$$-m(G''' - G') - M_t(E''' - E') = 0. \quad (J4)$$

Using Eq. (J2), this equation can be rewritten as

$$E'''_{\text{tot}} = E'_{\text{tot}}. \quad (J5)$$

This shows that the Maxwell construction is equivalent to the equality of the total energy of the two phases at the transition.

Appendix K: Asymptotic behavior of the transition mass

In this Appendix, we determine the asymptotic behavior of the transition mass M_t as $\delta \rightarrow 0$.

Let us first consider the dilute phase. For $M_t \rightarrow 0$, we can neglect the self-interaction terms in the energy [last two terms in Eq. (91)]. We can also use the asymptotic mass-radius relation $M_t \sim 2/R_t^{\text{dilute}}$ [see Eq. (106)]. Therefore, we get [35]:

$$(E_{\text{tot}})_t^{\text{dilute}} \sim -\frac{M_t^3}{4}. \quad (K1)$$

We note that $(E_{\text{tot}})_t^{\text{dilute}} \rightarrow 0$ when $\delta \rightarrow 0$.

We now consider the condensed phase. For $M_t \rightarrow 0$, we can neglect the self-gravity in the energy [second term in Eq. (91)]. Assuming the scalings $M_t \sim a\sqrt{\delta}$ and $R_t^{\text{dense}} \sim b\sqrt{\delta}$ when $\delta \rightarrow 0$, we obtain

$$(E_{\text{tot}})_t^{\text{dense}} \sim \left(\frac{a}{b^2} - \frac{a^2}{3b^3} + \frac{a^3}{b^6} \right) \frac{1}{\sqrt{\delta}}. \quad (K2)$$

At the transition point, the energy of the two phase must be equal: $(E_{\text{tot}})_t^{\text{dilute}} = (E_{\text{tot}})_t^{\text{dense}}$. Comparing Eqs. (K1) and (K2), we see that the term in brackets in Eq. (K2) must necessarily vanish otherwise the total energy would tend to infinity, instead of zero, when $\delta \rightarrow 0$. Therefore, $a/b^2 - a^2/3b^3 + a^3/b^6 = 0$. On the other hand, substituting the scalings $M_t \sim a\sqrt{\delta}$ and $R_t^{\text{dense}} \sim b\sqrt{\delta}$ into the mass-radius relation (101) we obtain a second equation $a^2/b^4 - a/6b + 1/3 = 0$. Solving these two equations, we get $a = 16\sqrt{3}$ and $b = 4\sqrt{3}$ implying $M_t \sim 16\sqrt{3}\delta$ and $R_t^{\text{dense}} \sim 4\sqrt{3}\delta$ when $\delta \rightarrow 0$. Comparing these results with Eqs. (113), we conclude that the transition point (R_t, M_t) asymptotically approaches the point (R_*, M_*) corresponding to the minimum radius when $\delta \rightarrow 0$.

Appendix L: Weak and strong self-interaction limits

In this Appendix, we try to clarify the notion of weak and strong self-interaction limits for axions.

1. $|\lambda| \ll 1$

The strength of the self-interaction can be measured by the dimensionless parameter λ . This parameter is usually very small with respect to unity ($|\lambda| \ll 1$) as required by particle physics and quantum field theory, meaning that axions are in a weak self-interaction regime. For QCD axions, one has $\lambda_{\text{QCD}} = -7.39 \times 10^{-49}$ and for typical ULAs, one has $\lambda_{\text{ULA}} = -3.10 \times 10^{-91}$. The condition $|\lambda| \ll 1$ corresponds to (i) $|a_s| \ll \hbar/mc = \lambda_C$, i.e., the scattering length of the axions is small as compared to their Compton wavelength; (ii) $f \gg mc^2$, i.e., the axion decay constant is large as compared to their rest mass energy. We shall say that the condition $|\lambda| \ll 1$ corresponds to the weak self-interaction limit from the viewpoint of particle physics. We note that gravity (G) does not enter into this criterion.

2. $1/\delta \gg 1$

The study of this paper, focusing on self-gravitating axion stars, shows that the strength of the self-interaction can be measured by another dimensionless parameter $1/\delta$. This parameter is usually very large ($1/\delta \gg 1$), meaning that axions are in a strong self-interaction regime. For QCD axions, one has $\delta_{\text{QCD}}^{-1} = 1.13 \times 10^{15}$ and for typical ULAs, one has $\delta_{\text{ULA}}^{-1} = 9.80 \times 10^7$. The condition $1/\delta \gg 1$ corresponds to (i) $|a_s| \gg 2Gm/c^2 = r_S$, i.e., the scattering length of the axions is large as compared to their effective Schwarzschild radius; (ii) $f \ll M_P c^2$, i.e., the axion decay constant is small as compared to the Planck energy; (iii) $|\lambda| \gg (m/M_P)^2$. We note that gravity (G) enters into this criterion. We shall say that the condition $1/\delta \gg 1$ corresponds to the strong self-interaction limit from the viewpoint of gravity.

In the strongly self-interacting regime $1/\delta \gg 1$, we have shown that (i) axion stars can be treated with Newtonian gravity (except for dense axion stars with a very large mass $M \sim M_{\text{max,GR}}^{\text{dense}}$); (ii) there is a critical mass $M_{\text{max,N}}^{\text{dilute}}$ marking the onset of a phase transition between dilute and dense axion stars.

In the weakly self-interacting regime $1/\delta \ll 1$, axion stars are Newtonian when $M \ll M_{\text{max,GR}}^{\text{dilute}}$ and general relativistic when $M \sim M_{\text{max,GR}}^{\text{dilute}}$.

Remark: We have already introduced the parameter $1/\delta$ (denoted σ) in [77] in a different, cosmological, context. In this context, the conditions $1/\delta \ll 1$ (weak self-interaction) and $1/\delta \gg 1$ (strong self-interaction) determine two different regimes in the evolution of a Universe dominated by a self-interacting complex SF with a purely

quartic potential (see the phase diagrams of Figs. 8, 18 and 19 of [77]).

3. $|\lambda| \gg (m/M_P)^2$

We note that the two conditions $|\lambda| \ll 1$ and $1/\delta \gg 1$ are both satisfied for axions, i.e., the axions are weakly self-interacting from the viewpoint of particle physics and strongly self-interacting from the viewpoint of gravity. It may seem strange that a particle with a coupling constant as small as $|\lambda|_{\text{QCD}} = 7.39 \times 10^{-49}$ or $|\lambda|_{\text{ULA}} = 3.10 \times 10^{-91}$ is considered to be strongly self-interacting (from the viewpoint of gravity). The reason is that $|\lambda|$ is small with respect to 1 but large with respect to $(m/M_P)^2$ which is itself extremely small: $(m/M_P)_{\text{QCD}}^2 = 6.71 \times 10^{-65}$ and $(m/M_P)_{\text{ULA}}^2 = 3.22 \times 10^{-100}$. In this sense, there is no paradox.

4. $|\lambda| \gg (M_P/M_{\text{ground}})^2 \sim 10^{-92}$

The previous criteria are relativistic in essence since they depend on the speed of light. In this section, we consider another criterion that does not depend on c .

Let us consider the most compact halo that we know and let us assume that it corresponds to the ground state ($T = 0$) of a self-gravitating BEC (see Appendix D of [77]). To be specific, we identify this halo with Fornax which has a mass $M_{\text{ground}} \sim 10^8 M_\odot$ and a radius $R_{\text{ground}} \sim 1 \text{ kpc}$. As shown in [35], the condition to be in the noninteracting regime is that $M_{\text{ground}} \ll M_a = \hbar/\sqrt{Gm|a_s|}$ or, equivalently, $M_{\text{ground}} \ll M_P/\sqrt{|\lambda|}$.⁴³ This condition can be rewritten as $|\lambda| \ll (M_P/M_{\text{ground}})^2 \sim 10^{-92}$. Therefore, in order to be able to neglect the self-interaction of the bosons, $|\lambda|$ has to be small with respect to 1.20×10^{-92} (!), not only small with respect to 1. This striking condition was stressed in Appendix A.3 of [35]. In many case, one has $10^{-92} \ll |\lambda| \ll 1$. This shows one more time that the self-interaction of the bosons (either attractive or repulsive) is of considerable importance in gravitational problems (axion stars, axionic DM halos...) even if their self-interaction parameter $|\lambda|$ looks very small at first sight.

Remark: As mentioned above, one cannot ignore the self-interaction of the axions when considering mini QCD axion stars and ULA clusters that form in the nonlinear regime of the cosmic evolution. Things are different, however, when considering the formation of structures

⁴³ For a repulsive self-interaction ($a_s > 0$), the noninteracting limit corresponds to $M \ll M_{\text{TF}} \sim \hbar/\sqrt{Gma_s}$ and the TF limit corresponds to $M \gg M_{\text{TF}} \sim \hbar/\sqrt{Gma_s}$. For an attractive self-interaction ($a_s < 0$), the noninteracting limit corresponds to $M \ll M_{\text{max}} \sim \hbar/\sqrt{Gm|a_s|}$; the halo becomes unstable when $M \sim M_{\text{max}} \sim \hbar/\sqrt{Gm|a_s|}$.

by Jeans instability in the linear regime of the cosmic evolution as investigated in [80]. In that case, we find that: (i) the attractive self-interaction of QCD axions cannot be neglected in the ultrarelativistic era; (ii) the self-interaction of QCD axions can be neglected in the matter era (they behave as CDM); (iii) the self-interaction of ULAs cannot be generally neglected in the matter era.

Appendix M: Condensation temperature

The GP equation is valid at $T = 0$, or for $T \ll T_c$, where

$$T_c = \frac{2\pi\hbar^2\rho^{2/3}}{m^{5/3}k_B\zeta(3/2)^{2/3}} \quad (\text{M1})$$

is the condensation temperature of the bosons (here $\zeta(3/2) = 2.6124\dots$). For self-gravitating BECs with attractive self-interaction close to the critical point ($M \sim M_{\text{max}}$ and $R \sim R_*$), using Eqs. (47) and (48), we find that the order of magnitude of the condensation temperature is

$$k_B T_c \sim m \left(\frac{\hbar G}{a_s^2} \right)^{2/3}. \quad (\text{M2})$$

It can be expressed in terms of f and λ as

$$k_B T_c \sim m \left(\frac{Gf^4}{\hbar m^2 c^6} \right)^{2/3} \sim m \left(\frac{Gm^2 c^2}{\lambda^2 \hbar} \right)^{2/3}. \quad (\text{M3})$$

It can also be written as

$$\begin{aligned} k_B T_c &\sim \left(\frac{r_s}{2|a_s|} \right)^{4/3} \left(\frac{M_P}{m} \right)^{1/3} M_P c^2 \\ &\sim (32\pi)^{4/3} \left(\frac{f}{M_P c^2} \right)^{8/3} \left(\frac{M_P}{m} \right)^{1/3} M_P c^2 \\ &\sim \left(\frac{8\pi}{|\lambda|} \right)^{4/3} \left(\frac{m}{M_P} \right)^{8/3} \left(\frac{M_P}{m} \right)^{1/3} M_P c^2. \quad (\text{M4}) \end{aligned}$$

For QCD axions with $m = 10^{-4} \text{ eV}/c^2$ and $a_s = -5.8 \times 10^{-53} \text{ m}$, we find $T_c \sim 2.11 \times 10^{23} \text{ K}$ and $k_B T_c \sim 1.82 \times 10^{10} \text{ GeV}$.

For ULAs with $m = 2.19 \times 10^{-22} \text{ eV}/c^2$ and $a_s = -1.11 \times 10^{-62} \text{ fm}$, we find $T_c \sim 4.19 \times 10^{38} \text{ K}$ and $k_B T_c \sim 3.61 \times 10^{25} \text{ GeV}$.

These values of the condensation temperature are considerable. Whatever the physical origin of the temperature T , it is clear that the condition $T \ll T_c$ will be fulfilled by many orders of magnitude. This implies that excited (thermal) states are completely negligible for self-gravitating BECs. Therefore, in excellent approximation, bosonic DM can be considered to be at zero thermodynamic temperature ($T = 0$) described by the GP equation. Still, DM halos may have an effective nonzero temperature $T_{\text{eff}} \neq 0$ responsible for their atmosphere as discussed in [78, 158, 178].

-
- [1] B. Moore, T. Quinn, F. Governato, J. Stadel, G. Lake, *MNRAS* **310**, 1147 (1999)
 - [2] G. Kauffmann, S.D.M. White, B. Guiderdoni, *Mon. Not. R. astr. Soc.* **264**, 201 (1993); A. Klypin, A.V. Kravtsov, O. Valenzuela, *Astrophys. J.* **522**, 82 (1999); B. Moore, S. Ghigna, F. Governato, G. Lake, T. Quinn, J. Stadel, P. Tozzi, *Astrophys. J. Letter* **524**, L19 (1999); M. Kamionkowski, A.R. Liddle, *Phys. Rev. Lett.* **84**, 4525 (2000)
 - [3] M. Boylan-Kolchin, J. S. Bullock, M. Kaplinghat *MNRAS* **415**, L40 (2011)
 - [4] M.R. Baldeschi, G.B. Gelmini, R. Ruffini, *Phys. Lett. B* **122**, 221 (1983)
 - [5] M.Yu. Khlopov, B.A. Malomed, Ya.B. Zeldovich, *Mon. Not. R. astr. Soc.* **215**, 575 (1985)
 - [6] M. Membrado, A.F. Pacheco, J. Sanudo, *Phys. Rev. A* **39**, 4207 (1989)
 - [7] S.J. Sin, *Phys. Rev. D* **50**, 3650 (1994)
 - [8] S.U. Ji, S.J. Sin, *Phys. Rev. D* **50**, 3655 (1994)
 - [9] J.W. Lee, I. Koh, *Phys. Rev. D* **53**, 2236 (1996)
 - [10] F.E. Schunck, [astro-ph/9802258]
 - [11] T. Matos, F.S. Guzmán, *F. Astron. Nachr.* **320**, 97 (1999)
 - [12] V. Sahni, L. Wang *Phys. Rev. D* **62**, 103517 (2000)
 - [13] F.S. Guzmán, T. Matos, *Class. Quantum Grav.* **17**, L9 (2000)
 - [14] W. Hu, R. Barkana, A. Gruzinov, *Phys. Rev. Lett.* **85**, 1158 (2000)
 - [15] P.J.E. Peebles, *Astrophys. J.* **534**, L127 (2000)
 - [16] J. Goodman, *New Astronomy* **5**, 103 (2000)
 - [17] T. Matos, L.A. Ureña-López, *Phys. Rev. D* **63**, 063506 (2001)
 - [18] A. Arbey, J. Lesgourgues, P. Salati, *Phys. Rev. D* **64**, 123528 (2001)
 - [19] M.P. Silverman, R.L. Mallett, *Class. Quantum Grav.* **18**, L103 (2001)
 - [20] M. Alcubierre, F.S. Guzmán, T. Matos, D. Núñez, L.A. Ureña-López, P. Wiederhold, *Class. Quantum. Grav.* **19**, 5017 (2002)
 - [21] M.P. Silverman, R.L. Mallett, *Gen. Rel. Grav.* **34**, 633 (2002)
 - [22] J. Lesgourgues, A. Arbey, P. Salati, *New Astron. Rev.* **46**, 791 (2002)
 - [23] A. Arbey, J. Lesgourgues, P. Salati, *Phys. Rev. D* **68**, 023511 (2003)
 - [24] T. Fukuyama, M. Morikawa, *Prog. Theor. Phys.* **115**, 1047 (2006)
 - [25] C.G. Böhm, T. Harko, *J. Cosmol. Astropart. Phys.* **06**, 025 (2007)
 - [26] T. Fukuyama, M. Morikawa, T. Tatekawa, *J. Cosmol. Astropart. Phys.* **06**, 033 (2008)
 - [27] A. Bernal, T. Matos, D. Núñez, *Rev. Mex. Astron. As-*

- trofis. **44**, 149 (2008)
- [28] T. Fukuyama, M. Morikawa, Phys. Rev. D **80**, 063520 (2009)
- [29] P. Sikivie, Q. Yang, Phys. Rev. Lett. **103**, 111301 (2009)
- [30] T. Matos, A. Vázquez-González, J. Magaña, Mon. Not. R. Astron. Soc. **393**, 1359 (2009)
- [31] J.W. Lee, Phys. Lett. B **681**, 118 (2009)
- [32] T.P. Woo, T. Chiueh, Astrophys. J. **697**, 850 (2009)
- [33] J.W. Lee, S. Lim, J. Cosmol. Astropart. Phys. **01**, 007 (2010)
- [34] P.H. Chavanis, Phys. Rev. D **84**, 043531 (2011)
- [35] P.H. Chavanis, L. Delfini, Phys. Rev. D **84**, 043532 (2011)
- [36] P.H. Chavanis, Phys. Rev. D **84**, 063518 (2011)
- [37] F. Briscece, Phys. Lett. B **696**, 315 (2011)
- [38] T. Harko, Mon. Not. R. Astron. Soc. **413**, 3095 (2011)
- [39] T. Harko, J. Cosmol. Astropart. Phys. **05**, 022 (2011)
- [40] A. Suárez, T. Matos, Mon. Not. R. Astron. Soc. **416**, 87 (2011)
- [41] P.H. Chavanis, Astron. Astrophys. **537**, A127 (2012)
- [42] H. Velten, E. Wamba, Phys. Lett. B **709**, 1 (2012)
- [43] M.O.C. Pires, J.C.C. de Souza, J. Cosmol. Astropart. Phys. **11** (2012) 024
- [44] C.-G. Park, J.-C. Hwang, H. Noh, Phys. Rev. D **86**, 083535 (2012)
- [45] V.H. Robles, T. Matos, Monthly Not. Roy. Astron. Soc. **422**, 282 (2012)
- [46] T. Rindler-Daller, P. R. Shapiro, Monthly Not. Roy. Astron. Soc. **422**, 135 (2012)
- [47] V. Lora, J. Magaña, A. Bernal, F.J. Sánchez-Salcedo, E.K. Grebel, J. Cosmol. Astropart. Phys. **02**, 011 (2012)
- [48] J. Magaña, T. Matos, A. Suárez, F. J. Sánchez-Salcedo, JCAP **10**, 003 (2012)
- [49] G. Manfredi, P.A. Hervieux, F. Haas, Class. Quantum Grav. **30**, 075006 (2013)
- [50] A.X. González-Morales, A. Diez-Tejedor, L.A. Ureña-López, O. Valenzuela, Phys. Rev. D **87**, 021301(R) (2013)
- [51] F.S. Guzmán, F.D. Lora-Clavijo, J.J. González-Avilés, F.J. Rivera-Paleo, J. Cosmol. Astropart. Phys. **09** (2013) 034
- [52] H.Y. Schive, T. Chiueh, T. Broadhurst, Nature Physics **10**, 496 (2014)
- [53] H.Y. Schive *et al.*, Phys. Rev. Lett. **113**, 261302 (2014)
- [54] B. Li, T. Rindler-Daller, P.R. Shapiro, Phys. Rev. D **89**, 083536 (2014)
- [55] D. Bettoni, M. Colombo, S. Liberati, JCAP **02**, 004 (2014)
- [56] V. Lora, J. Magaña, JCAP **09**, 011 (2014)
- [57] P.H. Chavanis, Eur. Phys. J. Plus **130**, 180 (2015)
- [58] E.J.M. Madarassy, V.T. Toth, Phys. Rev. D **91**, 044041 (2015)
- [59] A. Suárez, P.H. Chavanis, Phys. Rev. D **92**, 023510 (2015)
- [60] A. Suárez, P.H. Chavanis, J. Phys.: Conf. Series **654**, 012088 (2015)
- [61] P.H. Chavanis, Phys. Rev. D **92**, 103004 (2015)
- [62] A.H. Guth, M.P. Hertzberg, C. Prescod-Weinstein, Phys. Rev. D **92**, 103513 (2015)
- [63] J.C.C. de Souza, M. Ujevic, Gen. Relat. Grav. **47**, 100 (2015)
- [64] R.C. de Freitas, H. Velten, Eur. Phys. J. C **75**, 597 (2015)
- [65] J. Alexandre, Phys. Rev. D **92**, 123524 (2015)
- [66] K. Schroven, M. List, C. Lämmerzahl, Phys. Rev. D **92**, 124008 (2015)
- [67] D. Marsh, A.R. Pop, Monthly Not. Roy. Astron. **451**, 2479 (2015)
- [68] J.A.R. Cembranos, A.L. Maroto, S.J. Núñez Jareño, JHEP **03**, 013 (2016)
- [69] B. Schwabe, J. Niemeyer, J. Engels, Phys. Rev. D **94**, 043513 (2016)
- [70] J. Fan, Phys. Dark Univ. **14**, 84 (2016)
- [71] E. Calabrese, D.N. Spergel, Monthly Not. Roy. Astron. Soc. **460**, 4397 (2016)
- [72] D. Marsh, Phys. Rep. **643**, 1 (2016)
- [73] P.H. Chavanis, Phys. Rev. D **94**, 083007 (2016)
- [74] P.H. Chavanis, T. Matos, Eur. Phys. J. Plus **132**, 30 (2017)
- [75] L. Hui, J. Ostriker, S. Tremaine, E. Witten, Phys. Rev. D **95**, 043541 (2017)
- [76] J. Zhang, Y.S. Tsai, K. Cheung, M. Chu, arXiv:1611.00892
- [77] A. Suárez, P.H. Chavanis, Phys. Rev. D **95**, 063515 (2017)
- [78] P.H. Chavanis, Eur. Phys. J. Plus **132**, 248 (2017)
- [79] B. Li, T. Rindler-Daller, P.R. Shapiro, arXiv:1611.07961
- [80] A. Suárez, P.H. Chavanis, in preparation
- [81] E. Madelung, Zeit. F. Physik **40**, 322 (1927)
- [82] L. de Broglie, J. Physique **8**, 225 (1927)
- [83] L. de Broglie, Compt. Rend. Acad. Sci. Paris **185**, 380 (1927)
- [84] L. de Broglie, Compt. Rend. Acad. Sci. Paris **185**, 1118 (1927)
- [85] J.E. Kim, G. Carosi, Rev. Mod. Phys. **82**, 557 (2010)
- [86] R.D. Peccei, H.R. Quinn, Phys. Rev. Lett. **38**, 1440 (1977)
- [87] J. Preskill, M. Wise, and F. Wilczek, Phys. Lett. B **120**, 127 (1983)
- [88] L. Abbott and P. Sikivie, Phys. Lett. B **120**, 133 (1983)
- [89] M. Dine, W. Fischler, Phys. Lett. B **120**, 137 (1983)
- [90] R. L. Davis, Phys. Lett. B **180**, 225 (1986)
- [91] P. Sikivie, Q. Yang, Phys. Rev. Lett. **103**, 111301 (2009)
- [92] O. Erken, P. Sikivie, H. Tam, Q. Yang, Phys. Rev. D **85**, 063520 (2012)
- [93] C.J. Hogan, M.J. Rees, Phys. Lett. B **205**, 228 (1988)
- [94] E.W. Kolb, I.I. Tkachev, Phys. Rev. D **49**, 5040 (1994)
- [95] D.J. Kaup, Phys. Rev. **172**, 1331 (1968)
- [96] R. Ruffini, S. Bonazzola, Phys. Rev. **187**, 1767 (1969)
- [97] M. Colpi, S.L. Shapiro, I. Wasserman, Phys. Rev. Lett. **57**, 2485 (1986)
- [98] I.I. Tkachev, Sov. Astron. Lett. **12**, 305 (1986)
- [99] P.H. Chavanis, T. Harko, Phys. Rev. D **86**, 064011 (2012)
- [100] I.I. Tkachev, Phys. Lett. B **261**, 289 (1991)
- [101] F.S. Guzmán, L.A. Ureña-López, Astrophys. J. **645**, 814 (2006)
- [102] J. Barranco, A. Bernal, Phys. Rev. D **83**, 043525 (2011)
- [103] E. Braaten, A. Mohapatra, H. Zhang, Phys. Rev. Lett. **117**, 121801 (2016)
- [104] S. Davidson, T. Schwetz, Phys. Rev. D **93**, 123509 (2016)
- [105] E. Cotner, Phys. Rev. D **94**, 063503 (2016)
- [106] J. Eby, C. Kouvaris, N.G. Nielsen, L.C.R. Wijewardhana, JHEP **02**, 028 (2016)
- [107] E. Braaten, A. Mohapatra, H. Zhang, Phys. Rev. D **94**, 076004 (2016)
- [108] J. Eby *et al.*, JHEP **12**, 066 (2016)

- [109] Y. Bai, V. Barger, J. Berger, JHEP **12**, 127 (2016)
- [110] D.G. Levkov, A.G. Panin, I.I. Tkachev, Phys. Rev. Lett. **118**, 011301 (2017)
- [111] E. Braaten, A. Mohapatra, H. Zhang, Phys. Rev. D **96**, 031901(R) (2017)
- [112] T. Helfer *et al.*, JCAP **03**, 055 (2017)
- [113] J. Eby *et al.*, JHEP **04**, 099 (2017)
- [114] J. Eby *et al.*, arXiv:1705.05385
- [115] P. Tisserand *et al.* (EROS-2 Collaboration), Astron. Astrophys. **469**, 387 (2007)
- [116] K. Griest, A.M. Cieplak, M.J. Lehner, Phys. Rev. Lett. **111**, 181302 (2013)
- [117] P. Svrcek, E. Witten, JHEP **0606**, 051 (2006)
- [118] A. Arvanitaki, S. Dimopoulos, S. Dubovsky, N. Kaloper, J. March-Russell, Phys. Rev. D **81**, 123530 (2010)
- [119] S. Chandrasekhar, Astrophys. J. **74**, 81 (1931)
- [120] J.R. Oppenheimer, G.M. Volkoff, Phys. Rev. **55**, 374 (1939)
- [121] C. Sulem, P.L. Sulem, The Nonlinear Schrödinger Equation (Springer, 1999)
- [122] V.E. Zakharov, E.A. Kuznetsov, Phys. Usp. **55**, 535 (2012)
- [123] P.H. Chavanis, C. Rosier, C. Sire, Phys. Rev. E **66**, 036105 (2002)
- [124] C. Sire, P.H. Chavanis, Phys. Rev. E **66**, 046133 (2002)
- [125] C. Sire, P.H. Chavanis, Phys. Rev. E **69**, 066109 (2004)
- [126] P.H. Chavanis, C. Sire, Phys. Rev. E **70**, 026115 (2004)
- [127] J. Sopik, C. Sire, P.H. Chavanis, Phys. Rev. E **74**, 011112 (2006)
- [128] P.H. Chavanis, C. Sire, Phys. Rev. E **83**, 031131 (2011)
- [129] E.A. Donley, N.R. Claussen, S.L. Cornish, J.L. Roberts, E.A. Cornell, C.E. Wieman, Nature **412**, 295 (2001)
- [130] I.I. Tkachev, Sov. J. Exp. Theor. Phys. Lett. **101**, 1 (2015)
- [131] A. Iwazaki, Phys. Rev. D **91**, 023008 (2015)
- [132] S. Raby, Phys. Rev. D **94**, 103004 (2016)
- [133] A. Iwazaki, arXiv:1707.04827
- [134] Y. Bai, Y. Hamada, arXiv:1709.10516
- [135] M.S. Pshirkov, Int. J. Mod. Phys. D **26**, 1750068 (2017)
- [136] C.-P. Ma, E. Bertschinger, Astrophys. J. **455**, 7 (1995)
- [137] V. F. Mukhanov, H. A. Feldman, R. H. Brandenberger, Phys. Rep. **215**, 203 (1992)
- [138] E. Witten, Ann. Phys. (N.Y.) **128**, 363 (1980)
- [139] P. Di Vecchia, G. Veneziano, Nucl. Phys. B **171**, 253 (1980)
- [140] G.G. di Cortona, E. Hardy, J.P. Vega, G. Villadoro, JHEP **01**, 034 (2016)
- [141] F. Dalfovo, S. Giorgini, L.P. Pitaevskii, S. Stringari, Rev. Mod. Phys. **71**, 463 (1999)
- [142] S. Chandrasekhar, R.F. Tooper, Astrophys. J. **139**, 1396 (1964)
- [143] H. Poincaré, Acta Math. **7**, 259 (1885)
- [144] B.K. Harrison, K.S. Thorne, M. Wakano, J.A. Wheeler *Gravitation Theory and Gravitational Collapse* (University of Chicago Press, 1965)
- [145] V. Arnol'd, *Catastrophe Theory* (Springer, Berlin, 1992)
- [146] N.G. Vakhitov, A.A. Kolokolov, Radiophys. Quantum Electron. **16**, 783 (1973)
- [147] E. Seidel, W.M. Suen, Phys. Rev. Lett. **72**, 2516 (1994)
- [148] P.H. Chavanis, Int. J. Mod. Phys. B **20**, 3113 (2006)
- [149] D.W. Meltzer, K.S. Thorne, Astrophys. J. **145**, 514 (1966)
- [150] S. Weinberg, *Gravitation and Cosmology* (John Wiley & Sons, 1972)
- [151] S.L. Shapiro, S.A. Teukolsky *Black Holes, White Dwarfs, and Neutron Stars* (Wiley Interscience, 1983)
- [152] C. W. Misner, H. S. Zepolsky, Phys. Rev. Lett. **12**, 635 (1964)
- [153] T. Padmanabhan, Phys. Rep. **188**, 285 (1990)
- [154] N. Menci *et al.*, Astrophys. J. **836**, 61 (2017)
- [155] A. Diez-Tejedor, D. Marsh, arXiv:1702.02116
- [156] F. Hoyle, W.A. Fowler, Mon. Not. R. Astron. Soc. **125**, 169 (1963)
- [157] W.A. Fowler, Astrophys. J. **144**, 180 (1966)
- [158] P.H. Chavanis, M. Lemou, F. Méhats, Phys. Rev. D **92**, 123527 (2015)
- [159] N. Bilic, R.D. Viollier, Phys. Lett. B **408**, 75 (1997)
- [160] N. Bilic, G.B. Tupper, R.D. Viollier, Lect. Notes Phys. **616**, 24 (2003)
- [161] R. Ruffini, C.R. Argüelles, J.A. Rueda, Mon. Not. R. Astron. Soc. **451**, 622 (2015)
- [162] D.F. Torres, S. Capozziello, G. Lambiase, Phys. Rev. D **62**, 104012 (2000)
- [163] F.S. Guzmán, Phys. Rev. D **73**, 021501 (2006)
- [164] E. Seidel, W.M. Suen, Phys. Rev. D **42**, 384 (1990)
- [165] J. M. Lattimer and M. Prakash, in *From Nuclei to Stars*, Ed: S. Lee (Singapore, World Scientific, 2011), [arXiv:1012.3208]
- [166] P. B. Demorest, T. Pennucci, S. M. Ransom, M. S. E. Roberts and J. W. T. Hessels, Nature **467**, 1081 (2010)
- [167] O. Barziv, L. Karper, M. H. van Kerkwijk, J. H. Telging, and J. van Paradijs, Astron. Astrophys. **377**, 925 (2001)
- [168] H. Quaintrell, A. J. Norton, T. D. C. Ash, P. Roche, B. Willems, T. R. Bedding, I. K. Baldry, and R. P. Fender, Astron. Astrophys. **401**, 303 (2003)
- [169] M. H. van Kerkwijk, R. Breton, and S. R. Kulkarni, Astrophys. J. **728**, 95 (2011)
- [170] J. Antoniadis *et al.*, Science **340**, 6131 (2013)
- [171] D.D. Holm, J.E. Marsden, T. Ratiu, A. Weinstein, Phys. Rep. **123**, 1 (1985)
- [172] P.H. Chavanis, Astron. Astrophys. **432**, 117 (2005)
- [173] D. Lynden-Bell, R. Wood, Mon. not. R. astron. Soc. **138**, 495 (1968)
- [174] J. Katz, Mon. Not. R. Astron. Soc. **183**, 765 (1978)
- [175] H.A. Buchdahl, Phys. Rev. **116**, 1027 (1959)
- [176] S. Chandrasekhar, *An Introduction to the Theory of Stellar Structure* (Dover, 1942)
- [177] P. Ledoux, C.L. Pekeris, Astrophys. J. **94**, 124 (1941)
- [178] P.H. Chavanis, in preparation